DI (FH) Adrian Prüggler

Pre-collision Applications of Human Body Models - An Approach for Incorporating Reactive Occupant Kinematics when Modeling Critical Driving Situations

DOCTORAL THESIS

to achieve the university degree of
Doktor der technischen Wissenschaften
submitted to
Graz University of Technology

Supervisor
Assoc.Prof. Dipl.-Ing. Dr.techn. Arno Eichberger
Institute of Automotive Engineering Graz

Second supervisor
Jun.-Prof. Dr. Syn Schmitt

Graz, July 2015

EIDESSTATTLICHE ERKLÄRUNG

AFFIDAVIT

Ich erkläre an Eides statt, dass ich die vorliegende Arbeit selbstständig verfasst, andere als die angegebenen Quellen/Hilfsmittel nicht benutzt, und die den benutzten Quellen wörtlich und inhaltlich entnommenen Stellen als solche kenntlich gemacht habe. Das in TUGRAZonline hochgeladene Textdokument ist mit der vorliegenden Dissertation identisch.

I declare that I have authored this thesis independently, that I have not used other than the declared sources/resources, and that I have explicitly indicated all material which has been quoted either literally or by content from the sources used. The text document uploaded to TUGRAZonline is identical to the present doctoral dissertation

_____ _____

Datum / Date Unterschrift / Signature

Abstract

In order to further decrease the number of road fatalities and severely injured persons the automotive industry must devise new vehicle safety strategies and develop new safety measures and/or refine and combine existing technical vehicle safety measures. Vehicle safety can be split into three main parts: primary, secondary and tertiary safety. Although the focus in recent decades, has been mainly on the development of secondary safety measures, the combination of the three disciplines offers significant potential to achieve the desired decrease. Hence, the focus within the industry has expanded to include primary and tertiary safety and combine the strengths of all three research disciplines for the development of new safety measures (e.g. autonomous braking, dual stage airbags, automated emergency call system). The increase in computational power has given rise to a growing use of simulation using numerical dummy models to complement conventional dummy testing for the assessment of secondary safety systems. Unlike conventional numerical dummy models, human body models (HBM) allow for the direct identification of injury mechanisms and have therefore become a valuable tool for assessing secondary safety systems. In the pre-collision phase, occupant kinematics are strongly influenced by human muscle contributions, which conventional dummy models and purely passive HBMs cannot properly reproduce .

This thesis presents a method for incorporating for such contributions for such contributions by separating the HBM and the muscle actuator control that influences the model kinematics. The approach can be used for both multi-body and finite element models. Muscle groups are replaced by controlled beam elements that influence model kinematics. The methodology is demonstrated using a simplified version of *Total Human Model for Safety* -THUMS®, a commercial Finite Element Based human body model. The simplification included the replacement of deformable body parts with rigid bodies linked by kinematic joints. The development and validation of the methodology were based on data collected during one sled and two vehicle test series. Overall, 51 male and 6 female volunteers were investigated using various configurations of seat and restraint system.

The results of the numerical simulations are presented for these different test series and in particular for three different load cases. Large intra- and inter-individual differences in volunteers kinematic responses were observed, and the presented approach made it possible to simulate the complete range of movement. The approach of separating the controller and the HBM presented in this thesis is an important step towards the goal of using HBMs for pre-collision investigations. The implementation methodology allows for the flexible alteration of controller and model complexity.

Kurzfassung

Um die Zahl toter und schwerverletzter Personen im Straßenverkehr weiter abzusenken, erfindet die Automobilindustrie neue Fahrzeugsicherheitsstrategien, entwickelt neue Sicherheitssysteme und/oder kombiniert bereits bestehende technische Systeme. Die Fahrzeugsicherheit kann in drei Teilgebiete aufgespalten werden: Primäre, sekundäre und tertiäre Fahrzeugsicherheit. Obwohl der Fokus in den letzten Jahrzehnten auf der Entwicklung von sekundären Sicherheitssystemen lag, bietet die Kombination dieser drei Disziplinen beträchtliches Potenzial für weitere Verbesserungen. Deshalb hat sich der Fokus der Industrie erweitert, um auch primäre und tertiäre Fahrzeugsicherheit zu inkludieren und die Stärken der drei Disziplinen für die Entwicklung neuer Sicherheitsmaßnahmen (z.B.: Bremsassistent, zweistufiger Airbag, e-Call) zu kombinieren.

Die stetig steigende Rechnerleistung ermöglicht bei der Entwicklung neuer Sicherheitstechnologien die Ergänzung konventioneller Dummyversuche mit Simulationen numerischer Dummymodelle. Im Unterschied zu konventionellen numerischen Dummymodellen erlauben numerische Menschmodelle eine direkte Betrachtung von Verletzungsmechanismen und sind deshalb zu einem wertvollen Werkzeug für die Bewertung sekundärer Fahrzeugsicherheitsysteme geworden. In der Vorkollisionsphase wird die Insassenkinematik wesentlich von der Muskelaktivierung des Menschen beeinflusst, welche konventionelle Dummymodelle und rein passive Menschmodelle nicht reproduzieren können.

Diese Arbeit zeigt eine Methode, bei der mittels Separation des Menschmodells und des Aktuatorreglers, der Einfluss der Muskeln abgebildet werden kann. Der Zugang ist sowohl für Mehrkörpersysteme als auch für Finite Elemente Modelle einsetzbar. Muskelgruppen wurden durch geregelte Balkenelemente ersetzt welche die Modellkinematik beeinflussen. Die Methode wird am Beispiel von *Total Human Model for Safety* -THUMS®, einem kommerziellen Finite Elemente Methode basierten Menschmodell, präsentiert. Die Vereinfachungen inkludieren den Ersatz der verformbaren Körperteile durch Starrkörper welche mit kinematischen Gelenken verbunden sind. Die Entwicklung und Validierung der Methode basiert auf Daten welche im Zuge einer Schlittentestserie und zweier Fahrzeugtestserien gesammelt wurden und insgesamt 51 männliche und 6 weibliche Freiwillige für zahlreiche Konfigurationen von Sitz und Gurt betrachtet.

Ergebnisse numerischer Simulationen werden für drei Testserien, im Besonderen für drei unterschiedliche Lastfälle gezeigt. Große Unterschiede einzelner Individuen als auch zwischen den Individuen im Kinematikverhalten wurden beobachtet. Die präsentierte neuartige Methode erlaubt die Simulation der ganzen Bewegungsbandbreite sowie eine flexible Steigerung der Regler und Modellkomplexität. Die Methode, die den Regler

und das Menschmodell trennt ist ein wichtiger Schritt in Richtung des Einsatzes von Menschmodellen in der Vorunfallsphase.

Acknowledgement

I would like to express my special appreciation and thanks to my supervisor Assoc.Prof. Dipl.-Ing. Dr.techn. Arno Eichberger. I am very grateful for the time and ideas he contributed to make my Ph.D experience productive and stimulating. Furthermore I would like to express my profound gratitude to Jun.-Prof. Dr. Syn Schmitt, who agreed to be the second supervisor of this thesis.

My further thanks go to Dipl.-Ing. Dr. techn. Harald Schluder, Dipl.-Ing. Dr. techn. Andreas Rieser and DI Andreas Teibinger who provided me the opportunity to conduct this research at the vehicle safety division of the mechanics department of Virtual Vehicle Research Center in Graz. I am also especially grateful for the productive collaboration with my project colleagues, Dr. rer. nat. Philipp Huber, DI Thomas Steidl, DI Stefan Kirschbichler and Dipl.-Ing. Dr. techn. Kurt Steiner whose helpful advice contributed greatly to this thesis. Additionally, I would like to thank all of my colleagues from my working group, who have not only been helpful collaborators but also supportive friends.

My special thanks go to my parents, the rest of my family and my friends. Words cannot express how grateful I am to all of you for your love, support and patience. All of you encouraged me to follow my dreams. In particular I dedicate this thesis to my grandfather Alois, who passed away before I could start my career as an engineer, and my grandmother, Helene, who gave me the strength to finish this thesis.

Finally, I would like to thank the project partners and acknowledge the financial support of the COMET - Competence Centers for Excellent Technologies - programme by the Austrian Federal Ministry for Transport, Innovation and Technology (BMVIT), the Federal Ministry of Science, Research and Economy (BMWFW), the Austrian Research Promotion Agency (FFG), the province of Styria and the Styrian Business Promotion Agency (SFG).

Contents

Abbreviations

CC	Contractile component
CNS	Central nervous system
DoF	Degrees of freedom
EC	European Commission
EEA	European Environment Agency
EMG	Electromyography
EU	European Union
FE	Finite Element
FEM	Finite Element Method
GHMBC	Global human body model
HARB	Human arcticulated rigid body
HBM	Human body model
HUMOS	Human model for safety
ICOS	Independent co-simulation
ITARDA	Institute for Traffic Accident Research and Data Analysis (Japan)
MBS	Multi-body system
MoI	Mass moment of inertia
MTU	Muscle tendon unit
MVC	Maximum voluntary contraction
NHTSA	National Highway Traffic Safety Administration
OEM	Original equipment manufacturer
OOP	Out of postion
PD	Proportional-differential
PEC	Parallel elastic component
PMHS	Post-mortem human subjects
R&D	Research and development
SEC	Serial elastic component
THUMS	Total Human Model for Safety
UK	United Kingdom
VSI	Vehicle Safety Institute

Symbols

Variables and constants

a, b	Constant coefficients
a_x	Acceleration in x-axis direction (vehicle longitudinal acceleration)
a_y	Acceleration in y-axis direction (vehicle lateral acceleration)
E_1	Joint torque body 1
E_2	Joint torque body 2
i	Counting indices
i_1	Radius of gyration 1
i_2	Radius of gyration 2
$F_{Shoulderbelt}$	Shoulder belt force
F_{S_1}	Disturbance force on rigid body 1
F_{S_2}	Disturbance force on rigid body 2
J_{i-i}	Mass moment of inertia with respect to rotation axis i-i
$J_{a-a,S}$	Mass moment of inertia through point S with respect to rotation axis a-a
$J_{s-s,COG}$	Mass moment of inertia through COG with respect to rotation axis s-s
J_{S_1}	Mass moment of inertia through COG rigid body 1
J_{S_2}	Mass moment of inertia through COG rigid body 2
J_{xx}	Axial mass moment of inertia around x-axis
J_{xy}	Deviation or centrifugal moment xy
J_{xz}	Deviation or centrifugal moment xz
J_{yy}	Axial mass moment of inertia around y-axis
J_{yx}	Deviation or centrifugal moment yx
J_{yz}	Deviation or centrifugal moment yz
J_{zz}	Axial mass moment of inertia around z-axis
J_{zx}	Deviation or centrifugal moment zx
J_{zy}	Deviation or centrifugal moment zy
J_1	Axial mass moment of inertia around 1-axis
J_2	Axial mass moment of inertia around 2-axis
J_3	Axial mass moment of inertia around 3-axis
k	Counting indices
L_{Hxf}	Difference between muscle/actuator attachment points for head front in x direction

L_{Hzf}	Difference between muscle/actuator attachment points for head front in z direction
L_{Hzs}	Difference between muscle/actuator attachment points for head side in z direction
L_{LBR}	Length back rest
L_{LSBR}	Length side back rest
L_{LHR}	Length head rest
L_{LSP}	Length seat plate
L_{HSP}	Height seat plate
L_{Hys}	Difference between muscle/actuator attachment points for head side in y direction
L_{Txf}	Difference between muscle/actuator attachment points for torso front in x direction
L_{Tys}	Difference between muscle/actuator attachment points for torso side in y direction
L_{Tzf}	Difference between muscle/actuator attachment points for torso front in z direction
L_{Tzs}	Difference between muscle/actuator attachment points for torso side in z direction
L_{WBR}	Width back rest
L_{WBRB}	Width back rest bottom
L_{WBRT}	Width back rest top
L_{WHR}	Width head rest
L_{WSP}	Width seat plate
L_0	Muscle resting length
m	Mass
m_1	Mass of rigid body 1
m_2	Mass of rigid body 2
P	Muscle tension
P_0	Maximum isometric tension
Q_1	Generalized forces for generalized coordinate 1
Q_2	Generalized forces for generalized coordinate 2
Q_i	Generalized forces for generalized coordinate i
r	Perpendicular distance to rotation axis
s_1	Distance center of gravity rigid body 1
s_2	Distance center of gravity rigid body 2
t_c	Coupling time step
t_S	Simulation start time
T_1	Kinetic energy of rigid body 1
T_2	Kinetic energy of rigid body 2
Tr	Reaction time
u_i	Coupling input quantities
v	Velocity contraction velocity

v_x	Velocity in x-axis direction (vehicle longitudinal velocity)
v_2	Translational velocity of rigid body 2
V	Volume
V_i	Volume of body i
x	Position in x direction
x_{COG}	Position mass center of gravity in x direction
x_1	Position mass center of gravity of rigid body 1 in x direction
x_2	Position mass center of gravity of rigid body 2 in x direction
y	Position in y direction
y_{COG}	Position mass center of gravity in y direction
y_i	Coupling output quantities
z	Position in z direction
z_{COG}	Position mass center of gravity in z direction
z_1	Position mass center of gravity of rigid body 1 in z direction
z_2	Position mass center of gravity of rigid body 2 in z direction
α	Angle backrest to seatplate
β	Angle seatplate to xy plane
γ	First angle side support to backrest
Δt_i	Micro time step of system i
$\Delta T_{i,<m>}$	M-th Macro time of system i
ϕ_{Head}	Head segment angle
ϕ_{Torso}	Torso segment angle
$\varphi_{x,Head}$	Relative head segment angle around x-axis
$\varphi_{x,Torso}$	Relative torso segment angle around x-axis
$\varphi_{y,Head}$	Relative head segment angle around y-axis
$\varphi_{y,Torso}$	Relative torso segment angle around y-axis
φ_1	Generalized coordinate 1
φ_2	Generalized coordinate 2
$\dot{\varphi}_1$	Velocity of generalized coordinate 1
$\dot{\varphi}_2$	Velocity of generalized coordinate 2
ω	Vehicle yaw rate
ρ	Density
ρ_k	Density of body k
ζ	Second angle side support to backrest

Vectors

$\mathbf{b}$	Moment vector due to other forces
$\mathbf{F}$	Actuator force vector
$\mathbf{K_{High}}$	Input parameter vector after perceiving the maneuver
$\mathbf{K_{Low}}$	Input parameter vector preliminary to perceiving the maneuver
$\mathbf{T}$	Controller torque vector
$\mathbf{x}$	Translational displacement vector
$\dot{\mathbf{x}}$	Translational velocity vector
$\ddot{\mathbf{x}}$	Translational acceleration vector
$\bar{\mathbf{Q}}$	Generalized centrifugal moment vector and
$\boldsymbol{\alpha}$	Rotational displacement vector
$\dot{\boldsymbol{\alpha}}$	Rotational velocity vector
$\ddot{\boldsymbol{\alpha}}$	Rotational acceleration vector
$\boldsymbol{\varphi}$	Current outside model angles vector
$\boldsymbol{\varphi}_d$	Demand angles vector
$\dot{\boldsymbol{\varphi}}$	Current outside model angular velocities vector
$\dot{\boldsymbol{\varphi}}_d$	Demand velocities vector

Matrices

$\mathbf{J}^{(\mathbf{A})}$	Inertia tensor with respect to reference
$\mathbf{M}$	Mass matrix

1. Introduction

1.1. Mobility and motorization

Considering mankind's history from an engineering perspective, the Industrial Revolution, which took place from the 18^{th} to 19^{th} centuries, had a significant impact. This phase brought three important changes: the invention of machines to replace hand tools, the replacement of human and animal muscle power with other forms of power (e.g., steam), and the adoption of the factory system [Mus14, Mon14, Dea79]. This period provided a solid foundation for 21^{st} century society.

One invention that had an enormous impact on humans existence was the invention of the automobile about 130 year ago. Gottlieb Daimler (1834-1900) and Wilhelm Maybach (1846-1929) successfully tested a four-stroke gasoline engine in an experimental two wheeler (1885) and in a "motor carriage" (1887). In 1886, Carl Friedrich Benz (1844-1929) patented his invention, which is often seen as the first practical car powered by an internal combustion engine. [Eck01]

Figure 1.1.: Benz Patent motorcar [Mus14]

In the 19^{th} century, few people had the opportunity and the money to purchase a car. However, in modern society, the rise of mass production, in combination with other technical advances, have made automobiles affordable for many in industrialized and even developing countries. According to [Eur13], in 2011 nine of the EU-28 member states (Luxembourg, Italy, Malta, Lithuania, Cyprus, Finland, Austria, Germany and Slovenia) had at least one car per two inhabitants, with the lowest rates reported for Romania and Latvia. From 2006 to 2011, motorization rates increased in most member states

presented. Figures published by the European Environment Agency [Age11] in 2011 (also based on Eurostat data) show the significant increase in the number of passenger cars per 1000 inhabitants for 32 EEA (EEA-32)countries from 1995 to 2008, as shown in Figure 1.2.

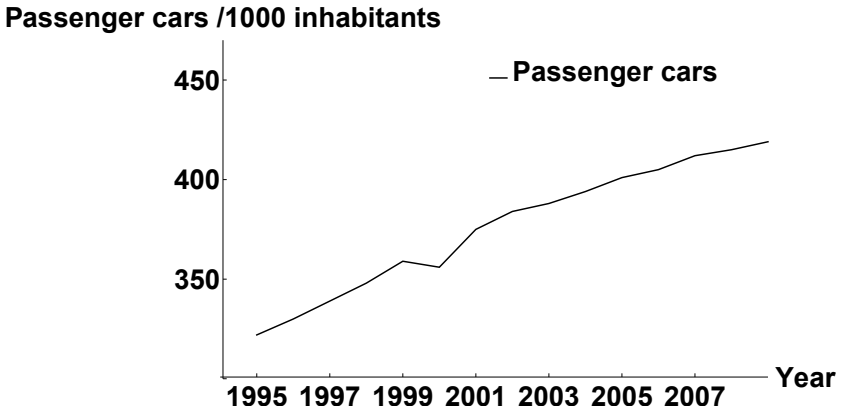

Figure 1.2.: Passenger cars per 1000 inhabitants from 1995 to 2008 for the EEA-32 countries. Adapted from [Age11]

The European Environment Agency [Age11] states that both the overall vehicle fleet in the EEA area and car ownership rates grew from 1995 to 2009. They identify several main factors to explain the observed growth of passenger cars per capita in the EEA area, including the "(a) decreasing number of persons per household, (b) increasing number of cars per household and (c) increases in the average travel distance, lower accessibility and flexibility by public transport and changes in lifestyle patterns." For many people in industrialized countries, the car is not only a means of transport for daily life, but rather an embodiment of mobility. According to [SEB+11] and [BS13] mobility basically involves the desire or the ability to travel across distances and reaching goals. The important human functions aided by mobility include leisure activities, work and shopping. The sum of all movement of human beings and goods is referred to as traffic, and leisure time traffic accounts for a substantial portion. The high percentage of motorized individual traffic is a result of the advantages of cars (e.g., time independent, broad and flexible use, transport of goods).

1.2. Accident statistics

However, in addition to its positive effects on society, the rising level of motorization also involves negative consequences that need to be addressed. The increasing number of road vehicles requires improvement and expansion of road networks, increases the consumption of natural resources, and increases emissions, thereby affecting the human environment and the global climate. Furthermore, injuries and deaths caused by traffic

accidents have become a major public health and socio-economic problem. In 2010 there were 1.24 millions deaths on the world's roads. Another 20 to 50 million sustain non-fatal injuries due to road traffic crashes. Traffic incidents are eight on the global list of estimated causes of death and the leading cause of death for people between the ages of 15 and 29. Road traffic injuries generate high financial costs that are estimated at over US $ 100 billion a year, which represent about 1-2% of low- and middle-income countries' gross' national product. Although some high-income countries have seen recent decreases in road traffic fatality rates, the global rate continues to rise as a result of the rapid increase in road traffic accidents in low and middle- income countries. Hence current trends suggest that road traffic injuries will be the fifth leading cause of death by 2030. To prevent road traffic injuries, national efforts are needed. Hence, in 2010, United Nations General Assembly adopted the resolution 64/255[1]. This resolution proclaimed a Decade of Action for Road Safety. As shown in Fig. 1.3, the goal is reverse the current upward trend in road fatalities in the decade from 2010 to 2020 by saving about 5 million lives. [TLPM13]

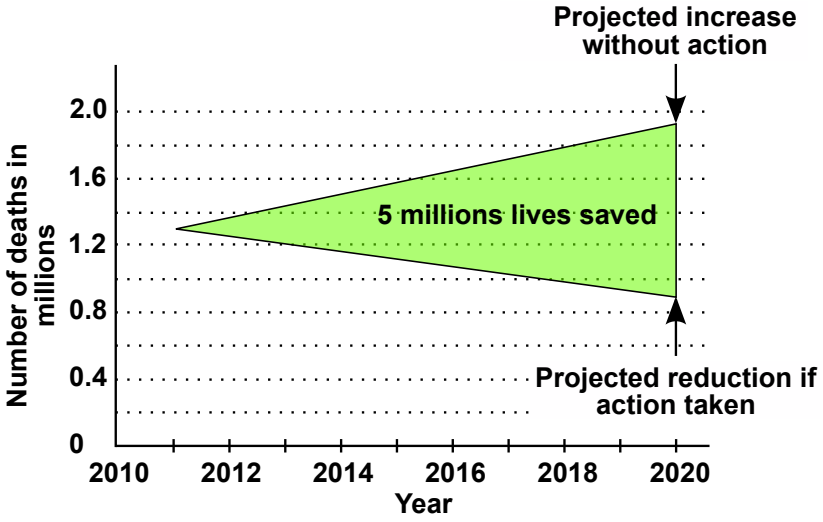

Figure 1.3.: Goal of the Decade of Action for Road Safety 2011-2020, [TLPM13]

Figure 1.4 shows the number of fatalities in Europe from 2001 to 2013. Although there has been a significant decrease in the number of fatalities, the ambitious target of halving the number of road traffic fatalities by 2010, which was set in 2001 in its white paper "European transport policy for 2010: time to decide", has not been completely met, as the number of fatalities has fallen more slowly than envisaged. [BBY+12]

In 2011, the European Commission (EC) again adopted an ambitious road safety programme that calls for a near elimination of road transport fatalities by 2050. The goal

[1]Download: http://www.who.int

is to first cut the number of road fatalities in half by 2020. To achieve this, initiatives in the areas of technology, enforcement, education and closer attention to vulnerable road users have been identified as key aspects. [Com11]

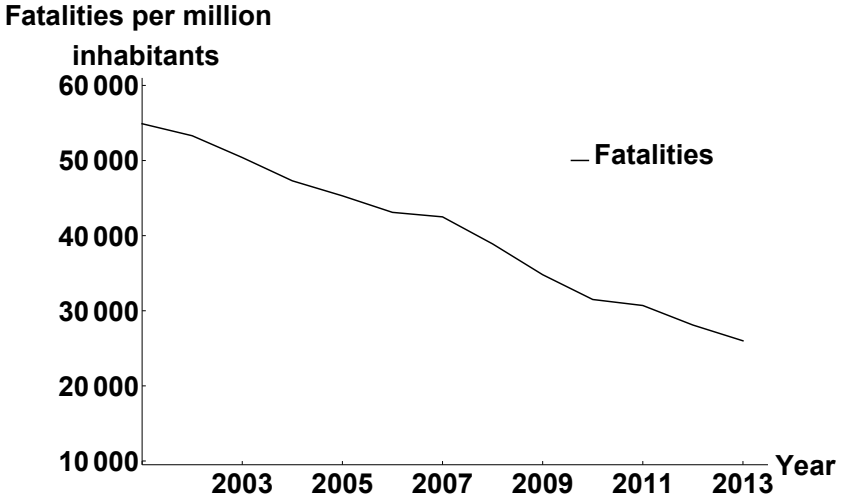

Figure 1.4.: Number of EU road accident fatalities per million inhabitants from 2001 to 2013 [Com14b]

1.3. Primary, secondary and tertiary vehicle safety

Vehicle safety plays an important role in decreasing road casualties on national and international levels [Com14a]. According to Kramer [Kra08], the field of vehicle safety is mainly divided into two parts: primary and secondary safety. In recent years, the post-crash treatment has also gained more importance. Hence, throughout this thesis, vehicle safety is divided into three parts: primary, secondary and tertiary safety. According to [BM07], road safety consists of three main components. The human being (traffic participant), the vehicle (means of transport) and the environment (infrastructure). Primary safety covers all measures geared towards avoiding accidents or reducing accident severity (e.g., brake assistant, collision avoidance). Primary safety measures act in the time interval between the recognition of a critical situation and the first contact between the collision participants. Secondary safety comprises all measures used to mitigate the consequences to the human in the event of an unavoidable accident (e.g., restraint systems, driver and passenger airbags, deformable vehicle structures). This phase starts spans the time between initial contact of the collision participants and the point of standstill. Tertiary safety comprises all measures taken after the accident for rescue and injury treatment. [Com14a, Eic10, Kra08, SS08] The combination of the three disciplines is expected to have great potential to further decrease fatalities. Hence the current approach is to combine the strengths of these three research disciplines to

develop new safety measures (e.g., autonomous braking, dual-stage airbag, automated emergency call system). Figure 1.5 shows examples of primary, secondary and tertiary safety measures for the driver, the vehicle and the environment. As the figure shows, the different disciplines are no longer considered completely separate.

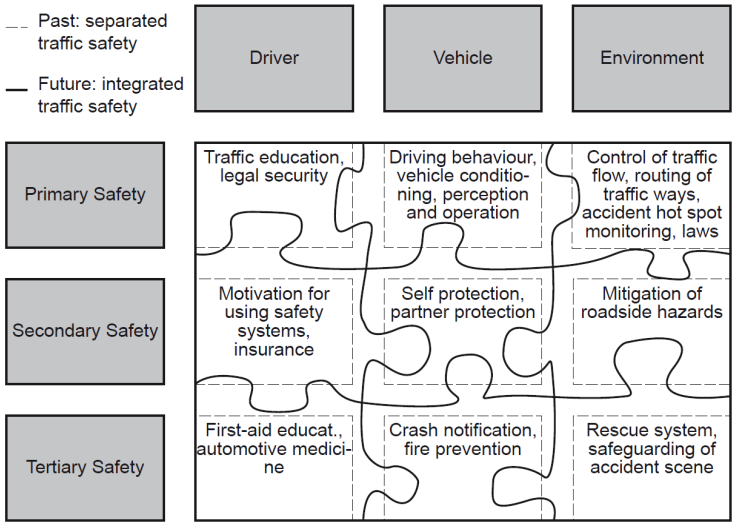

Figure 1.5.: Examples of safety measures divided for driver, vehicle and environment and for the different phases [Eic10]

The last five decades have seen significant progress in vehicle safety has made significant progress. In 2002, Leen [LH02] presented a figure that considering different safety systems with respect to their safety potential and their level of assistance. Due to the novelty of tertiary systems, Leen's figure excluded such systems and only covered passive safety and active safety systems. As evident can be seen in Fig. 1.6, the passive safety systems introduced between 1960 and 1980 had significant safety potential. Since 1985, the safety potential of the passive systems has decreased, while this trend has gone in the opposite direction for active systems. Between 1960 and 1990, only two active systems were introduced: the antilock brake system and electronic traction control. After 1990, the number of active systems began to increase can be observed. These systems offer a high safety potential. Besides the systems already introduced on the market, Leen also estimated the potential of future active safety systems, such as autonomous driving. In addition to the safety potential, the level of driver assistance is also shown. As evident there is a trend toward autonomous active safety systems. The combination of primary and secondary vehicle safety systems, referred to as integrated safety ([SG14]), offers the potential for a further significant decrease in road casualties. The main idea of integrated safety is to support the driver to as much as possible to help avoid the accident, but if the accident is unavoidable, the secondary safety systems should provide the optimum protection for the accident parties involved, depending on the accident scenario. Primary vehicle safety systems currently on the market (semi-autonomous braking sys-

tems) have proven to be effective in avoiding accidents. Primary vehicle safety systems that monitor drivers, vehicles and environmental conditions, alert drivers of potentially dangerous situations, and assist them or act autonomously to prevent a crash or mitigate its severity can significantly contribute to EU road safety. Since many primary vehicle safety systems interact with occupants in the pre-crash phase, their value in preventing or reducing injuries depends on how the system influences the vehicle and/or the occupants' kinematics. The ability to model and simulate this interaction in order to derive the occupant kinematics is of crucial importance to the industry. Primary safety systems can override driver input and act autonomously. On the one hand, this circumvents some of the weaknesses of a human driver (e.g., reaction time, direction of attention), but on the other hand, it increases the pressure on the industry to prove that these systems do indeed increase safety.

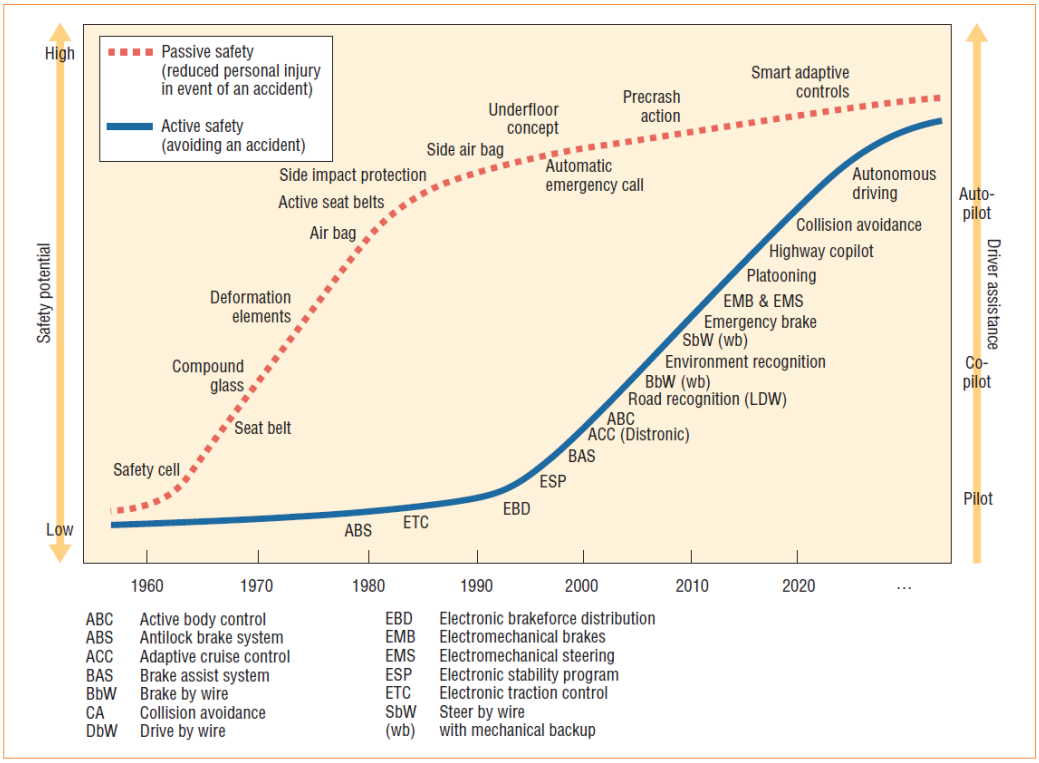

Figure 1.6.: Past and future primary and secondary safety measures [LH02]

The current vehicle safety evaluation process is based on standardized tests. These laboratory tests evaluate the effectiveness of safety systems starting with the first contact of the accident participants. For these tests, vehicle occupants are assumed to be in a standardized initial position. However, in real-life scenarios, a phase in which the occupants are exposed to longitudinal and/or lateral acceleration forces frequently precedes the collision event (emergency braking or skidding). Such accelerations, which could be

the result of either a driver input (braking, steering, etc.) or the intervention of primary safety system (autonomous braking, electronic stability control), lead to occupant displacements. Hence, if the pre-collision phase is followed by a collision phase, the occupants' real positions differ from the assumed initial laboratory test position. Such an *out of position* (OOP) before a collision can decrease the effectiveness of restraint systems designed and optimized for normal driving posture and therefore directly influence the injury outcome [BCUM10], a fact which highlights the importance of a combined consideration of both the pre-collision and collision kinematics of occupants.

In particular, the use of mechanical and numerical dummy models is well established for investigations of the collision phase and severe impacts. Due to the fact that mechanical dummy models have been built to withstand high accelerations, their potential for use in low-acceleration scenarios is limited and they cannot be used to assess of primary systems effectively. Adapting these hardware dummies or developing new ones for use in low-acceleration scenarios would be time consuming. [MVHB$^+$12]. Furthermore, the efforts would lead to increased development cost, and the ability to reproduce results obtained with such a hardware dummy would remain unknown. Within the last decade, there has been an additional focus on developing computer human models, also referred to as numerical human body models (HBM). Unlike to dummies which are a mechanical representation of the human being, numerical human body models are a more detailed representation of human beings and offer the chance to directly to consider injuries and injury mechanisms.

Figure 1.7 shows the two development paths in vehicle safety. Starting with a human or more precisely, a defined group of humans with a certain anthropometry, either an HBM or a dummy model can be developed. The development of both anthropometry and anatomical data requires, post-mortem human subject (PMHS) tests and material data. The development of HBMs also involves volunteer tests. Based on the dummy response (accelerations, velocities and displacements), the injury risk for the human being can be estimated using injury risk criteria. As mentioned above, using an HBM enables the direct investigation of injuries and injury mechanisms.

Due to their potential to directly consider injury mechanisms in simulations within the crash phase, human body models (HBM) have become a valuable tool for secondary safety system assessment. The vision is to use these models for low-severity impacts as well, such as pre-collision car maneuvers. In the pre-collision phase, volunteer kinematics are strongly influenced by human contributions (e.g., active steering or body stabilization). Several studies have highlighted the importance of muscle activity that influences human kinematics during pre-collision car movements, see [EOH$^+$07, EZS$^+$08, BKMD11, BKM$^+$12, KBD11, KBMD14]. These contributions are among the main reasons why existing purely passive HBMs cannot accurately reproduce occupant pre-collision kinematics. Hence, to enable the use of HBMs in the pre-collision phase, the incorporation of human contributions is an important issue for the further development of advanced safety systems.

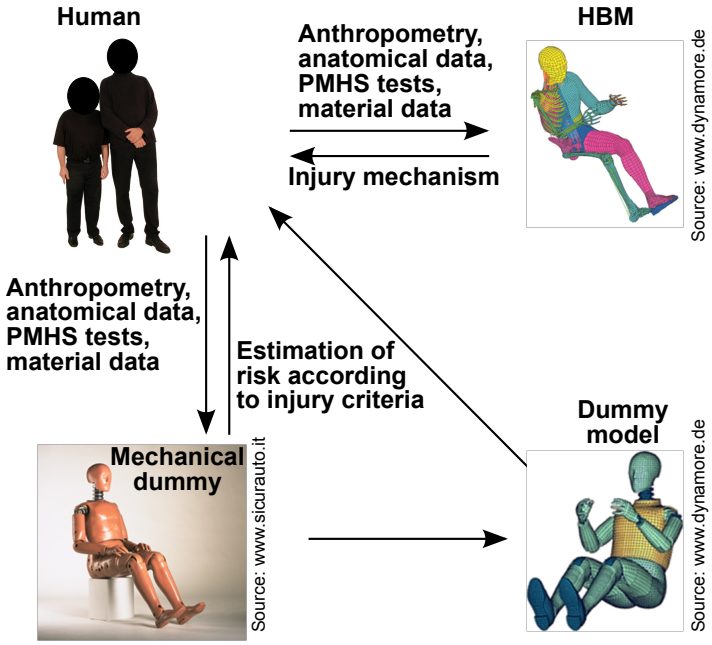

Figure 1.7.: Two development paths: Human body model vs. dummy. Adapted from [Hub13]

1.4. Objective

As described in the previous section, the knowledge of human pre-collision kinematics is essential for the further development of integrated safety systems and therefore offers great research potential. The aim of this thesis was to develop a methodology for incorporating reactive human occupant kinematics in an HBM. In this thesis, reactive human kinematics is the kinematics of human occupants caused by muscle contributions that counteract external low-acceleration disturbances (up to several g). This method requires the description of the kinematics of the biological system "*human*" during pre-collision maneuvers, as well as the development of a numerical representation within the simulation. Based on these two fields, known as testing and simulation, the following thesis research questions were derived:

1. What kind of approach to incorporating reactive human behavior or human movement patterns is necessary to enable the use of both MB and FE HBMs for pre-collision considerations?
2. What load cases have already been investigated, and what load cases are needed?
3. What kind of modeling strategy is needed to enable the simulation of volunteer responses?

After offering some insight into the current state of the art and the weaknesses of HBMs, this thesis presents an alternative modeling strategy for the use of an HBM in pre-collision investigations. Furthermore it shows a modular implementation methodology based on kinematics data gathered during two projects conducted at the Virtual Vehicle in cooperation with the Graz University of Technology (Vehicle Safety Institute- VSI) and the other partners mentioned in the acknowledgement section of this thesis.

2. Fundamentals

The development of a methodology for incorporation of pre-collision occupant kinematics into a numerical human body models requires knowledge in several disciplines, including biomechanics, testing methods and simulation. In order to clarify the incorporation methodology and the limits of the chosen approach, this chapter provides basic information about these disciplines, as well as the current state of the art in passive HBMs.

2.1. Biomechanics

According to [Hat74], biomechanics is "The study of the movement of living things using the science of mechanics". In biomechanics, the principles of mechanics are applied to biological systems [SNW04]. Mechanics, an important field of physics, is the study of force and motions and their relations [GHS08, Knu07].

2.1.1. Skeletal system

The human is a complex mechanical system. According to [GL18] the human skeleton consists of about 206 distinct bones. This number varies from person to person, and due to the fusion of bones, this number decreases with age. The skeletal system protects and supports the human body, assists with movement, stores important minerals, and even produces blood cells [EBB05], p. 111. The bones are the major supporting elements of the body and protect vital organs. The skull consists of 8 cranial bones, 14 facial bones, 6 auditory ossicles and one hyoid bone. The vertebral column consists of 33 to 34 vertebrae, including 7 cervical, 12 thoracic and 5 lumbar vertebrae, followed by the sacrum and the coccyx. These last two consist of 5 fused vertebrae each [Pla09], p. 36. The vertebral column carries the head and enables the movement of head and trunk. Furthermore, it protects the spinal cord and provides exits for spinal nerves. Due to its importance for this thesis and the understanding of the incorporation methodology, chapter 3 provides further information about the vertebral column.

The 12 thoracic vertebrae are also part of the thoracic cage. This thoracic cage consists of 12 pairs of ribs, cartilage and the sternum, also referred to as the breastbone. The thoracic cage plays a major role during ventilation in preventing the collapse of the thorax and protecting the organs. The bones of the trunk where the upper limbs are attached to the trunk form the shoulder girdle. The shoulder girdle is formed by the scapula and clavicles. The bone in the upper arm is referred to as the humerus, while

the lower arm contains the ulna and radius. The skeleton of the hand can be divided into three segments: carpal bones (wrist bones), the metacarpals (bones in the palm) and the phalanges (bones in the digits).

The bones of the trunk where the lower limbs are attached to the trunk form the pelvic girdle. The pelvic girdle is formed by the hip bones. The two hip bones, the sacrum and the coccyx form the pelvis. The upper bone of the lower extremity is called the femur. It is the longest and strongest bone in the human skeleton. The triangular bone in front of the knee is called the patella. The tibia, the fibula and the foot form the lower part of the lower extremity. The skeleton of the foot consists of three parts: the tarsals, metatarsals and phalanges. Figure 2.1 illustrates the bones of the skeletal system. The hyoid bone is not shown.

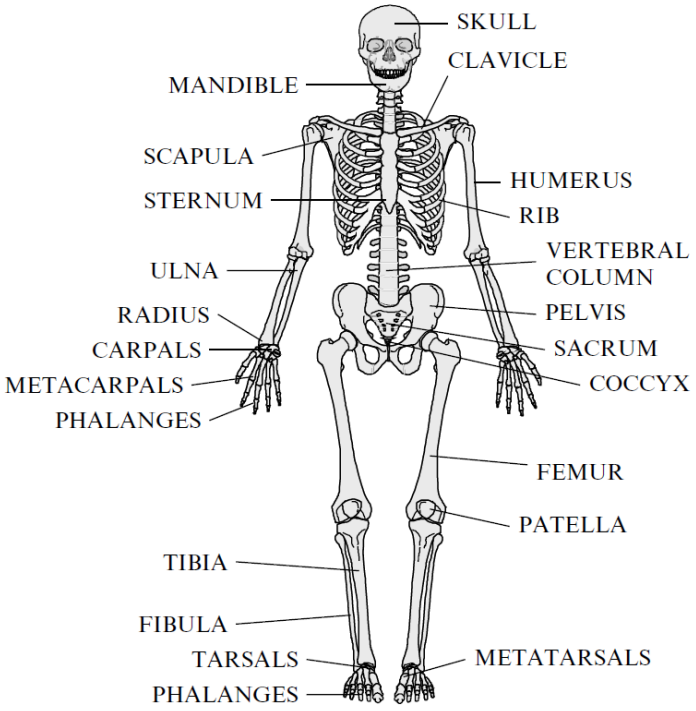

Figure 2.1.: Bones of the skeletal system (hyoid bone not included) [EBB05]

The connections that join two bones at different parts of their surfaces are called joints or articulations [GL18]. There are three types of joints within the skeletal system: fibrous[1], cartilaginous and synovial joints [2]. In multi-body dynamics, joints are classified, based on the degrees of freedom (DoF) they provide. Figure 2.2 shows the six different types

[1]Fibrous connective tissue tightly binds together articulating bones
[2]Joints with fluid-filled joint cavities, cartilage in articulating bones and ligaments

of synovial joints based on their structural DoF: gliding joints, hinge joints (the most common type, such as elbow), pivot joints, condyloid joints (allow flexion-extension and rotation, e.g. fingers), saddle joint (multiaxial, e.g. thumbs) and ball and socket joints (most freely movable, e.g. shoulders) [EBB05].

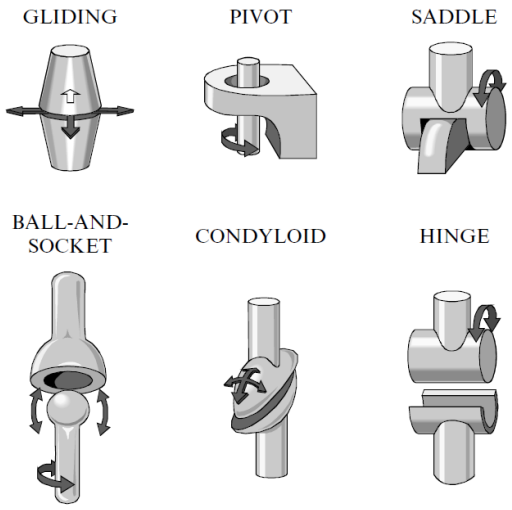

Figure 2.2.: Different synovial joint types found in the human skeletal system [EBB05]

2.1.2. Muscles

Within the human body, composed bundles of specialized cells are responsible for producing motion, moving substances within the body, providing stabilization and generating heat. These bundles are referred to as muscles [RHMY06]. The human body contains three different types of muscle tissue:

1. Smooth muscles
2. Cardiac muscles
3. Skeletal muscles

Smooth muscles are non-striated muscles. In contrast to skeletal muscles, smooth muscles are involuntary, meaning that they cannot be influenced by human will. Smooth muscles are responsible for the contractility of hollow organs (e.g. blood vessels, the gastrointestinal tract, the bladder, or the uterus) [BB02, Pla09]. Cardiac muscle tissue, also referred to as heart muscle, is a specialized muscle tissue only found in the heart. Cardiac muscles have high endurance and contractile strength. The third type, which is the most relevant muscle type for this thesis, is skeletal muscle. This type of muscle tissue is responsible for movement and maintenance of posture. In contrast to smooth

muscle tissue, skeletal muscles can be voluntarily and involuntarily controlled by the central nervous systems (CNS).

Figure 2.3 shows the structure of skeletal muscles. Muscle fibers , which are composed of smaller protein filaments called myofibrils, are multinucleated. The connective tissue which covers the muscle fibers is called endomysium. Skeletal muscle tissue is composed of groups muscle fibers arranged in an orderly manner. The distinct bundles of muscle fibers are called fascicles. Each fascicle consists of hundreds of muscle fibers and is covered by connective tissue called perimysium. The connective tissue that surrounds the entire muscle is called epimysium. At the end of the muscles, the connective tissue components form tendons that attach to the body's skeletal structures.

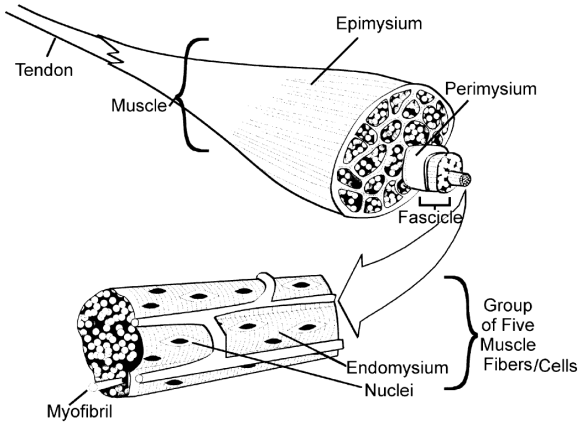

Figure 2.3.: The skeletal muscle structure: Layers of connective tissue and fascicles; muscle fibers are composed of many myofibrils. [Knu07]

A detailed examination of myofibrils shows that they are made up of even smaller fibers, which are well organized and aligned with adjacent myofibrils within a fiber. This gives the skeletal muscle the characteristic appearance of a consistent pattern of dark and light bands. The smallest functional unit of the myofibril is the sarcomere. Sarcomeres are the basic contractile structures of muscle. Active muscle tension is often modeled based on the interaction of two contractile proteins in sarcomeres: actin (a thin-protein element) and myosin (a thicker-protein element). When the muscle fiber is activated, the actin and myosin chains connect via cross-bridges [Knu07]. The excitation and contraction of the muscle is triggered by impulses delivered from the brain and spinal cord to motor nerve endings. Sensory nerve endings send impulses to the brain via the spinal cord. For detailed information on the excitation process, see [EBB05], p. 119 ff.

Muscle structure and activation are complex. For the modeling of the mechanical properties of muscle tissue, Winters and Stark [WS87] distinguish between two modeling approache:. phenomenological models, which are often based on the work of Hill [Hil38]; and and biophysical cross-bridge models based on the findings of Huxley [Hux57]. Bio-

physical models incorporate molecular processes during the cross-bridge building, since this leads to complex mathematical descriptions, they are of only minor importance for practical applications. Hence, phenomenological, Hill-type models are used, which feature less complexity and more accurate force responses, in a wide range of conditions. The Hill-type-based relation between the contraction velocity v and muscle tension P reads

$$(a + P)(v + b) = b(P_0 + a) \tag{2.1}$$

where a and b are constant coefficients, and P_0 is the maximum isometric tension. Therefore, the equation has the unit of energy. As is evident, for the calculation of the resulting muscle tension, this equation only takes the contraction velocity into account. In 1966, [GHJ66] also showed the relationship between muscle tension and fiber length.

The modeling of a muscle and its mechanical properties requires the consideration of two different sources of tensile force. The first source, the active tension, is the force created by contractile proteins, actin and myosin in the sarcomeres of activated motor units. The second force, the passive tension of a muscle, arises from the elongation of the connective tissue of the muscle-tendon unit. The left part of Fig. 2.4 shows the force-length relationship of human skeletal muscles. The characteristic performance of the active component results from the changing number of cross-bridges over the length of a muscle. If the muscle is stretched beyond its resting length L_0, the passive component increases. The total tension of the muscle is the sum of these two components. The right side of Fig. 2.4 shows the force-velocity relationship. As is evident, the force generated by a muscle decreases as the velocity of shortening (right branch) increases, while increasing velocity of lengthening also increases the muscle resistance force (left branch). Using the Hill-model, one can model both the active and the passive tension of a muscle. The model is a three-component model, with two elements in series and one element in parallel. The active tension component is represented by the contractile element (CE), while the passive tension is represented by the parallel elastic component (PEC) and the series elastic component (SEC). Figure 2.5 shows the three components of a muscle model. [Knu07]

Besides the force-length and force-velocity relationships, a third mechanical characteristic of the muscle-tendon unit (MTU) is relevant for muscle modeling. This is the force versus time relationship and refers to the delay in the muscle tension development of the MTU. Thus, there is a delay between the motor action potential (measured using electromyography) and the actual increase in muscle tension. The delay can be split into two components. The first one is related to the rise in muscle stimulation, also known as excitation dynamics, and the second component of the delay is called contraction dynamics (which is the actual build-up of tension). [Knu07]

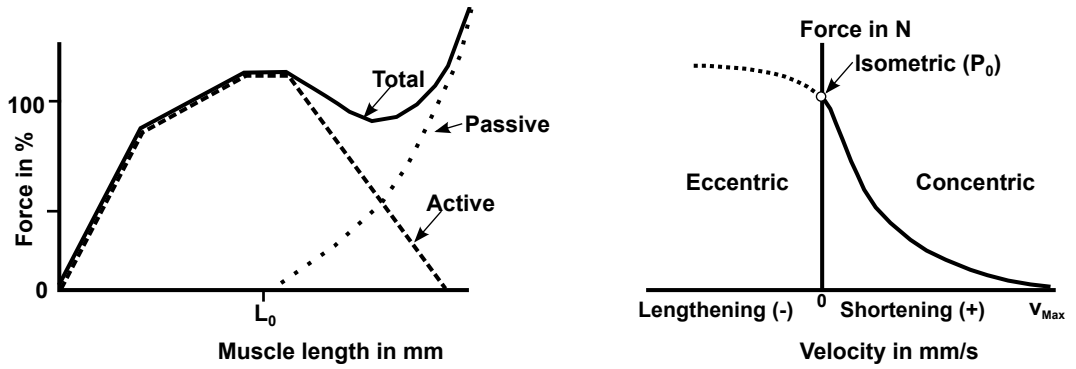

Figure 2.4.: Qualitative description of human skeletal muscle force–length and force-velocity relations. Adapted from [Knu07], pages 84 and 79

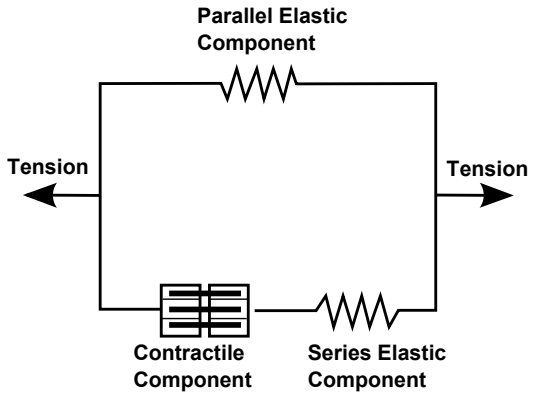

Figure 2.5.: Three-component muscle model

2.2. Testing

2.2.1. Kinematic measurement

The application of motion capture systems enables the collection of data for the illustration and analysis of human body dynamics during different kinds of motion. According to [Men00], there are three different types human motion capture systems:

1. Outside-in systems: External sensors (cameras) collect data from sources placed on the body (reflective markers)
2. Inside-out systems: Sensors placed on the body that collect external sources (e.g. sensors moved in externally generated fields)
3. Inside-in systems: Sources and sensors placed on the body (e.g. electromechanical

suits with potentiometers as sensors and the actual joints as sources

This thesis focusses outside-in systems. In human motion science, optical motion capture, which was developed for medical applications, has become a helpful tool. Optical motion capture systems are an accurate method for capturing certain motions. Extensive post-processing is required in order to make the collected optical suitable for use. The subject is equipped with markers and moves within a certain space. The marker 3D position is calculated using the information from at least two cameras. If there are occlusions that influence the markers' visibility, markers could be lost. This loss of markers requires additional efforts in order to reconstruct marker trajectories. The identification of markers in each sequence frame is referred to as tracking [HFP+01]. For the reconstruction of the marker position, the investigated body segments are considered non-deformable (rigid bodies) and are connected via kinematic joints. If markers are assigned to deformable structures of the human body, new challenges arise. Detailed information on human movement analysis using stereophotogrammetry, including the necessary theoretical background information and the relevant challenges, can be found in Cappozzo et al. ([CDCLC05]), Chiari et al. ([CDCD+05]), Leardini et al. ([LCDCC05]) and Della Croce et al. ([CLCC05]).

2.2.2. Surface electromyography

As mentioned above, muscles are responsible for active human motions. For the analysis of human movement, the contribution of certain muscles is often of interest. Neuromuscular activities during muscle contraction generate electrical currents, which can be measured using EMG (electromyography). The origins of EMG can be found already back in 1966 [RHMY06]. The measured signal depends on the anatomical and physiological properties of the muscle. In former times, invasive methods were used. Small needles were inserted into the muscle and then measured. Depending on the motion, this could be very painful for the volunteers. Nowadays, so called surface EMG is used. This is a non-invasive test wereby the EMG detector is placed on the skin above the muscle.

One of the difficulties in measuring EMG is the complexity of the signal. In traveling through different tissues, an EMG signal acquires noise. Furthermore the detector may collect signals from different motor units. Hence, when measuring EMG signals, one should consider the signal-to-noise ratio which is the ratio of the energy in EMG signal to energy in the noise signal, as well as the signal distortion (the relative contribution of any frequency in the EMG signal should not be altered)[RHMY06]. EMG signals can be either positive or negative voltage. In the present thesis, EMG was only measured in the initial testing stages. Further information on EMG measurements and the challenges involved can be found in [DL93, DL03, RHMY06]

2.3. Simulation

2.3.1. General information

In recent decades, simulation has become an important tool in engineering. According to Nigg [Nig91], "Simulation is the process of performing experiments on a numerical model." The process consists of two components: creating a numerical model and performing experiments with this model. According to Westermann [Wes10], model creation can be further divided in three components:

- Physical modeling: Defining a problem using equations
- Mathematical modeling: Equation interpretation
- Numerical models: Discrete formulation

Once the model has been created, the numerical simulations can be performed. Numerical simulation can be split in three steps:

- Pre-processing
- Solution
- Post-processing

Pre-processing comprises the activities of geometry determination, assignment of material properties, particularly for FEM, selecting a mesh type and meshing. The solution is the process of choosing the boundary conditions and solving the model equations. The final step, post-processing, is the visualization and interpretation of the results. [Wes10]

2.3.2. Finite element or multi-body systems

In vehicle safety, two solution approaches are common.

1. Multi-body systems (MBS)
2. Finite Element Method (FEM)

According to [dJB94], a multi-body system is an assembly of interconnected rigid bodies. The linking between the rigid bodies, which is called kinematic pair or joint, allows for a relative movement of the rigid bodies. Depending on the application and the modeling complexity of the real system, different types of joints are used (e.g. revolute, prismatic, cylindrical, spherical, universal). Every rigid body needs to have a defined mass, a center of gravity and a mass moment of inertia. If the rigid body is in contact with the environment the shape of the body is also relevant. [Tas10] Non-connected rigid bodies are often interrelated via force transmission elements (springs, dampers). The use of multi-body systems leads to a system of ordinary differential equations that must be solved. To solve this system of ordinary differential equations, a numerical integration

procedure is used (e.g. Euler or Runge-Kutta integration). One of the strengths of MB models compared to FE models is the shorter computational time due to lower model complexity, which makes it possible to conduct parameter studies. Further information on multi-body system can be found in [dJB94].

The second method is the Finite Element Method. In contrast to the MBS approach, the structure investigated is deformable. The detailed and complex structure is divided into a finite number of elements, which are connected by nodes. Material properties are assigned to these elements. The resulting system of partial differential equations is solved using approximate solutions within these elements. The use of FE models provides insight into the deformation of structures, but due to the model complexity, it requires, more computational power than MBS. Further information on FEM can be found in [Zie71, BW76].

2.3.3. Review of human body models

As stated in chapter 1.3, HBMs are used in vehicle safety simulation and make it possible to consider injuries and injury mechanism in the collision phase. Human body models are numeric representations of human beings. Human modeling requires information about the anatomy, anthropology and material properties of human tissue, which has to be integrated into the model. One of the greatest challenges in human modeling is the variation from individual to individual. Geometry, mass distributions and material properties depend on the gender, age and personal constitution of the individual. Furthermore the geometry is affected by posture [HKC94a]. In vehicle safety applications, models are mainly available in two postures; standing position, to determine pedestrian impact responses; seated position, to determine injury and injury mechanisms of occupants during collisions.

Due to the importance of the 50^{th} percentile[3] dummy model for collision tests, the development of human body models has also concentrated mainly on this type. Human body models are available as MB models, FE models or hybrid models that combine the two approaches. The brief historical review of human body models in this thesis focusses on multi-body and FE models of the whole human body, which the author believes are the most relevant for this thesis. Besides these whole human body models there are also models available for distinct body regions. Further information on the history of models of different body regions presented at STAPP conference can be found in Yang et al. [YHWK06].

The first whole human body MB model using the MB software MADYMO® was presented by Huang et al. in 1994 ([HKC94b]). Happee et al. ([HHK+98]) then presented a model in 1998, which served as a basis for further improvement and studies on multi-body human modeling using MADYMO. As of 2014, multi-body models using MADYMO are well established and often used for simulation in vehicle safety.

[3] According to [SRPS83], height=175cm; weight= 76.7kg

The first FE whole-body model was developed by Huang et al. in 1994 ([HKC94a]). With respect to its application (i.e., the prediction of occupant side impact response), the model had a very simplified geometry of head, neck, shoulder, pelvis and limbs.

In 1998, Lizee et al. ([LRS+98]) presented another whole human body model with a more detailed geometry for most body parts, particularly for the spine.

In 1999, Choi et al. presented ([CEKL99]) the H-model. This model consists of a whole body model, referred to as HARB (Human Articulated Rigid Body) that serves as basis model, to which other body part modules can be added.

The work presented by Robin in 2001, ([Rob01]) emerged from the HUMOS (Human Model for Safety) programme which started in 1997 withe the goal of producing a refined HBM that would gain wide acceptance in the crashworthiness community. Further information on the HUMOS model can be found in Serre et al. ([SBB+06]).

Another model was presented by Iwamoto et al. in 2002 ([IKW+02]). This model is referred to as THUMS® (Total Human Model for Safety). The aim of the work of Iwamoto et al. was to develop a model of the entire human body for the estimation of total behaviors and overall injuries in traffic accident situations. This model is also based on a mid-sized male occupant and consists of a base model and detailed models (head/face, shoulder and individual internal organs). Chapter 3 provides more information on this model, including which THUMS® versions are available and the number of elements.

In 2005, Zhao and Narwani ([ZN05]) presented another model for an adult male. This model is an amalgamation of finite element models for different body regions (e.g., the thorax, abdomen, shoulder and head-neck) which had been developed earlier at Wayne State University. The aim of this research was to develop a robust reliable human body model for restraint system R&D applications.

The last whole human body FE model mentioned in this thesis is the GHBMC (Global Human Body Models Consortium ™) model ([PKC+13]). Figure 2.6 shows the history of whole FE HBM's from 1994 to 2014.

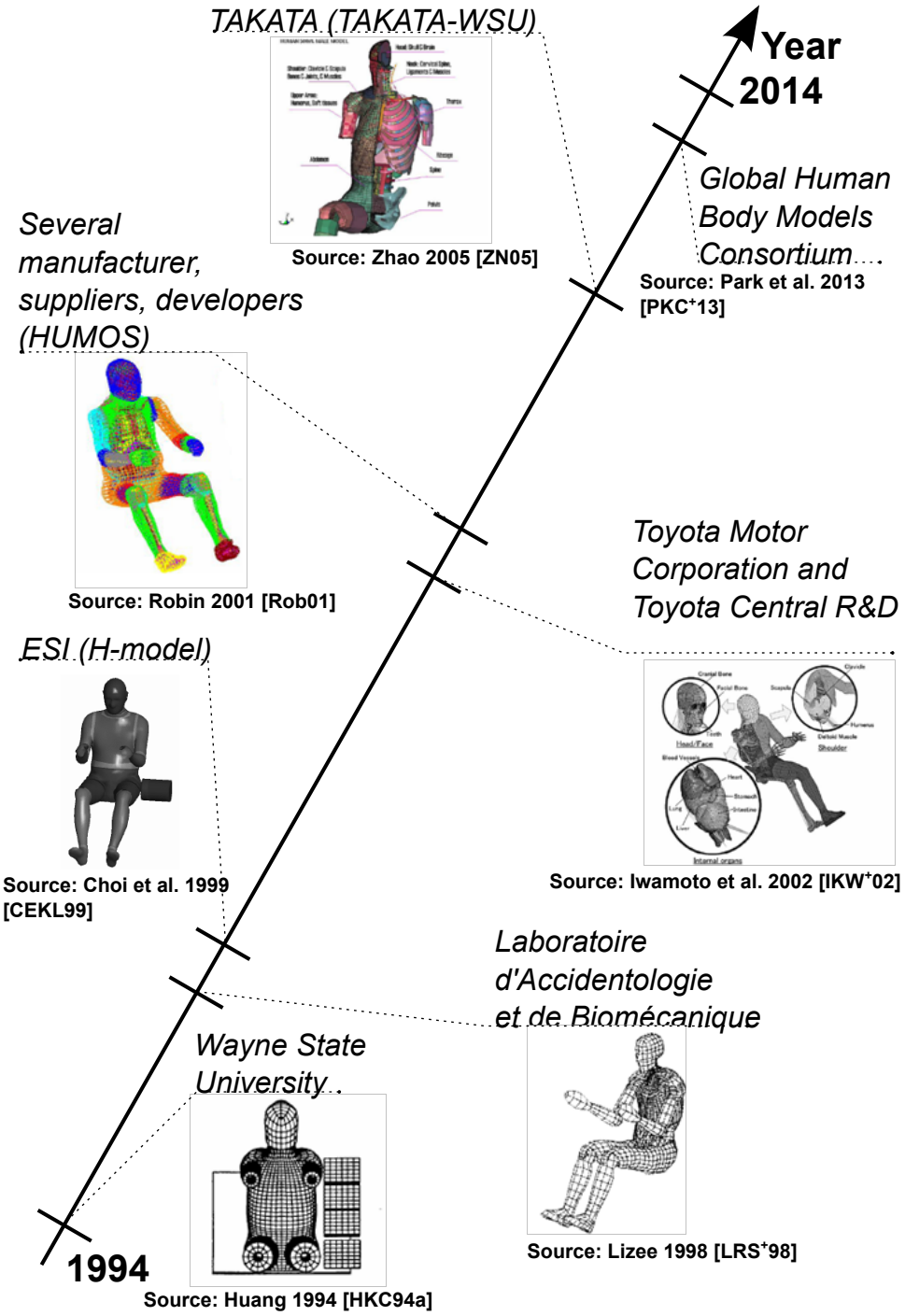

Figure 2.6.: Whole human body FE models from 1994 to 2014

3. Methodology

3.1. General information

As mentioned above, this thesis is a further step towards the goal of using human body models for pre-collision simulations. Based on this general aim, the research questions presented in the introduction of this thesis were derived. For the sake of completeness, these research questions are stated here again.

1. What kind of approach to incorporating reactive human behavior or human movement patterns is necessary to enable the use of both MB and FE HBMs for pre-collision considerations?
2. What load cases have already been investigated, and what load cases are needed?
3. What kind of modeling strategy is needed to enable the simulation of volunteer responses?

Based on the questions above, the complete process for the development of the methodology was divided into four main steps. Figure 3.1 shows the major steps for the development of the methodology. The process started with the definition of pre-collision scenarios based on accident research. After the current state of the art and the relevant load cases had been determined, work continued with the devising of a modeling approach that allows for the implementation of reactive human occupant kinematics in an HBM. One essential component for the successful definition and subsequent validation of the modeling approach was movement studies. Movement studies comprise the process of collecting occupant kinematics data based either on literature or on tests performed to provide a framework for this thesis. The last step was model validation. Simulation model response was compared to occupant kinematics data, and the approach was refined step by step. The following sections present the main ideas and assumptions of the different development steps. Validation will be presented in chapter 4.

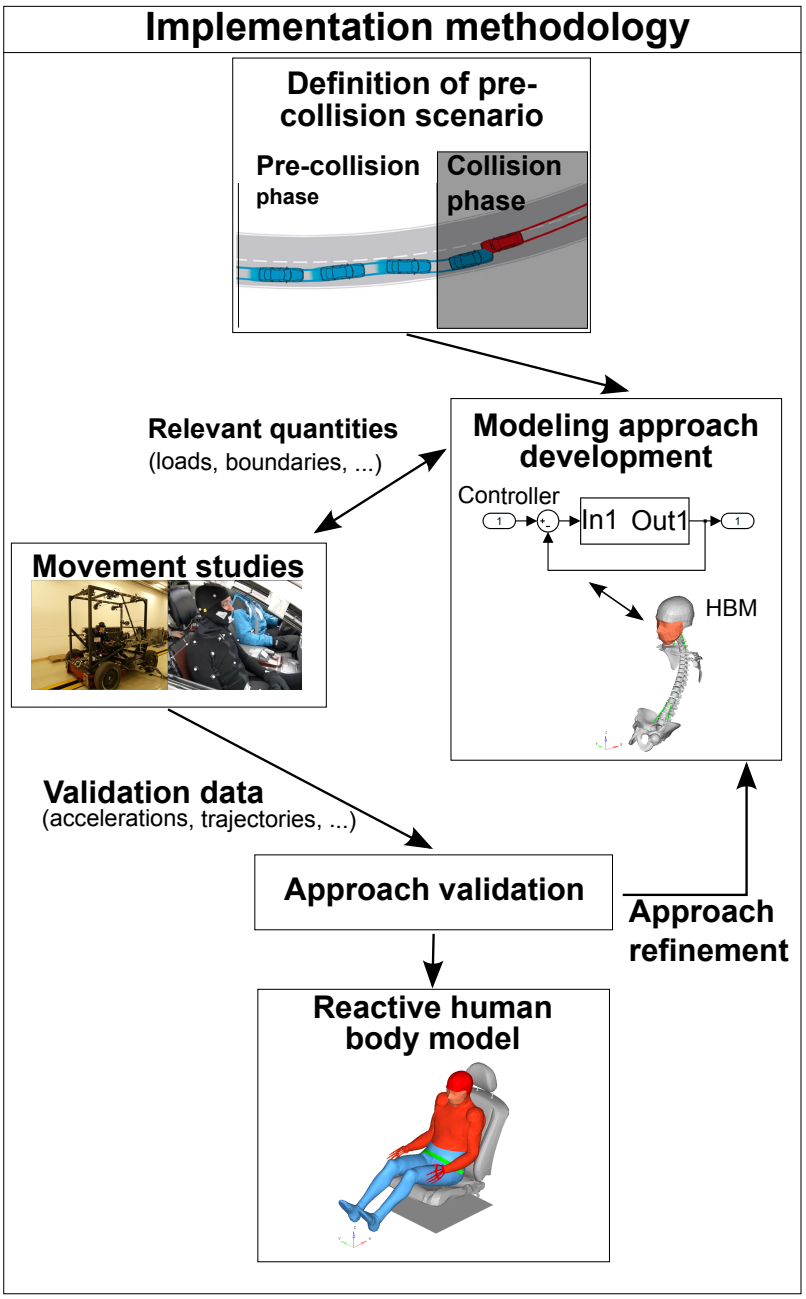

Figure 3.1.: Main steps for the development of a methodology for incorporating reactive occupant pre-collision kinematics. Within the movement studies and the modeling approach development, information on the loads, boundary conditions etc. are exchanged. Furthermore, movement studies results are used to validate the approach

3.2. Definition of pre-collision scenario

For simulations of the collision phase, simulation boundaries (e.g., vehicle speed, accelerations and occupant positions) are strictly defined. For investigations of occupant kinematics in the pre-collision phase, there were no existing standards. Hence, the definition of relevant load cases was a major step for the development of the overall methodology. The pre-collision phase within this thesis starts with a critical driving state and continues until the first contact between the collision opponents. In this phase, primary safety features can be activated, which support and override the driver input to prevent an accident. Within this phase, vehicle occupants are exposed to comparably low accelerations, with a maximum of about 1g[1]. Occupant behavior during this phase consists of an active component (e.g., steering, goal-directed movements) and a passive, or reactive, component, whereby occupants reacting to the accelerations (e.g., bracing, stabilizing). This thesis addresses the reactive component.

The choice of relevant load cases was based on traffic safety statistics of 2008, published by the National Highway Traffic Safety Administration (NHTSA) [Adm08]. Figure 3.2 shows the relative distribution of the initial points of impacts within the total number of crashes. The total number of crashes includes single-vehicle and multiple-vehicle crashes, as well as three different crash severities: fatal, injured and property damage only. As is evident, the most common crash type is front, followed by side and rear. Hence, for testing and the subsequent incorporation, maneuvers which could lead to such impact scenarios were selected. Section 3.3.3 provides detailed information on the load cases investigated.

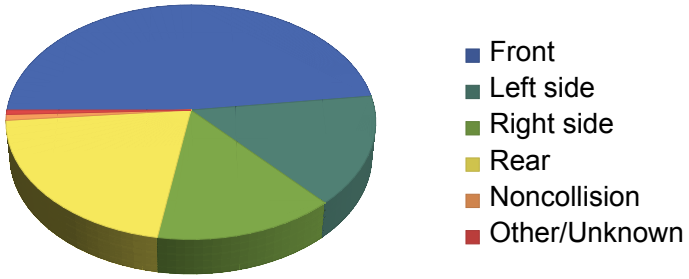

Figure 3.2.: Percentage of initial points of impact in the total number of crashes; data from [Adm08]

[1]This acceleration is approximately the maximum that can be achieved with a conventional series production car with standard production tires.

3.3. Modeling approach development

3.3.1. Main concept

The thesis objective of "developing methodology for incorporating reactive human occupant kinematics in a numerical human body model" consists of two major components: occupant pre-collision kinematics and a numerical human body model. As a complex biological system, human kinematics mainly depend on two aspects: physiological factors and psychological factors. Physiological factors cover a wide range of parameters, such as age, gender, body size, mass distribution, and body constitution. Psychological factors could include driving experience, fatigue and state of awareness. When considering these parameters, it is clear that the parameters must be restricted to ensure a reasonable development of the methodology. Section 3.3.3 describes the psychological and physiological parameters that were taken into account.

As stated in section 2.3.3, HBMs are available as : FE models and MB models. Within this thesis, a modular approach was developed that enables the modeling of the biological system for pre-collision considerations and can be applied for FE models as well as for MB models. Figure 3.4 illustrates the main difference between current common modeling approaches and the approach described here. In the common approaches, the controller that influences model kinematics is directly applied on the model level, which means that the controller is modeled using the input code of the simulation software (e.g., controller within LS-Dyna® environment). Although this is a practical approach, it leads to increased effort if the same controller must be used for the same HBM in a different solver environment or for another HBM because the controller has to be modeled for the second code or the new HBM. Hence, this thesis presents an alternative way of simulating occupant pre-collision kinematics by using co-simulation. Within co-simulation, different subsystems are coupled to a system. Interacting subsystems are simulated over a time step referred to as *macro* time step $\Delta T_{i,<m>}$ where i denotes the system index and $<m>$ the m-th macro time step. Within this time interval subsystems use individual time steps, referred to as micro time steps Δt_i where $\Delta T_{i,<m>} \geq \Delta t_i$. After the time

$$t_{c,i} = t_S + \sum_{m=1}^{M} \Delta T_{i,<m>}, \tag{3.1}$$

where t_S denotes simulation start time, in- and output quantities $\mathbf{u_i}$ and $\mathbf{y_i}$ are exchanged. During the exchange, simulations tools are stopped [BW13, Ben14]. Figure 3.3 shows the main concept for $i = 1, 2$.

This co-simulation approach splits the two systems, i.e. the controller that influences model kinematics and the HBM. As is evident in Fig. 3.4(a), the controller and the HBM are connected via an interface and exchange relevant quantities. The presented approach accepts additional computational effort in order to gain the potential to increase the complexity of the controller and exchange the underlying model.

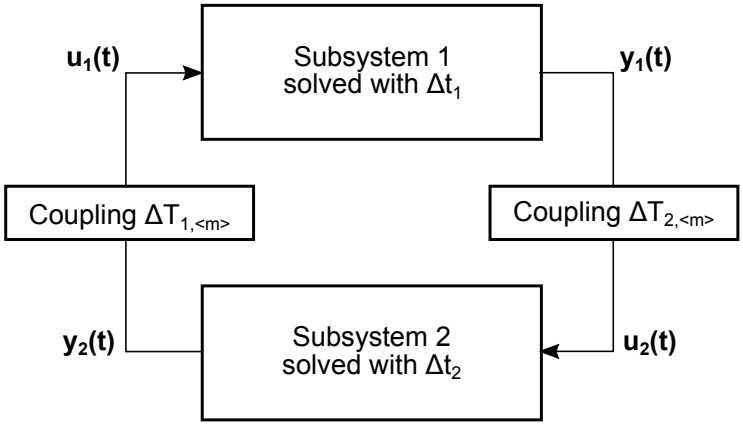

Figure 3.3.: Coupling concept, adapted from [Ben14]

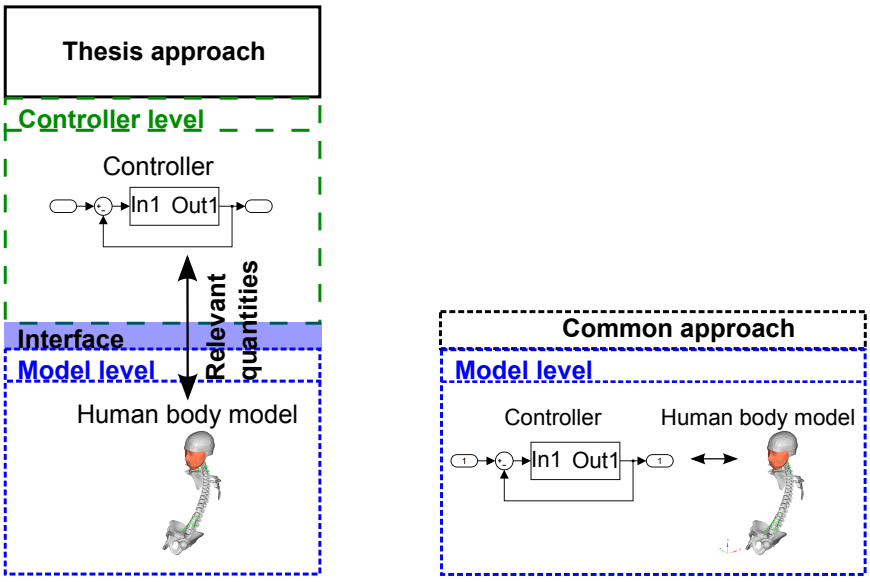

(a) Thesis approach (b) Common approach

Figure 3.4.: Comparison of thesis simulation (a) and common simulation approach (b)

The application of the co-simulation for dynamic mechatronic systems was presented by Cresnik et al. [CRS09]. For simulating the occupants' pre-collision kinematics, a prototype version of the co-simulation tool was used. The co-simulation tool, which is now also also commercially available, is called ICOS®. The main concept of the approach

is that the controller generates a force $\mathbf{F}$, which is computed from translational $\mathbf{x}, \dot{\mathbf{x}}, \ddot{\mathbf{x}}$ and rotational nodal quantities $\boldsymbol{\alpha}, \dot{\boldsymbol{\alpha}}, \ddot{\boldsymbol{\alpha}}$. The controller that generates this force was developed in Matlab/Simulink®, and the model that was controlled was an FE model (in LS-Dyna®). Force is applied on predefined bar elements in axial direction. The *Macro* time step $\Delta T_{i,<m>}$ can be determined by the user. Information could either be exchanged after each FE time step or after several time steps. This influences the calculation speed. The principle is shown in Fig. 3.5.

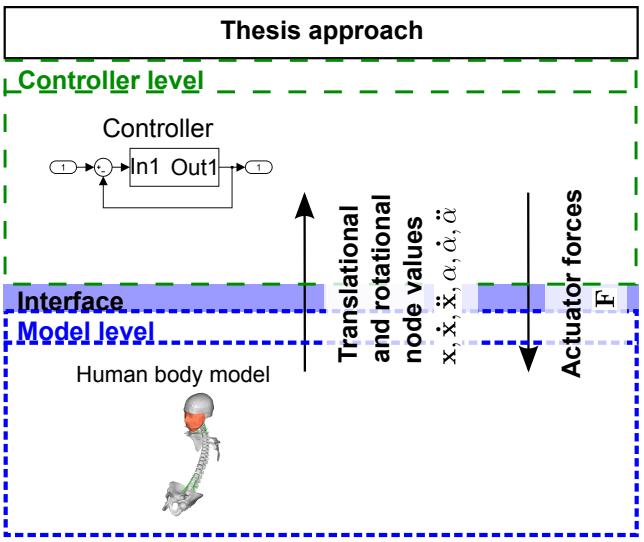

Figure 3.5.: Basic principle of co-simulation approach with the controller as master level exchanging an actuator force $\mathbf{F}$ and nodal quantities $\mathbf{x}, \dot{\mathbf{x}}, \ddot{\mathbf{x}}$, $\boldsymbol{\alpha}, \dot{\boldsymbol{\alpha}}, \ddot{\boldsymbol{\alpha}}$

Within the FE environment, model parts can be assigned pre-defined material types or a user-material can be created. In the co-simulation approach, data is exchanged via a user-material, specifically an LS-Dyna® usermaterial. In addition to exchanging the relevant nodal quantities, this user-material is also responsible for establishing the communication between Matlab/Simulink® and LS-Dyna®. Further information on the necessary input and settings for the coupling can be found in Appendix A.

The coupling approach for HBM application was tested on a simple FE model representing the leg. Foot, shank and thigh were modeled as rigid shell elements connected via joints with a single degree of freedom. Muscles were represented by actuated beam elements. The origin and insertion of the actuator elements were not anatomically correct [PHR+11]. An open-looped control with a constant actuator force was used. Figure 3.6 shows the simple model. Rigid body shell elements are indicated in grey color. The green cylindrical element (i.e.,the first element at the top of the figure) represents the actuator beam element, which can contract and extend. This element was connected to seatbelt elements. Seatbelt elements are specific FE elements that, in combination with a slipring element, allow for a continuous sliding of the belt through a sharp change of

angle, as can be seen in the knee area. Simulations showed that the chosen approach worked adequately, and that the co-simulation approach in combination with a seatbelt and slipring modeling made it possible to take into account sharp changes of angle.

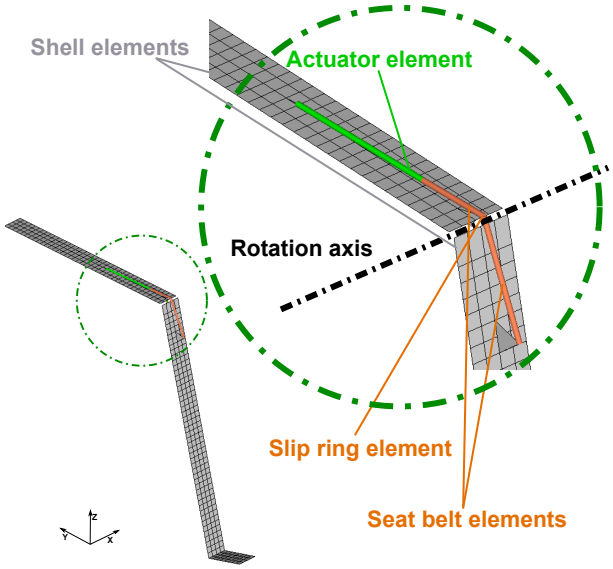

Figure 3.6.: Leg model to check co-simulation and modeling approach

The second model built, was more complex and consisted of parts of the HybridIII[2] 50th-percentile male and BIORID-II[3] crash test dummy models. Once again, joints were modeled as kinematic joints with a single degree of freedom. The body parts (extremities and spine) were modeled as rigid bodies. Similar to the first step, the leg of the model was controlled. All model parts except the legs had their six DoF constrained. The objectives of this step were to check the modeling approach in a more realistic geometry and to determine if this approach could also be used to control the upper parts of the human body. One further goal was to devise a modeling approach, that made it possible to apply the controller for different FE models with a reasonable effort. One solution for modeling the actuator elements in such a way that the controller could also be used for different models was to implement separate beam nodes to define the actuator elements. The nodes defining these elements are connected to the rigid bodies.

The third co-simulation approach test was performed on the upper body parts of the BIORIDII/HybridIII model. To control upper body kinematics, a closed-loop control was used. The control variable was the actuator length. The aim was to reach its initial length. A simple proportional-differential (PD) controller was used. Figure 3.7 shows

[2]The HybridIII originally developed by General Motors (GM), is the most widely used dummy for crash tests in the world[Hum14b].

[3]The BioRID-II is a dummy that was originally developed by Chalmers University to assess seat restraints in a rear impact scenario [Hum14a].

an overlay of the controlled model (blue) and the initial model position shown (grey). The model has been exposed to a 4g acceleration square pulse in the frontal direction with a duration of 50 ms starting at the beginning of the simulation. The amplitude of acceleration pulse was chosen to check joint stability. As is evident, the controlled model moved forward (in the negative x-axis direction). After about 1000 ms, the model reached its initial position. This simulation showed that the co-simulation approach works well enough for closed-loop control. Furthermore, the simulation showed that joint and model stability were not an issue.

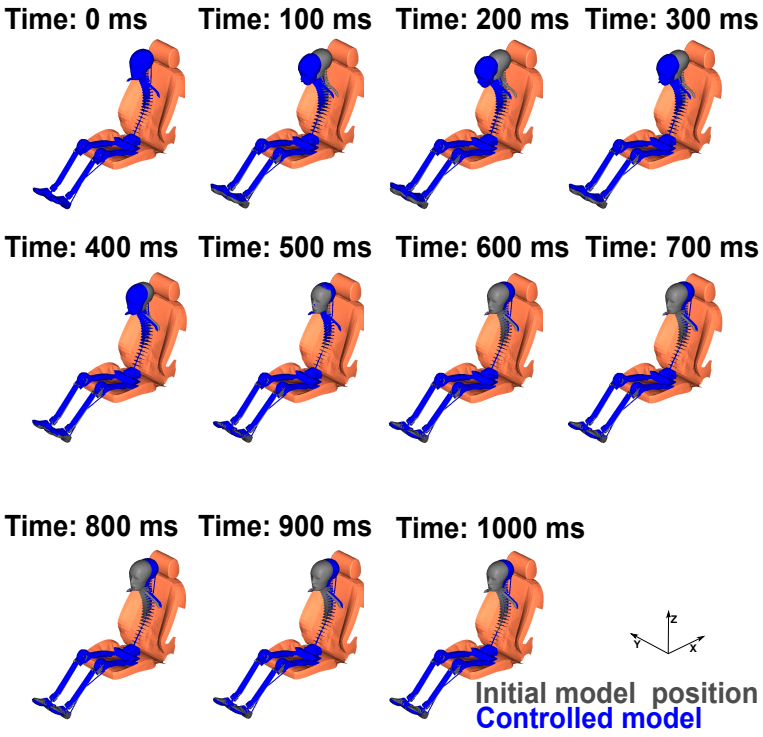

Figure 3.7.: Controlled (blue) model consisting of BIORID-II and HybridIII parts overlaid with initial model position

3.3.2. Movement studies

3.3.2.1. Definition of load cases

A literature review showed that the majority of research dealing with the influence of muscle activation on occupant kinematics in low-acceleration scenarios can be divided into two fields: sled tests and vehicle tests. The kinematic responses of males and females during low-speed impacts were investigated by Ejima et al. in several studies [EOH+07, EZS+08, EIS+12]. Volunteers were exposed to accelerations of about 1g [EOH+07] or

0.8g [EZS+08] in the frontal direction, and 0.4g and 0.6g [EIS+12] in the lateral direction. Studies were carried out in relaxed and braced muscle states. Additional frontal sled tests with 2.5g and 5g were carried out by Beeman et al. [BKMD11, BKM+12], and Kemper et al. [KBD11] conducted 5g frontal tests, as well as 2.5g and 5g frontal tests [KBMD14]. All of these studies concluded that volunteer pre-collision kinematics are strongly dependent on individual muscle contribution.

In 2005, Muggenthaler et al. [MAS05] carried out sinusoidal vehicle tests and compared volunteer kinematics to dummy kinematics. Muscle activity was determined using electromyography (EMG). The authors concluded that dummy response cannot be used for the determination of human occupant pre-collision response. Furthermore, EMG data revealed muscle activation in this phase. Also in 2005, Morris and Cross [MC05] published the results of their qualitative study dealing with passenger pre-collision kinematics. They investigated a total of 49 volunteers subjected to frontal and lateral accelerations and classified occupant responses based on recordings of five cameras mounted in the test vehicle. They stated that occupant trajectory during pre-collision braking is mainly influenced by two pre-event factors: seat belt use and foot location. Holding on to the vehicle structure with the arm or with the hand (bracing) is more likely during long duration events, and is less often seen with belted passengers. For the lateral maneuvers, they found that the head and neck tend to stay upright, in order to maintain the field of vision and the occupant trajectory. In violent lateral accelerations, it is almost entirely due to inertia in the initial phase.

In 2011, Carlsson and Davidsson [CD11] investigated occupant kinematic responses during autonomous braking maneuvers while driving on public roads. Eight female and nine male volunteers were selected. The kinematics of both drivers and passengers exposed to three different acceleration levels (i.e., 0.3g, 0.4g and 0.5g) over 1.5 s were determined using planar film analysis. The results showed that the overall motion during braking was very small, and it was hypothesized that the size and gender of the volunteers, the position in the driver or passenger seat, the vehicle deceleration and the seat belt properties influence the forward movement.

Van Rooij et al. [RPdCJ13] carried out experiments with a professional driver on a test track. Head forward displacement was evaluated for driver voluntary braking, autonomous braking, and autonomous braking with distraction. The driver's forward head displacement showed significant differences between driver braking and autonomous braking scenarios. This may be caused by the driver's anticipation in the voluntary braking case.

Östh et al. [OODB13] and Òlafsdòttir et al. [OsDB13] published their results investigating passenger kinematics and muscle responses in autonomous braking events with standard and reversible pre-tensioned restraints. They investigated 20 subjects (11 male and 9 female) with a production car with two different braking test cases of about 1.1g. Kinematic data was collected with a video- tracking system, and muscle activity was measured with EMG. They observed a significant reduction of head-forward movement in pre-tensioned belt conditions.

Figure 3.8 summarizes the relevant literature for the determination of occupant pre-collision kinematics for sled and vehicle tests. Based on the published literature, it was decided to perform tests in parallel to the development of the implementation methodology. As shown above, kinematic investigations concentrated either on the driver or the passenger kinematics.

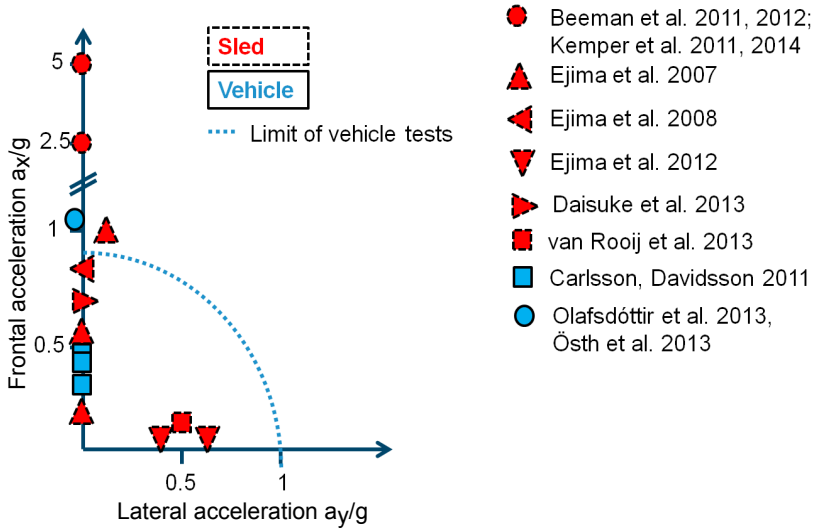

Figure 3.8.: Overview of literature on vehicle and sled tests with low g acceleration levels, adapted from [Hub13]

Although [Age10] found that the average number of passengers per car for the Western European countries sampled (UK, Denmark, the Netherlands, Norway, Germany, Austria, Spain and Italy) was 1.54 passengers per vehicle in 2007, driver kinematics were not investigated for three reasons. First, to focus on the driver kinematics, the drivers would need to have the maneuver information, or the steering wheel and the braking intervention would have to be automated. Second, the drivers can brace on the steering wheel, if they are aware of the upcoming accident. Results published by Beeman et al. in 2011 and Kemper et al. in 2014 [KBMD14], who investigated human occupants in low-speed frontal sled tests (2.5g, Δv = 5 km/h and 5g, Δv = 10 km/h), showed that there was a significant reduction in forward excursion due to bracing. The third reason for not investigating the driver kinematics is the increase in the complexity of the test set-up. To evaluate the kinematics response of a driver, quantities like steering wheel forces, belt tension and seat forces must be measured additionally. The complexity of the simulation boundary conditions and the model complexity itself would increase significantly. Especially in the initial model development stages, this was not reasonable. In addition, due to the novelty of combining the Vicon motion capture system with measurement of the muscle activity using EMG and their dynamic application, it was decided to investigate passenger kinematics. This thesis distinguishes between three different movement stud-

ies to determine occupant movements: sled tests, vehicle test series A and vehicle test series B. The distinction was made based on the general underlying boundary conditions. Based on the three test series, three different models were created. Figure 3.9 shows the three different model types, based on the three test series: a 2D sled test model, a 2D vehicle model and a 2.5D vehicle test model. Model development was based on the relevant test maneuvers. Individual model kinematics are influenced by a controller. For the sled test and vehicle test model of test series A, the same planar controller was used. The model for vehicle test series B is referred to as a 2.5D model because the kinematics are influenced by combining two planar controllers. Further information on the different models is presented in sections 3.3.3 and 3.3.4.

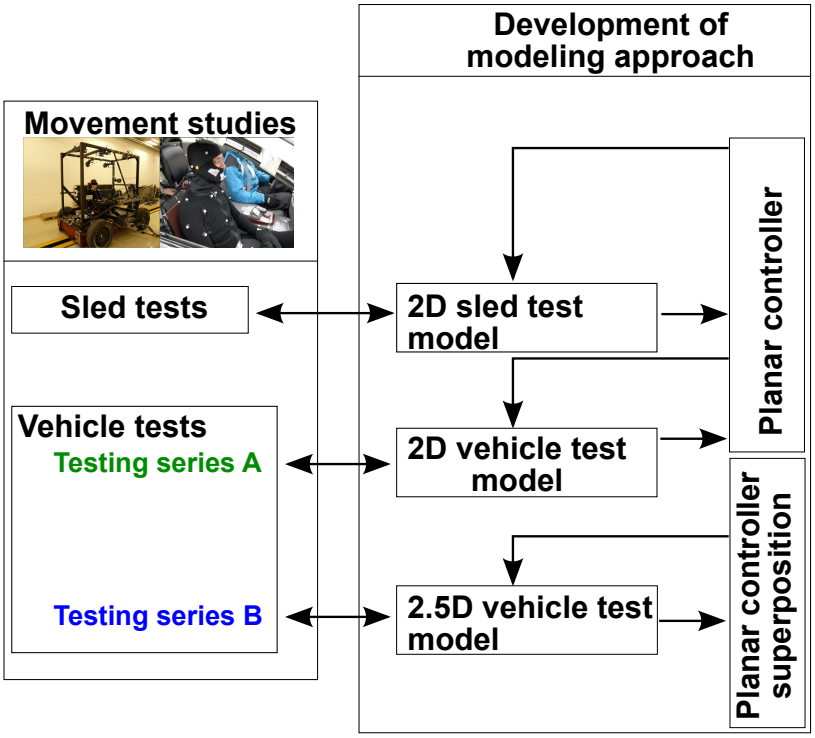

Figure 3.9.: Overview of movement studies and the models developed based on these studies.

Within the different test series, a further distinction was made with respect to the vehicle maneuvers. Figure 3.10 provides an overview of the maneuvers. The green solid line shows the maneuvers performed during test series A, while the blue dotted line shows the maneuvers form test series B. The velocity next to the arrows shows the initial vehicle velocity.

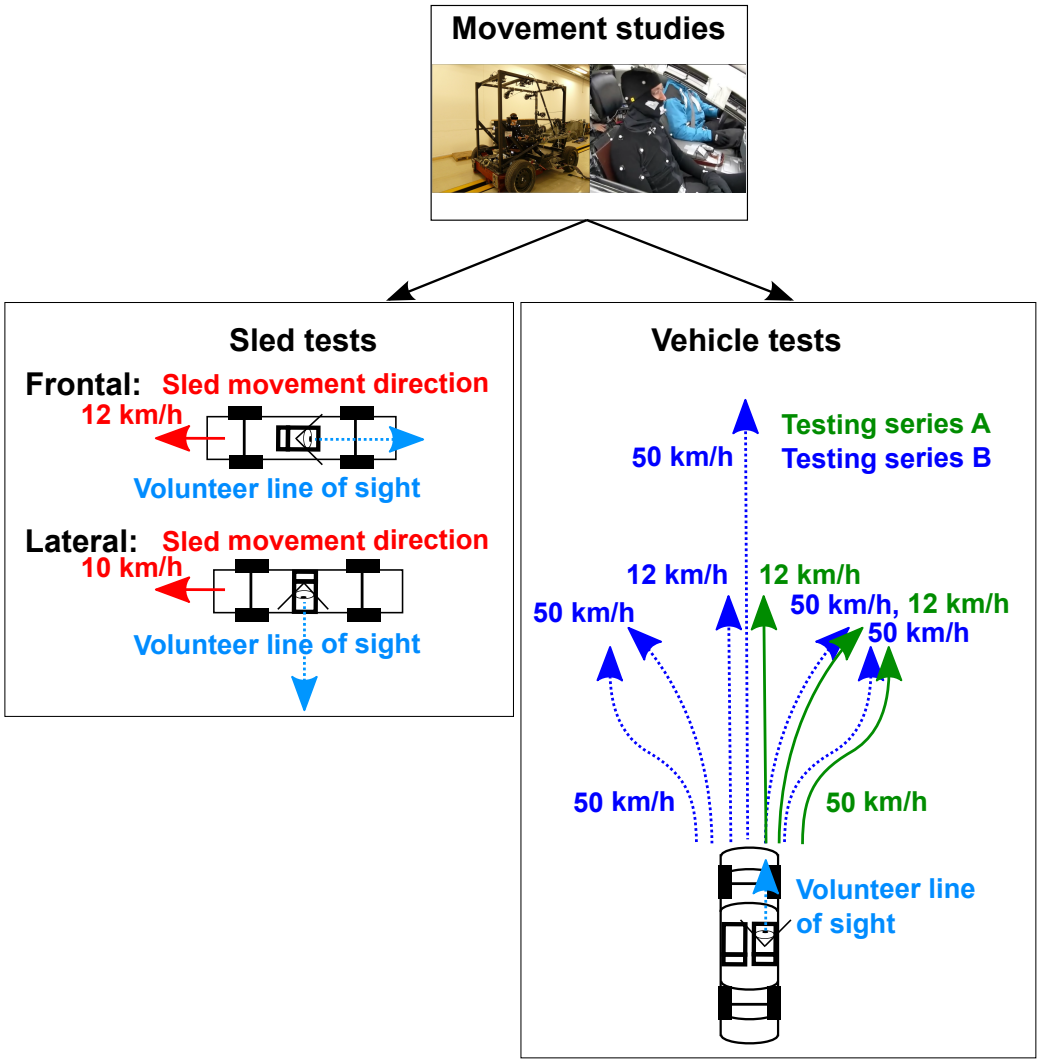

Figure 3.10.: Overview of movement studies performed to collect data for the methodology development

3.3.2.2. Sled testing

As shown in Fig. 3.9, the first model development step using an HBM was sled test movement studies. Sled test movement studies were carried out in parallel to the model development, which allowed for an exact definition of the boundaries used for this study. Sled tests were carried out at the crash test bench of the Vehicle Safety Institute (VSI), Graz University of Technology. The main aims of these tests were to collect initial data sets for simulation, to gain knowledge in the field of EMG, to determine the relevant

muscle groups for vehicle tests, and to evaluate two different camera systems that could be used for vehicle tests. Further information on these tests can be found in Kirschbichler et al. [KSP+11]. Figure 3.11(a) shows a volunteer seated on the reference seat on the sled with frame constructed for the camera mounting.

(a) Sled (b) Sled test reference seat

Figure 3.11.: Sled with camera frame, reference cameras and volunteer(a); and sled test reference seat(b), from [KSP+11]

One major issue for the test series was the elimination of vehicle-related influences on volunteer kinematics, which are difficult to implement in a simulation. For a vehicle occupant, the following three main influences were identified: seat, restraint system and voluntary bracing using vehicle structure or the hands on the thighs. A conventional series production seat is cushioned, and depending on the vehicle type and the OEM, this seat supports the occupant upper body during lateral maneuvers to a greater or lesser extent. For investigations of a pure frontal passenger kinematics such a seat may affect the occupant kinematics. Hence, a modified seat, also referred to as reference seat, was used. Figure 3.11 (b) shows the reference seat used. Detailed information on the modified seat can be found in section 3.3.3.4. The next test environmental component with a major influence on occupant kinematics was the seat belt. Also further information on the belt can also be found in section 3.3.3.4. The third and final major influence was voluntary bracing using the vehicle interior structure or the hands on the thighs. Before the tests, volunteers were instructed not to use parts of the structure or brace themselves. Furthermore, volunteers were given a piece of cardboard which to hold with both hands. The mass of this cardboard was in the range of a few grams, so it did not significantly affect volunteer kinematics.

Sled tests were carried out using two setups. In the first setup, the volunteer was seated in the direction opposite to the acceleration direction, and in the second setup, the seat was rotated by 90 degrees clockwise to simulate a lateral loading (see Fig. 3.10). The inverse setup for the frontal maneuver was necessary due to sled control. Basically, the original plan was to use a normal braking maneuver to decelerate the sled. The necessary braking force would have been generated by disc brakes actuated by braking cylinders mounted on the sled. Using such a system for the investigation in the test

facility environment with a floor coated with a slippy layer would have led to problems in the repeatability of the results. Hence, such a set-up was not reasonable. Alternatives would have been to externally brake the sled using a rope or a bolt bending a metal. The test bench is normally used for crash tests. Vehicles are accelerated using a rope system, which is mounted to the vehicles. Due to the strict regulations of crash tests, this system is able to accelerate the vehicles to a certain velocity with high accuracy. Hence, this rope system was used, in combination with a volunteer seated backwards.

Volunteers were fixed to the seat using a lap belt. In total, 11 volunteers with anthropometry matching the 50^{th} percentile-male were chosen. For seven volunteers, kinematics was captured using a standard optical Weinberger high-speed video system. For four volunteers, movement was captured using a Vicon V612 motion-capturing system featuring eight near-infrared cameras. Each volunteer was tested three times in frontal direction with an acceleration of 0.8g and a velocity of 12 km/h and three times laterally with an acceleration of 0.4g and 10 km/h. The muscular activity of eight different muscles on both sides of the body was measured using surface EMG. Before the tests maximum voluntary contraction tests (MVC) were conducted to obtain the quantitative measure of muscle strength.

The evaluation of the two different motion capture systems showed the beetif of the Vicon system over the standard optical Weinberger high-speed video system. The accuracy of both systems was in the same range, but the infrared systems have significant advantages regarding because no additional lighting is needed. [KSP+11]. This made it possible to use this system for vehicle tests without needing additional power for lighting. However, one drawback of the Vicon system was that this motion capture system was developed for static investigations. Cameras are normally mounted to a fixed static frame with given inter-camera distances and capture the motion of objects moving within a certain space. Even though the cameras were fixed to the frame using threaded bolts, the assumption about fixed inter-camera distances and static positions was no longer valid. This led to problems during recording and reconstructing the 3D motion of an object. For this reason, Huber et al. [HCM11] developed a correction algorithm to address this issue, which makes it possible to apply this motion capture system for vehicles.

3.3.2.3. Vehicle tests

Sled tests were mainly used to collect initial data sets for the development of the methodology and to gain experience with EMG measurements. The sled tests started from a standstill. Due to the absence of movement, the volunteers' kinematics may be different than they would be in a moving system. Furthermore, sled tests were performed under laboratory test conditions, and a total of 11 volunteers were tested. Vehicle tests were therefore performed to create a more realistic test scenario. In addition to the vehicle movement that was sensed by the volunteers, there was also different visual input (test track environment and vehicle interior), which could also affect volunteer responses. The total number of investigated volunteers was increased, and vehicle testing consisted of

two series. Both test series were performed using a Mercedes-Benz S-500 (type: type: W221, length: 5.23 m, wheelbase: 3.17 m and width: 1.78 m).

Vehicle test series A

In the first test series (series A), two maneuvers were investigated: an emergency braking maneuver at 12 km/h and a single lane change maneuver to the right at 50 km/h. As mentioned in section 3.3.2.2, for the development of the methodology, the seat influence was reduced by removing the seat cushion and using leather-covered wooden plates. For test series A, this reference seat was used again. Figure 3.12 shows the reference seat. The seating surface, with a width of 440 mm and a length of 490 mm has been inclined by 10 degrees. The rear edge of the seating surface was 180 mm above the footwell. The back rest of the seat with a width of 550 mm and a length of 512 mm and the seating surface enclosed an angle of 104 degrees. The headrest was not changed. In contrast to the sled tests, where a separate lap belt was used, the series seatbelt was used for both vehicle test series. In order to obtain a lap-belt-only configuration, the upper part of the belt was routed behind the seat. The length of the lap belt was fixed using a clamp close to the belt buckle. For every volunteer, the clamp was adjusted to ensure the tightness of the belt, thereby reducing the relative movement between the volunteers and the seat and providing reproducible boundary conditions for simulation.

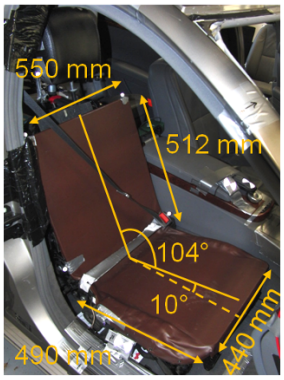

Figure 3.12.: Reference seat for vehicle test series A, from [KHP+14]

As described in Kirschbichler et al. [KHP+14], in test series A, 22 male subjects who were chosen close to 50th-percentile male were tested. Within the different maneuvers, also different awareness states were also investigated: *unaware*, where no information was given to the subject, *anticipated*, where the subject could anticipate the maneuver due to the velocities and *informed*, where the maneuver was announced by a countdown. The different awareness states were investigated in order to identify the influence of training and habituation effects. Maneuvers were performed on a closed test track in a fixed order. The location of the maneuver was chosen arbitrarily to avoid a pre-bracing of volunteers. All subjects held a valid driving license and gave their written consent for the test procedure. Before testing, the test procedure was reviewed and approved by

the local ethics committee. Table 3.1 shows the number of volunteers, their gender, the average values, and the standard deviations of mass, height and age of the volunteers participating in test series A.

Table 3.1.: Information for human volunteer subjects in test series A, averages and standard deviations

Number of volunteers	**Gender**	**Mass in kg**	**Height in cm**	**Age in years**
22	Male	77.4 ± 6.7	179.4 ± 4.3	32.2 ± 8.6

The occupant kinematics were captured using a Vicon V612 motion- capturing system. Due to the large dimensions of the test vehicle it was possible to mount eight near-infrared cameras. Occupant kinematics were recorded with a sample frequency of 100 Hz. Volunteers were equipped with retro-reflective markers on specific locations on the body. The vehicle state was determined using a Dewetron Dewe5000 recording the vehicle speed at 10 Hz, frontal and lateral accelerations at 50 Hz, and steering wheel angle and angular velocity at 100 Hz. Other channels were also sampled at 50 Hz. The low sampling frequency can be explained by the fact that the channels were recorded using the vehicle CAN bus instead of a separat measurement system.

(a) Test vehicle with Vicon V612 motion-capturing system (b) Volunteer front view (c) Volunteer side view

Figure 3.13.: Test series A; vehicle (a) and occupant (b and c), from [HCD+13]

The volunteers' muscle activity was measured bilaterally using surface EMG. Three neck muscles (m. sternocleidomastoideus, m. trapezius p. cervicalis and p. descendens) and four trunk muscles- m. rectus abdominis, m. obliquus externus abdominis, m. latissimus dorsi and erector spinae (lumbar region) were investigated. Further information on the results of the EMG measurement can be found in Huber et. al [HCD+13]. The combination of three different systems to measure the vehicle state, occupant kinematics data and EMG required the synchronization of these systems for the data acquisition

systems to detect the beginning of the maneuver. Systems were synchronized by an event trigger. A manual trigger located on the backseat was switched before to the maneuver. The trigger event induced a change in the voltage of the trigger signal, which was received by the vehicle kinematics and the EMG acquisition system. In order to synchronize the infra-red motion capture system with the other systems, an infrared-led emitting diode signal of a diode located behind the volunteer's head in one of the camera signal was used.

Figure 3.13(a) shows the test vehicle equipped with the Vicon V612 motion-capturing system. The vehicle's windshield was removed to prevent reflections of the infrared strobes, which were located on the cameras. Furthermore, the serial passenger door was changed to a passenger door with a cut-out so it would be possible to capture occupant movement in the passenger compartment without occlusions. Figures 3.13(b) and 3.13(c) show an occupant wearing a motion capturing suit with reflective markers.

Vehicle test series B

Within this series, the maneuvers performed in series A were repeated and extended. In addition to the emergency braking maneuver at 12 km/h, a braking maneuver at 50 km/h was performed, and in addition to the single lane change to the right at 50 km/h, a single lane change maneuver to the left at 50 km/h was also performed. Furthermore, combined maneuvers (a combination of braking and steering to the left and braking and steering to the right) at a velocity of 50 km/h were performed. Test results were presented by Kirschbichler et al. [KHP$^+$14] and Huber et al. [HCD$^+$13, HKAS14]. In contrast to series A, the seat was equipped with a lateral support structure with a geometry similar to the series production seat. The lateral support and the backrest enclosed an angle of 120 degrees. The distance between the left and the right support was 314 mm. Furthermore the wooden plates of the seat surface and the back rest from test series A were coated with a layer of foam of 40 mm thickness. Figure 3.14 shows the reference seat of test series B mounted in the car. The black cover of the seat is a layer of light-absorbing material, which reduced reflections in the infrared spectrum. In test series B the standard three-point belt was used, but the pretensioner which would activate during critical driving situations, was disabled.

Figure 3.14.: Reference seat of vehicle test series B, from [KHP+14]

In this study, 27 male subjects and six female subjects were tested. Table 3.2 shows the number of volunteers, as well as their gender, mass, height and age. Instead of three different awareness states, this study concentrated on the *unaware* condition for reasonons which will be explained in chapter 5 below. Before testing, the maneuvers were reviewed and approved by the local ethics committee. This test series was also performed on a closed test track, and volunteers gave their written consent to the test procedure. Occupant kinematics were once again captured using a Vicon V612 motion-capturing system with eight near-infrared cameras, recording with a sample frequency of 100 Hz. The vehicle state was determined using a Dewetron Dewe5000. The volunteers' muscle activity was measured bilaterally using surface EMG. The following muscles and locations were measured: M. vastus medialis, M. obliqus externus abdominis, M. rectus abdominis, M. latissimus dorsi, M. trapezius, M. sternocleidomastoideus, M. erector spinae and midcervical (C-4) paraspinal placement. In contrast to test series A, muscle activity was determined for a small subset of 5 volunteers.

3.3.3. Model development

Figure 2.6 showed that there are several FE HBM on the market or being developed within other research projects. In addition to these FE HBMs, MB models are also available. The approach developed in this thsis for the incorporation of reactive human body models is generally applicable for different FE HBMs, as well as for multi-body

Table 3.2.: Human volunteer information test series B, averages and standard deviations

Number of volunteers	Gender	Mass in kg	Height in cm	Age in years
27	Male	77.8 ± 8.4	179.1 ± 4.7	25.4 ± 9.6
6	Female	63.0 ± 10.4	169.0 ± 4.1	31.5 ± 9.3

systems.

For the development of the methodology, a modified THUMS® model was used. The model has been developed by Toyota Central R&D Labs since about 2000 in cooperation with other research institutes (e.g., Wayne State University). As with other HBMs, it is a numerical representation of the human body with assigned material properties of bones, skin, tendons, ligaments and other tissues. HBMs were originally developed and validated for simulation of the collision phase. In particular, these models were designed to provide a reasonable kinematic response in this phase, similar to dummy models; however these models were also intended to envable the consideration of injuries and injury mechanisms directly. The model is based on a 50^{th}-percentile American male with a height of 175 cm and a mass of 77 kg. Currently, there are three generations of THUMS® available. In 2004, the first commercially available generation was introduced, referred to as version 1.4/1.6. Since the beginning of 2008, the second generation, version 3.0, has been available. The last and current generation, version 4.0, was introduced in 2010. Table 3.3 shows an overview of the different THUMS® versions presented by Toyota [Dyn11, Fre12, Dyn14].

Table 3.3.: Overview of different THUMS versions [Dyn11, Fre12, Dyn14]

Generation	**Version**	**Year**	**Number of elements**	**Short description**
1	1.4/1.6	2004-2006	91000	Kinematic model with simple inner organs and simple head model
2	3.0	2008	143044	Refined head model, small improvement of geometry and material properties
3	4.0	2010	1755284	Significantly refined model, internal organs, 3D ligaments

In addition to the versions shown in table 3.3, Daimler AG developed their own versions based on a modified version of the first and second generation THUMS® called THUMS®-D . Models have been continuously improved in terms of mesh quality, material properties (additional validation) and extensive work on model stability (contacts, mesh, connections). This THUMS® version was used as an FE HBM model starting point for the development of a reactive HBM. The reason for using an FE model instead of an existing MB model (e.g., Madymo model) to develop the methodology was the vision to use one model for both the pre-collision and the collision phase in the future.

After deciding on a co-simulation approach and choosing the THUMSD® as an FE model, the development of the implementation methodology began. The main questions

that had to be answered were:

1. What kind of psychological details must be considered?
2. What physiological details should be included?
3. Which simulation and test boundaries should be chosen?

Ad 1.) The focus of this thesis was on kinematics. Except for the different awareness states that were considered during vehicle test series A, psychological factors were beyond the scope of this thesis. In order to address issues 2 and 3, a model creation process was developed. This is shown in Fig. 3.15. The physiological details were split into three categories: part modeling, joint modeling and muscle modeling. The test and simulation boundaries were defined in one step, referred to as "Definition of boundary conditions".

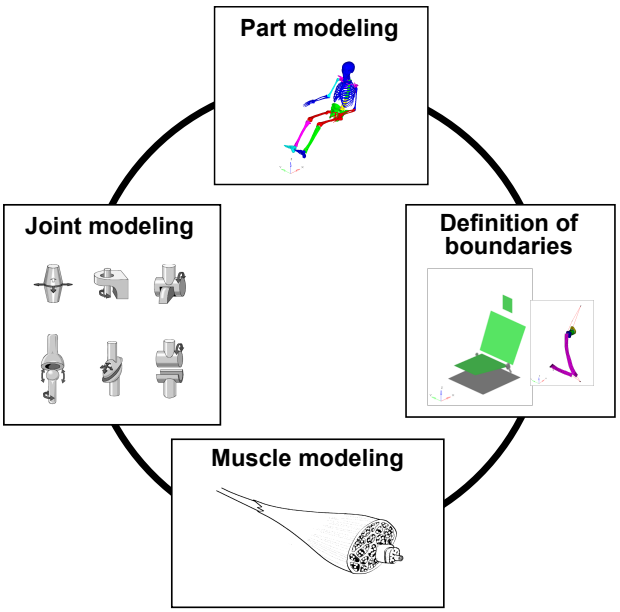

Figure 3.15.: Model-creation process

3.3.3.1. Part modeling

Part modeling addresses the issue of what physiological details with respect to the HBM components had to be included, and what type of part formulation was chosen.

The original THUMS® model had a driver position with the hands approximately in the steering wheel position. In movement studies (sled and vehicle tests), volunteers were instructed to have their arms resting on their thighs. In order to obtain the same

simulation model position as the volunteers had, the following rotations were performed. The arms were rotated around an axis, parallel to global y-axis through a constructed shoulder close to the center geometric center of the humeral head by -35 degrees (shoulder extension). Simulations showed initial penetrations of the upper arm flesh and the torso. Hence, an arm abduction by +5 degrees for the right and -5 degrees for the left, through constructed shoulder rotation point around an axis parallel to global x-axis was performed. Furthermore, the model had a different leg position than the volunteers. The hip joint is formed by the head of the femur and the acetabulum of the pelvis. A rotation point in the geometric center of the spherical femoral head was constructed, and hip extension around an axis parallel to global y-axis by -15 degrees was performed[4].

Figure 3.16 shows an overlay of the standard THUMS® model (gray) and the model used for further simplification (blue), with descriptions of the rotations performed.

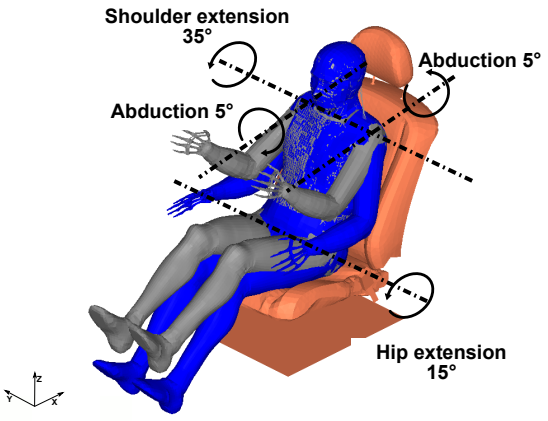

Figure 3.16.: Standard THUMS® model (gray) and model used for further simplification (blue) with descriptions of the rotations performed

Essentially, the development of the implementation methodology was based on the standard HBM or on a simplified model. As shown in table 3.3, the number of elements within the FE HBMs has increased significantly over the different model versions. The development of a controller which can influence model kinematics requires several iterations, which leads to a high number of simulations, and the considered time interval of 1 to 2 s is challenging in terms of the numerical stability of the FE HBM. Furthermore the HBM was too stiff, and without modifications it was not suitable for pre-collision simulations. In retrospect, this corresponds to findings published by Yigit et al. in 2014 [YWK+14], who showed a comparison of simulations varying shell thicknesses and Young's modulus based on literature. They concluded that in pre-collision simulations using THUMS® not only the muscle contribution, but also the stiffness of the soft tis-

[4]Note: The used coordinate system is the model coordinate system. This coordinate system is not in agreement with the recommendations on definitions of joint coordinate systems of various joints for the reporting of human joint motion given by Wu et al. [WSA+02, WvdHV+05]

sue affects model kinematics. Hence, for the development of the methodology, it was decided to use a bottom-up approach, starting with a simplified surrogate model and then increasing the complexity of the model in a stepwise fashion.

In particular, the derivation of a surrogate model requires a modeling of the human spine that makes it possible to accurately capture volunteer kinematics and then model them within the controller.

As stated in section 2.1.1 the human spine consists of 7 cervical, 12 thoracic, 5 lumbar vertebrae, as well as the sacrum and the coccyx. The vertebrae are separated from each other by intervertebral discs. Within THUMS®, the vertebral system is a high-fidelity model. Figure 3.17 shows the human spine and the FE spine representation of a seated THUMS®. Movement of the spine is enabled by using contacts between the participating parts. This modeling results in a high computational effort, which was not beneficial for the development of the methodology. Due to the focus on volunteer kinematics and the minor importance of modeling anatomical details, it was decided to split the human spine into segments. In particular, the spine was divided into two segments, representing the torso and the head-neck area. In order to further decrease the computational effort the two segments were modeled as rigid bodies. Rigid bodies were connected using two kinematic joints. Figure 3.18 shows the modeling approach and the main dimensions of the rigid bodies.

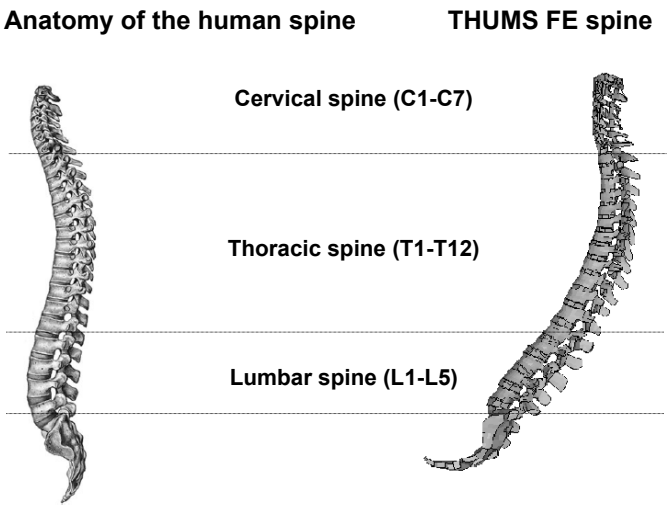

Figure 3.17.: Human spine (left), adapted from [SNW04] and FE spine representation of seated THUMS®(right)

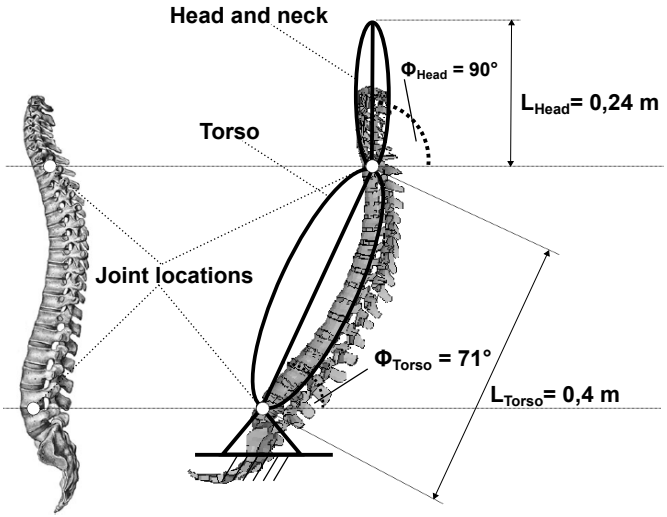

Figure 3.18.: Overlay of the FE spine of extracted THUMS® and MB representation with its main dimensions

In order to derive the surrogate model, it was necessary to determine the mass and inertia properties of the model. Figure shows 3.19 the part modeling and segmentation process for deriving the surrogate models. The positioned FE THUMS® was split with respect to the chosen joint location in four parts, which are colored in gray, green, blue and turquoise and represent the head, torso, pelvis and lower extremity section. The model parts within this section, including all bones, flesh and organs, were used to determine the mass and mass moment of inertia of this section. The bowels were in the transition zone between torso and pelvis. Although they are mainly within the defined pelvis section, these parts were assigned to the torso section. This assignment is based on the assumption that they influence torso kinematics due to contact with other parts of the HBM and therefore increase the resistance of the torso against frontal movements.

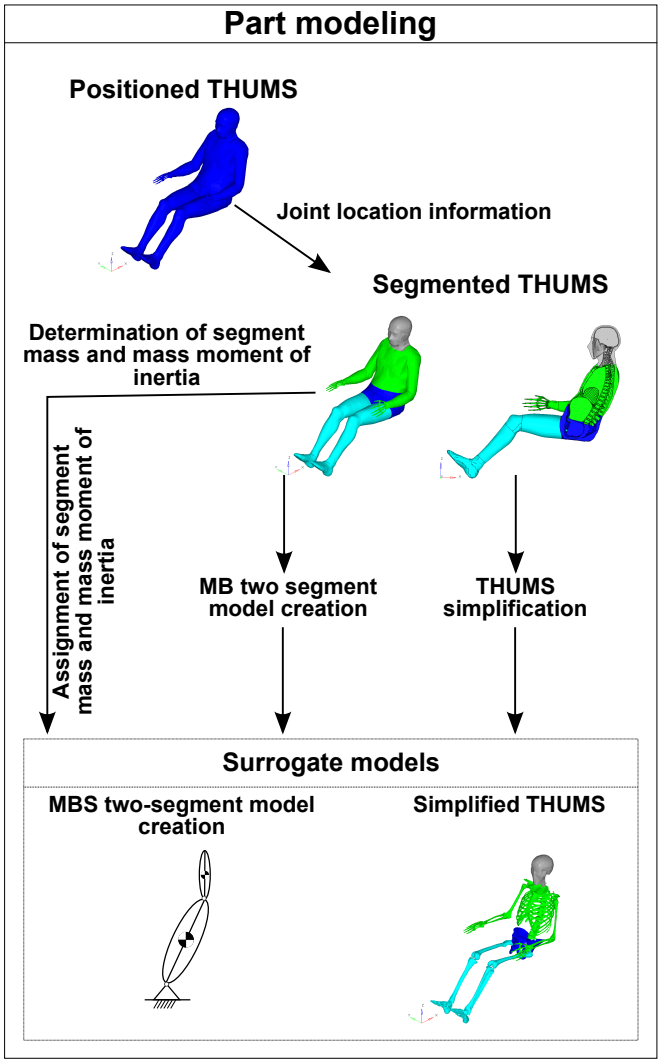

Figure 3.19.: Part modeling and segmentation process for deriving surrogate models

There are two approaches available for determining the mass and moment of inertia; information could be derived using either the individual segment or the whole body model. Furthermore, the mass could be determined using either pre-processor tools or the solver output (3.20). Within this thesis, it was decided to use the whole-body model in combination with a solver-based approach, although the common approach is based primarily on pre-processor tools. This decision was made because the comparison of different pre-processor tools showed a large variety of up to ten percent in mass output between the different tools and the mass values provided within THUMS® documentation. This large variety in pre-processor output may be explained by the different abilities of the tools to read all components within the model. For a methodology development, this variation

was too large. Using the solver output of the simulation ensures that the masses and moments of inertia assigned to the model and used for simulation are identical. Furthermore, in contrast to a segment-based approach, this approach allows for a fast adaption of the part assignment to individual segments. The co-simulation approach was originally developed for LS-Dyna® solver version R4.2.1. Hence, the output file obtained by using this solver was used.

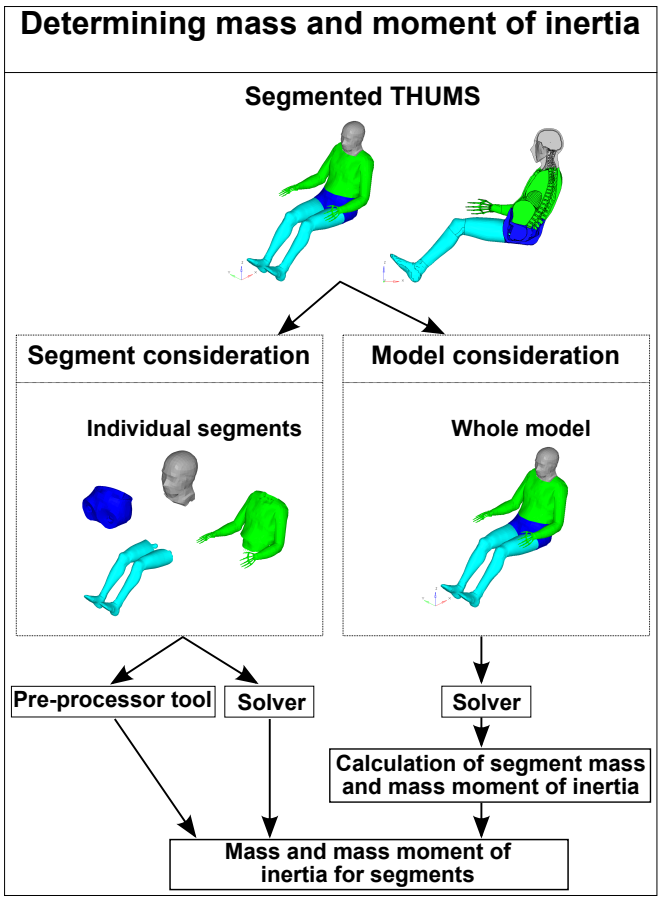

Figure 3.20.: Process of THUMS® segmentation and determination of mass

The solver output file was created by exposing the positioned whole THUMS® to gravity in an arbitrary simulation environment. Within the solver, the mass and moment of inertia for every part were calculated. The previous segmentation of the whole model provided the information about which part was assigned to which segment. By using the section part lists, individual parts were located within the solver output file. Figure 3.21 shows one sample entry of the simulation output file. The part identification number (Part id) is framed in solid green line, the mass and center of gravity (COG) information is in the dashed blue box and inertia tensor is in the red dashed-dotted box. .

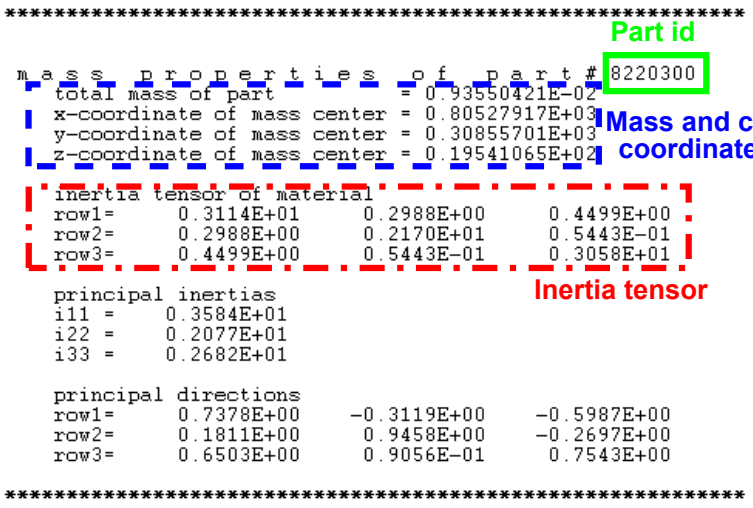


```
*************************************************************
 m a s s   p r o p e r t i e s   o f   p a r t #  8220300
   total mass of part              = 0.93550421E-02
   x-coordinate of mass center = 0.80527917E+03
   y-coordinate of mass center = 0.30855701E+03
   z-coordinate of mass center = 0.19541065E+02

   inertia tensor of material
   row1=      0.3114E+01      0.2988E+00      0.4499E+00
   row2=      0.2988E+00      0.2170E+01      0.5443E-01
   row3=      0.4499E+00      0.5443E-01      0.3058E+01

   principal inertias
   i11 =     0.3584E+01
   i22 =     0.2077E+01
   i33 =     0.2682E+01

   principal directions
   row1=      0.7378E+00     -0.3119E+00     -0.5987E+00
   row2=      0.1811E+00      0.9458E+00     -0.2697E+00
   row3=      0.6503E+00      0.9056E-01      0.7543E+00

*************************************************************
```

Figure 3.21.: Sample of simulation output file entry with color marked entries of part id (green, solid), mass and COG information (blue, dashed) and inertia tensor (red, dashed-dotted)

The COG information is given in the global coordinate system and contains part mass and the coordinates of the part COG. According to [GHS08], p. 96 ff. the coordinates of the COG of a body located on the surface of Earth and, exposed to gravity can be determined using the relations

$$\begin{aligned} x_{\mathrm{COG}} &= \frac{\int_V x\rho \, dV}{\int_V \rho \, dV}, \\ y_{\mathrm{COG}} &= \frac{\int_V y\rho \, dV}{\int_V \rho \, dV}, \\ z_{\mathrm{COG}} &= \frac{\int_V z\rho \, dV}{\int_V \rho \, dV}, \end{aligned} \tag{3.2}$$

where x, y and z denote the coordinates and ρ the density of the body. If a body is composed of k bodies with the volumes V_i and constant densities ρ_i and the individual COG components x_i, y_i, x_i are known, the denominator of 3.2 can be written as

$$\begin{aligned} \int_V \rho dV = \int_{V_1} \rho_1 \, dV + \int_{V_2} \rho_2 \, dV + \ldots + \int_{V_k} \rho_k \, dV = \\ \rho_1 \int_{V_1} dV + \rho_2 \int_{V_2} dV + \ldots + \rho_k \int_{V_k} dV = \rho_1 V_1 + \rho_2 V_2 + \ldots + \rho_k V_k = \sum_{i=1}^{k} \rho_i V_i. \end{aligned} \tag{3.3}$$

Reconsidering equation (3.2) under the assumption of constant density, it could be rewrit-

ten as

$$\begin{aligned} x_{\mathrm{COG}} &= \frac{1}{V}\int_V x\,dV \\ y_{\mathrm{COG}} &= \frac{1}{V}\int_V x\,dV \\ z_{\mathrm{COG}} &= \frac{1}{V}\int_V z\,dV \end{aligned} \tag{3.4}$$

This leads to

$$x_i = \frac{1}{V_i}\int_{V_i} x\,dV \Rightarrow \int_{V_i} x\,dV = x_i V_i \tag{3.5}$$

for the x-component. For the numerator of equation (3.2) for x_{COG} this leads to

$$\begin{aligned} \int_V x\rho\,dV &= \rho_1 \int V_1 x\,dV + \rho_2 \int V_2 x\,dV + \ldots + \rho_k \int V_k x\,dV \\ &= \rho_1 x_1\,V_1 + \rho_2 x_2\,V_2 + \ldots + \rho_k\,x_k\,V_k = \sum_{i=1}^{k} \rho_i\,x_i\,V_i. \end{aligned} \tag{3.6}$$

The same holds true for the y- and z-component. This yields

$$\begin{aligned} x_{\mathrm{COG}} &= \frac{\sum_{i=1}^{k} x_i\,\rho_i\,V_i}{\sum_{i=1}^{k} \rho_i\,V_i} \\ y_{\mathrm{COG}} &= \frac{\sum_{i=1}^{k} y_i\,\rho_i\,V_i}{\sum_{i=1}^{k} \rho_i\,V_i} \\ z_{\mathrm{COG}} &= \frac{\sum_{i=1}^{k} z_i\,\rho_i\,V_i}{\sum_{i=1}^{k} \rho_i\,V_i} \end{aligned} \tag{3.7}$$

.

This was used to determine the segment COGs.

Figure 3.21 shows that the inertia tensor comprises 9 entries. The mass moment of inertia with respect to a rotation axis i-i is generally defined as

$$J_{i-i} = \int r^2 dm \tag{3.8}$$

where dm denotes a mass element of the body in the perpendicular distance r to the rotation axis i-i. Due to its reference to the axis, it is also denoted as the axial mass moment of inertia. The inertia tensor comprises the three axial mass moment of inertia values (MoI) (x-, y-, z-axis) and six further entries referred to as moments of deviation (see [GHSW06], p. 170 ff.).

$$\mathbf{J}^{(A)} = \begin{bmatrix} J_{xx} & J_{xy} & J_{xz} \\ J_{yx} & J_{yy} & J_{yz} \\ J_{zx} & J_{zy} & J_{zz} \end{bmatrix} \tag{3.9}$$

The individual components are calculated as follows:

$$\begin{aligned} J_{xx} &= \int_m (y^2 + z^2)\, dm, \\ J_{xy} = J_{yx} &= -\int_m xy\, dm, \\ J_{yy} &= \int_m (z^2 + x^2)\, dm, \\ J_{yz} = J_{zy} &= -\int_m yz\, dm, \\ J_{zz} &= \int_m (x^2 + y^2)\, dm, \\ J_{zx} = J_{xz} &= -\int_m zx\, dm, \end{aligned} \tag{3.10}$$

Because J_{xy}=J_{yx}, J_{yz}=J_{zy} and J_{zx}=J_{xz}, this tensor is a symmetrical tensor. It is important to note that when using the tensor, the inertia properties are described with respect to a reference point A. All entries of the tensor therefore depend on the choice of the reference point, as well as on the axis orientation of the x-, y-, and z-axes. For every reference point a special axis system with three orthogonal axes *1*,*2* and *3* can be found for which the deviation moments are equal to zero. For such a system, the axial mass moment of inertia values are extremal values. The tensor can then be written in the form:

$$\mathbf{J}^{(A)} = \begin{bmatrix} J_1 & 0 & 0 \\ 0 & J_2 & 0 \\ 0 & 0 & J_3 \end{bmatrix} \tag{3.11}$$

To determine the mass moment of inertia within certain points on the rigid body, the parallel axis theorem[5] can be used. This theorem states that the moment of inertia of a rigid body around a given axis can be determined using the moment of inertia through the center of mass of the body around a parallel axis and the perpendicular distance between the axes.

[5] also known as Huygens–Steiner theorem, after C. Huygens and J. Steiner

$$J_{a-a,S} = J_{s-s,COG} + mr^2 \tag{3.12}$$

where $J_{s\text{-}s,COG}$ denotes the moment of inertia around rotation axis s-s through the center of mass, $J_{a\text{-}a,\ S}$ denotes the moment of inertia around parallel rotation axis a-a through point S, m denotes the mass of the body and r is the perpendicular distance of the axis.

The mass moments of inertia for all parts where given in global coordinate system with with respect to the global coordinate origin. Using the mass, the mass moment of inertia information and the part center of gravity information in the global coordinate system, the segment masses and mass moments of inertia were determined. Table 3.4 shows the masses which were determined for different body regions and table 3.5 shows the coordinates of the segment center of gravity, given with reference to the model global coordinate origin.

Table 3.4.: Surrogate model segment masses

Segment name	**Mass in kg**
Head and neck	7.60
Torso and upper extremities	31.72
Pelvis	9.42
Lower extremities	28.36
Total	**77.10**

Table 3.5.: Surrogate model segment COG (from origin)

Segment name	**COG position measured from origin in m**		
	x	y	z
Head and neck	1.74	-0.37	0.73
Torso and upper extremities	1.66	-0.37	0.39
Pelvis	1.55	-0.37	0.14
Lower extremities	1.18	-0.37	0.11

These determined masses were assigned to the surrogate models, which were an MB model realized in Matlab/Simulink® and a simplified FE THUMS® model with explicit FE solver LS- Dyna®. For the two segment MB model, the masses of the pelvis and the lower extremities were not relevant. For the simplified THUMS® model, the masses were added to the remaining parts. The mass determination also included the parts which remained after the simplification process. Hence, the density of the remaining THUMS® simplified model components was set to $7.85 \times 10^{-9}\,\mathrm{kg/m^3}$. This ensures that the remaining model components were not contributing twice to the mass. The mass of the remaining model components was less than one percent of the original mass. For the first stage of model development, the masses were assigned to the parts using an

Element Mass in LS-Dyna®. The whole mass of the segment was concentrated in one certain point of the model, which, in the first modeling step, was exactly the midpoint of a line element connecting the two joints of the surrogate model for the torso and the midpoint of a line in the vertical axis direction, connecting the joint in the cervical region and the top of the head. As shown in 3.22, the human spine has a curvature, and this point is therefore normally not a point on the spine. This midpoint was added to the spine using a rigid body constraint, which makes it possible to add arbitrary points in space to rigid bodies without the need for additional connection elements. The mass distribution within the segments was not modeled in this first model development stage. Figure 3.22 shows a comparison of the original THUMS® center of gravity of the head and the torso with the upper extremities in blue and the sled test model COGs in red. The original THUMS® head COG is slightly higher (z- distance of 14.45 mm) and anterior to the constructed head midpoint (x-distance of 6.32 mm). The original THUMS® torso and upper extremities COG and the constructed torso midpoint are at about the same height (z- distance of 1.98 mm), and the original THUMS® torso and upper extremities COG is once again anterior to the midpoint (x-distance of 20.45 mm).

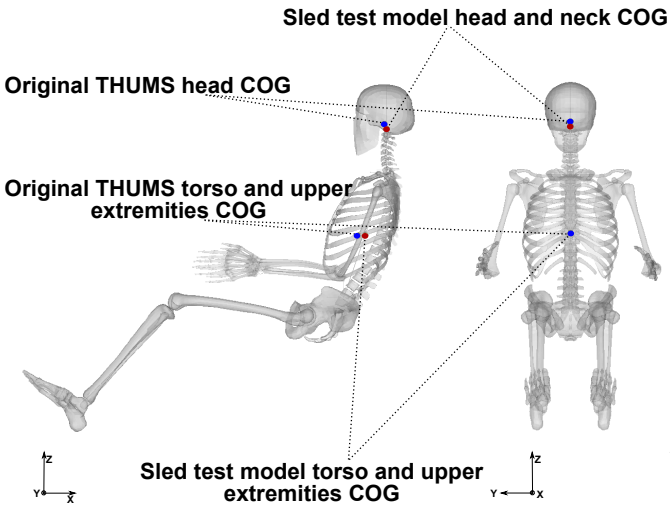

Figure 3.22.: Overlay of COG THUMS® complex and COG sled test model

Vehicle test models

The part modeling for deriving the vehicle test models remained the same as for the sled test model, but instead of using a concentrated mass in the middle of the segments, the exact inertia properties of the basis model were used for the surrogate models. Parts were assigned the same masses as in table 3.4. The process for determining inertia properties was described above. Table 3.6 shows the derived mass moment of inertia values for different body segments. The values are related to the origin of the global coordinate system.

Table 3.6.: Derived mass moments of inertia for different body segments (Reference point global Origin)

Segment name	**MoI in 10^6kgmm^2**					
	J_{xx}	$J_{xy} = J_{yx}$	$J_{xz} = J_{zx}$	J_{yy}	$J_{yz} = J_{zy}$	J_{zz}
Head and neck	6.12	-4.47	-9.91	24.50	-2.28	20.46
Torso and upper extremities	13.83	-19.70	-26.13	90.47	-6.26	87.20
Pelvis	1.56	5.28	-2.02	22.42	0.48	23.56
Lower extremities	4.75	12.39	-3.96	41.23	1.11	44.85

3.3.3.2. Joint modeling

For the part modeling, the locations of the joints had to be defined. As shown in Fig. 3.18, the joint locations were chosen between C7 and T1 and L4 and L5 respectively. The main reason for choosing these locations was the assumption that the fixation of the pelvis allowed only minor rotations. The rotation of the spine was therefore assumed to start in the lumbar section. The head rotation was assumed to start with the seventh cervical vertebrae.

The joint DoF were also determined based on occupant test data. Occupant kinematics test data of the frontal and lateral sled tests, as well as of the emergency braking and lane change maneuvers of vehicle test series A and B, indicated that the main contribution to the occupant movement was in the x-z plane for braking and the y-z plane for lateral maneuvers respectively.

The maneuvers investigated in vehicle test series B, and in particular the combined maneuver with a braking and a steering either to the right or the left in combination with the seat with lateral support and a three-point belt configuration, no longer allowed for a planar model consideration. Hence, for vehicle test series B, a joint modeling approach had to be found that makes it possible to simulate a multi-directional occupant movement.

To add further degrees of freedom, one can think of a spherical joint, which allows three rotations around defined axes. For a pure passive model without any control, this approach is sufficient. As soon as the model response is controlled, the main problem when using a spherical joint becomes obvious. The control of a spherical joint requires at least one actuator per degree of freedom, resulting in a total of three actuators. The combination of the simplified muscle modeling approach with a spherical joint did not allow for the stabilization of the model. The reason was that the beam element that was used as an actuator can only apply force to the model in the axial direction. If the model moves in two directions, this axial force introduces force components in all three directions. In order to allow multi-directional movement without major chances of both the muscle modeling and the underlying controller concept, the necessary three model DoF were split into three separate ones. This was done by introducing a level concept,

whereby the different levels represent the different model DoF. At each level, a revolute joint and a hierarchy of the three rotations was introduced. The first and master rotation is around the rotation axis 1 which is equal to a model forward movement in the x-z plane. The second rotation is a rotation around the rotated rotation axis 2, which is a lateral movement, and the third and last rotation is around the rotated rotation axis 3, which is a rotation around the vertical model axis. Figure 3.26 illustrates the main concept shown on a cuboid model. In the actual modeling, the three rotation axes are in the same plane. For a better understanding Fig. 3.26 shows the rotation axis in an exploded view. The grey plane symbolizes the ground level. The blue level is the plane carrying the master rotation axis 1, the green plane carries the second rotation axis and the vertical axis of the cuboid is equal to rotation axis three. The example shows rotations of 15 degrees around rotation axis 1, 20 degrees around the rotated rotation axis 2, and a final rotation of the cuboid by 25 degrees around rotation axis 3. For the HBM modeling, only two revolute joints per joint were used. Based on test data, the rotation around rotation axis 3 was omitted.

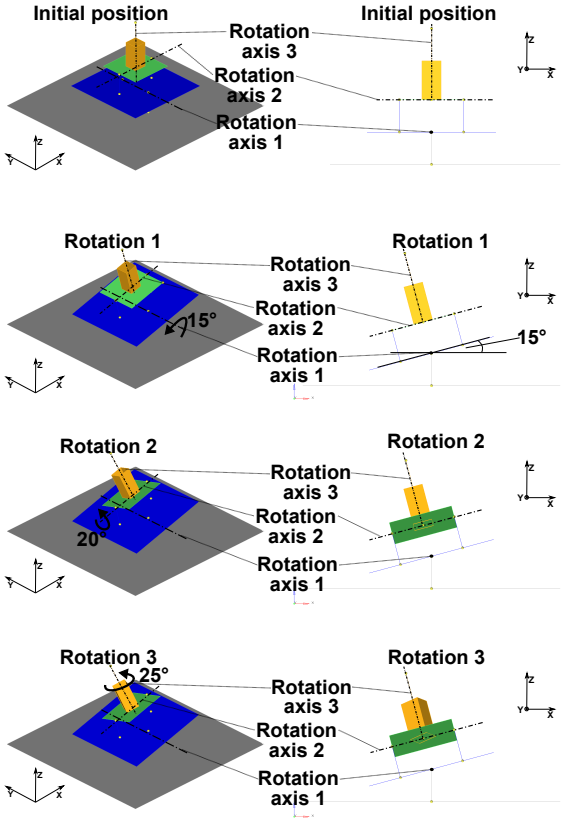

Figure 3.23.: Joint modeling concept for 2.5D model

3.3.3.3. Muscle modeling

Muscle modeling within this thesis addresses the implementation of actuators that can actively influence model kinematics. As stated in section 2.1.2, within the human body, muscles are responsible for active movements. The contracting muscle, referred to as agonist, produces any particular movement. This muscle is always paired with an antagonist which produces the opposite effect on the same bones [Knu07]. In most cases, the agonist is supported by other muscles. Muscles that help to stabilize a movement and reduce extraneous movements are referred to as synergist. As stated in section 2.1.2, besides their active components, human muscles also have passive properties which determine muscles' mechanical properties. Compared to the active part this passive part, is of a smaller order. Östh [Öst14] described different studies which considered active or passive muscle modeling. In 1987, Deng and Goldsmith presented a first implementation of muscle properties in an HBM for cervical spine. As shown in [Öst14], in the past, the main focus was on the development of muscle models for simulations of the collision phase. Implementation of active muscles for either the whole human body or the spine and for consideration of pre-collision scenarios were presented by van Rooij, 2011 [Roo11], Meijer et al., 2012 [MVHB+12] and Meijer et al., 2013 [MBE+13, MEBvH13]. In general modeling the torques of muscles around joints could be done either by implementing the muscles or by substituting the muscle elements and applying joint torques directly [Pan01].

For all of the above mentioned models, a torque generator or a Hill-type material model was used for active modeling. To create a model that can mimic occupant pre-collision kinematics accurately, it was a question of which details regarding the muscle should be taken into account. The modeling approach using torque generators instead of muscle line elements was not possible, due to the coupling. The quantities that could be transferred from a controller built in Matlab/Simulink® to an explicit FE solver or MB solver were only actuator forces. Therefore, it was not possible to build a controlled torque motor, so the approach with actuated beam elements was created. Due to the novelty of the implementation approach and the part simplifications, the actuated beam elements were modeled without using the Hill-type model and did not account for the underlying force-length and force-velocity relations. Nevertheless, the approach makes it possible to implement these relations. In addition, the lines of muscle action were not based on anatomy either. To achieve active planar movement of body segments in both directions, at least two contracting muscle elements per revolute joint (creating opposite torques around the joint) must be used. In contrast to real muscles, the actuated beam elements used within the co-simulation approach allow an active elongation. Hence, to achieve an active planar movement in both directions, only one actuator element was needed. It was decided to fix the muscle attachment points to a virtual plane, which is attached to the segment to be moved. Figure 3.24 shows the muscle/actuator elements implemented in the model. The top of the figure shows the muscle/actuator elements implemented to control frontal and lateral model movement. The bottom of the figure shows the distances between the attachment points for front and side. The subscript of length L

denotes the segment with H for head and T for torso followed by the coordinate direction x, y or z and the movement direction which will be influenced by the muscle/actuator element with letter f for frontal and letter s indicating lateral movement.

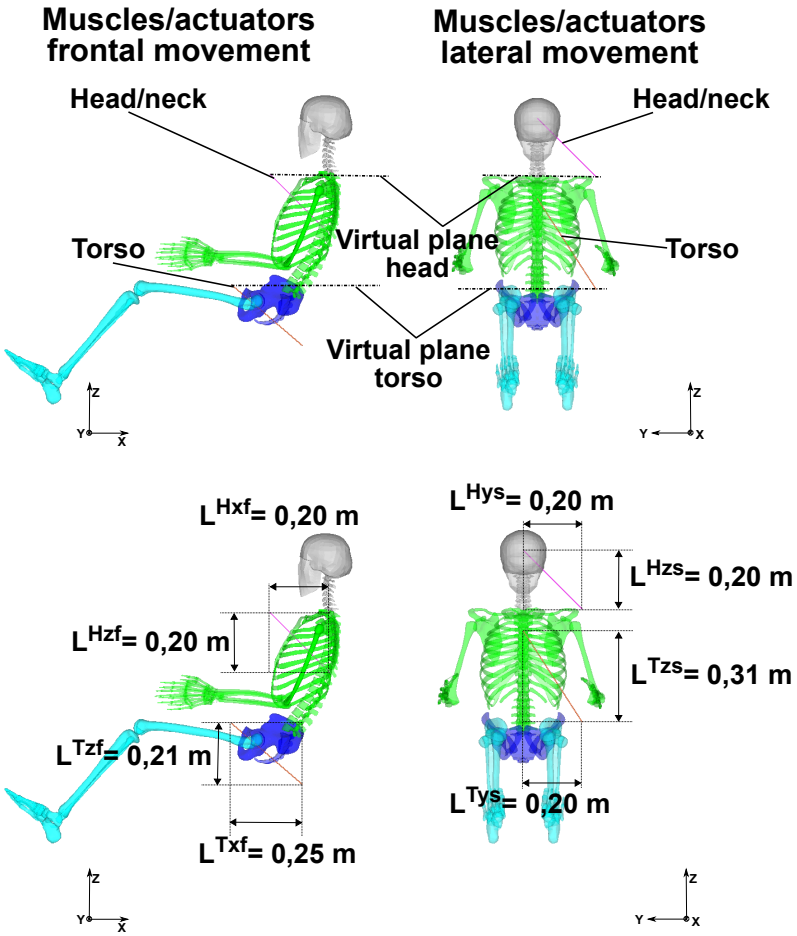

Figure 3.24.: Muscle/actuator elements with virtual attachment plane and main dimensions for frontal and lateral elements

For the model in vehicle test series B, the additional degree of freedom in joint modeling also required the introduction of two further actuator elements. It is important to mention that not all of the included actuator elements which are directly attached to the segment that should be moved. The first muscle element is responsible for the rotation around the y-axis and is in the x-z plane attached to the pelvis and virtual plane, which also carries the second rotation axis. The second muscle element is attached to the first virtual plane and to the second virtual plane. The third and last muscle element would have been between the second plane and the segment which should be moved.

For the present work the third rotation was not controlled. Hence there was no muscle element between these two planes. The implementing of such a muscle element structure in combination with the joint modeling ensures that an actuated muscle element only applies forces around the assigned rotation axis and in no other direction.

3.3.3.4. Definition of boundary conditions

As mentioned above, volunteers were seated on a modified seat and fixed to the seat using either a lap belt for the sled test series and vehicle test series A or a three-point belt for vehicle test series B.

Sled test boundary conditions

Specifically, the seat was a production seat of a Mercedes S500 (W221), with the seat cushion removed. On the seat frame, wooden plates covered with leather were mounted to achieve a planar seat plane. This simplification reduced the seat influence on occupant kinematics and in particular importance for simulation, allowed for the modeling of the seat as a rigid body. This reduced FE instabilities and provided comparable boundary conditions. For the sled tests, the seat was mounted on the sled using the standard seat mounting bolts. The electrical seat adjusting mechanism was still operable and allowed the seat to be positioned according the 50^{th}-percentile seat position. The reason for using a lap belt instead of a three-point belt was that a three-point belt directly affects the translational and rotational DoF of the torso and head of the volunteers. The maximum torso and head excursion would therefore be the result of human muscle contribution and seat belt characteristics. A lap belt was used to minimize the belt influence while still ensuring a safe test with reproducible boundary conditions. The lap belt was tightened for every volunteer prior to performing the tests. Hence the elongation of the belt was mainly due to material elongation. The tightening and fixation minimized the relative movement between volunteer and seat, leading to a defined boundary condition for simulation. Using a lap belt ensured that the upper body movement of volunteers was mainly due to human contribution. Due to the combination of the modified seat and the lap belt, the velocities and the accelerations were set to the low level of 12 km/h and 0.6g for frontal and 10 km/h and 0.4g for lateral maneuvers. Fig. 3.25 (a) shows the sled test environment and (b) shows the FE reference seat with its main dimensions.

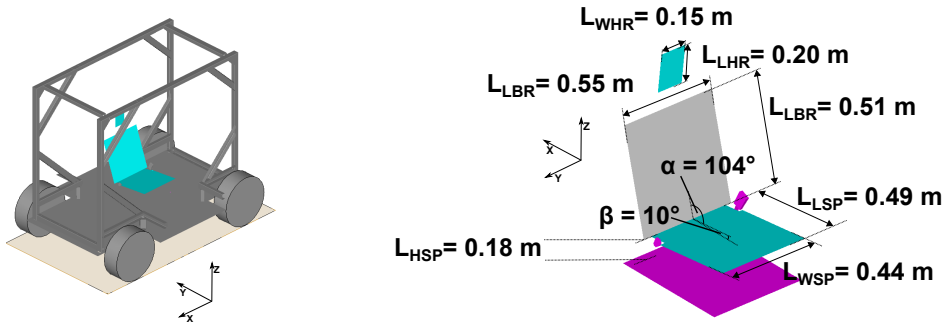

(a) FE sled with reference seat mounted for lateral maneuver

(b) FE reference seat

Figure 3.25.: Sled test environment with sled, camera frame and reference seat (a) FE reference seat with main dimensions (b) ,

The main difference between the sled tests and vehicle test series A was that the reference seat was mounted in the vehicle. In order to gain further information about the occupant kinematics without the influence of a three-point belt, a lap belt configuration was also used for vehicle test series A. In order to avoid injuries to the volunteers caused by the contact of head or torso with the vehicle structure, both the passenger door and the B-pillar were coated with foam. This had no influence on the simulation boundaries. Once again the lap belt was assumed to fix the volunteers movement so that there was no significant translation of the volunteer relative to the reference seat.

For test series B, the reference seat was equipped with lateral support, and instead of the lap belt, a three-point belt was used. Hence for the simulation, these two components had to be adjusted. The rigid FE reference seat was equipped with two lateral and also rigid supports. Figure 3.26 shows the seat with its main dimensions. For the three-point belt, a Daimler seat belt model was used. This model was composed of components of different vehicle models and was therefore not an exact representation of the seat belt used during the tests. In order to be able to modify the belt force and therefore mimic the measured belt forces, a beam element was introduced. Fig. 3.27 shows the FE three-point belt with the beam element that was used.

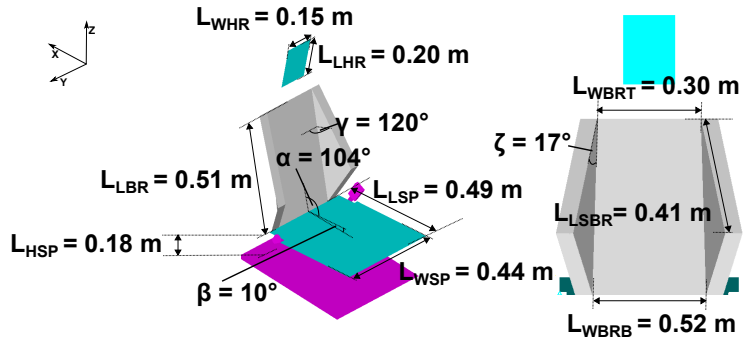

Figure 3.26.: FE reference seat with lateral support elements and main dimensions

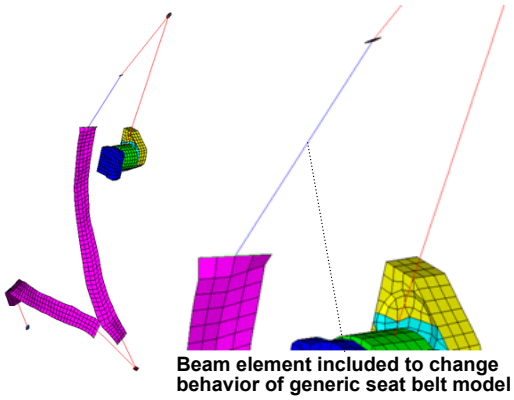

Figure 3.27.: Generic FE three-point belt, including FE shell and beam elements

3.3.4. Controller development

The development of a controller required the definition of a controller strategy. Massion [Mas92] stated that human motor acts can be divided into two categories: the maintenance of a reference position, also referred to as postural control and a goal-directed movement. The main difference between the two is that for postural control, the CNS often applies stabilizing muscle activations without conscious awareness. In the case of the goal-directed movement, a limb is actively moved along a trajectory towards a pre-determined goal. A movement is composed of these two types.

Simulations of the collision phase do not require model stabilization because the duration between the start of the simulation and the collision is too short to change the model position significantly. However, pre-collision maneuvers are characterized by long durations of up to several seconds. Within this phase, the occupants are exposed to gravity and other disturbances caused by the maneuver. Hence, occupants have to stabilize their bodies against these disturbances. The controller strategy used within this

thesis is based on the assumption that, before an emergency situation, the human body in postural maintenance state in order stabilize itself against gravity and disturbances due to vehicle/road interaction during normal driving, and it tries return to this initial position after being exposed to disturbances with higher amplitudes. As described in sections 3.3.3.1 and 3.3.3.2, the human upper body was divided into two rigid bodies, representing the body region between L5 and C7 and the region between C7 and the top of the head. Rigid bodies were connected using kinematic joints. The main idea of the controller concept was to use an internal model representation to determine the actuator forces that are needed to move the FE or MBS model in its demand position.

The starting point was the task of finding a suitable and feasible method to directly influence the nonlinear dynamic system

$$\dot{\mathbf{x}} = \mathbf{f}(\mathbf{x}, \mathbf{u}), \tag{3.13}$$

where $\mathbf{x}$ denotes the n - dimensional state vector, $\mathbf{u}$ denotes the m - dimensional control input and $\mathbf{f}$ is the n - dimensional vector function of the system. This task is a path following problem. The selected solution approach was the flatness-based approach, which is similar to an exact linearization. The main idea is to create a specific linear surrogate system by using non-linear state transformations. The internal controller representation of the model is equal to the dynamic model, which consists of two connected rigid bodies representing the torso and the head. The equations of motion of the two-segment kinematic chain were derived by using the Lagrange equations of second kind. Based on test data, the movement of the pendulum was assumed to be planar. The two rigid bodies were assumed to have a homogenous mass distribution (see, Fig. 3.28).

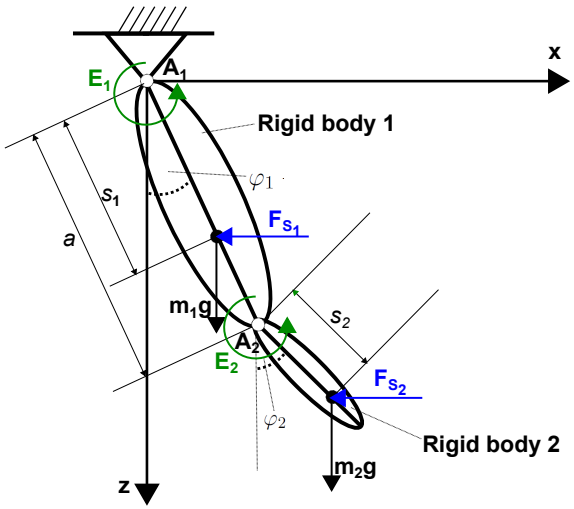

Figure 3.28.: Double pendulum with rigid body lengths a, rigid body masses m_1, m_2, moment of inertia J_1, J_2, center of gravity distances s_1, s_2 and generalized coordinates φ_1 and φ_2 exposed to gravity and disturbance forces F_{S_1} and F_{S_2}

The Lagrangian equations of motion can be written in the form:

$$\frac{d}{dt}\left(\frac{\partial T}{\partial \dot{q}_i}\right) - \frac{\partial T}{\partial q_i} = Q_i \qquad (i = 1, 2, \ldots, n) \tag{3.14}$$

where T denotes the kinetic energy, q_i the generalized coordinates and Q_i the generalized forces.

The kinetic energy of the first pendulum is given by

$$T_1 = \frac{1}{2}(J_{S_1} + m_1 \, {s_1}^2) \, \dot{\varphi}_1^2 \tag{3.15}$$

and of the second by

$$T_2 = \frac{1}{2}(m_2 \, {v_2}^2 + J_{S_2} \, \dot{\varphi}_2^2) \tag{3.16}$$

For the velocity v_2 it can be written

$${v_2}^2 = \dot{x}_2^2 + \dot{z}_2^2 = a^2 \, \dot{\varphi}_1^2 + s_2^2 \, \dot{\varphi}_2^2 + 2 \, a \, s_2 \dot{\varphi}_1 \dot{\varphi}_2 \, \cos(\varphi_1 - \varphi_2) \tag{3.17}$$

with

$$\begin{aligned} x_2 &= a \, \sin(\varphi_1) + s_2 \, \sin(\varphi_2), \\ z_2 &= a \, \cos(\varphi_1) + s_2 \, \cos(\varphi_2), \end{aligned} \tag{3.18}$$

The introduction of the radii of gyration i_1 and i_2 with respect to the joint points A_1 and A_2 with

$$\begin{aligned} J_{S_1} + m_1\, s_1^2 &= m_1\, i_1^2, \\ J_{S_2} + m_2\, s_2^2 &= m_2\, i_2^2 \end{aligned} \tag{3.19}$$

leads to

$$T = \frac{1}{2}\left[(m_1\, {i_1}^2 + (m_2\, a^2)\, \dot{\varphi}_1^2 + m_2\, i_2^2\, \dot{\varphi}_2^2 + 2\, a\, m_2\, s_2 \dot{\varphi}_1 \dot{\varphi}_2\, \cos(\varphi_1 - \varphi_2)\right] \tag{3.20}$$

Friction forces were not included. Hence, the model is exposed to a joint torque N_1 acting on rigid body 1 and N_2 acting on rigid body 2. Furthermore, the model is under gravity loading and exposed to disturbance forces F_{S_1} and F_{S_2}.

With

$$\begin{aligned} \frac{\partial T}{\partial \dot{\varphi}_1} &= (m_1\, i_1^2 + m_2\, a^2)\, \dot{\varphi}_1 + a\, m_2\, s_2\, \dot{\varphi}_2\, \cos(\varphi_1 - \varphi_2), \\ \frac{\partial T}{\partial \dot{\varphi}_2} &= m_2\, i_2^2\, \dot{\varphi}_2 + a\, m_2\, s_2\, \dot{\varphi}_1\, \cos(\varphi_1 - \varphi_2), \\ \frac{\partial T}{\partial \varphi_1} &= -a\, m_2\, s_2\, \dot{\varphi}_1\, \dot{\varphi}_2\, \sin(\varphi_1 - \varphi_2), \\ \frac{\partial T}{\partial \varphi_2} &= a\, m_2\, s_2\, \dot{\varphi}_1\, \dot{\varphi}_2\, \sin(\varphi_1 - \varphi_2), \\ Q_1 = E_1 - (m_1\, s_1 + m_2\, a)\, g\, \sin(\varphi_1) &- (F_{S_1}\, s_1 + F_{S_2}\, a)\, \cos(\varphi_1), \\ Q_2 = E_2 - m_2\, s_2\, g\, \sin(\varphi_2) &- F_{S_2}\, s_2\, \cos(\varphi_2) \end{aligned} \tag{3.21}$$

the Lagrangian equations can be written:

$$\begin{aligned} (m_1\, i_1^2 + m_2\, a^2)\, \ddot{\varphi}_1 + a\, m_2\, s_2\, \ddot{\varphi}_2\, \cos(\varphi_1 - \varphi_2) + \\ a\, m_2\, s_2\, {\dot{\varphi}_2}^2\, \sin(\varphi_1 - \varphi_2) + (m_1\, s_1 + m_2\, a)\, g\, \sin(\varphi_1) + \\ + (F_{S_1}\, s_1 + F_{S_2}\, a)\, \cos(\varphi_1) = E_1 \\ m_2\, i_2^2\, \ddot{\varphi}_2 + a\, m_2\, s_2\, \ddot{\varphi}_1\, \cos(\varphi_1 - \varphi_2) - a\, m_2\, s_2\, \dot{\varphi}_1^2\, \sin(\varphi_1 - \varphi_2) + \\ + s_2\, m_2\, g\, \sin(\varphi_2) + F_{S_2}\, s_2\, \cos(\varphi_2) = E_2. \end{aligned} \tag{3.22}$$

After reorganization, the Lagrangian equations can be written in the form:

$$\mathbf{M} \cdot \ddot{\boldsymbol{\varphi}} + \mathbf{b} + \bar{\mathbf{Q}} = \mathbf{E} \tag{3.23}$$

where

$$\mathbf{M} = \begin{bmatrix} m_1\, i_1^2 + m_2\, a^2 & a\, m_2\, s_2\, \cos(\varphi_1 - \varphi_2) \\ m_2\, s_2\, a\, \cos(\varphi_1 - \varphi_2) & m_2\, i_2^2 \end{bmatrix} \tag{3.24}$$

denotes the mass matrix,

$$\mathbf{b} = \begin{bmatrix} s_2\, m_2\, a\, \dot{\varphi_2}^2\, \sin(\varphi_1 - \varphi_2) \\ -s_2\, m_2\, a\, \dot{\varphi_1}^2\, \sin(\varphi_1 - \varphi_2) \end{bmatrix} \tag{3.25}$$

denotes the generalized centrifugal moment vector and

$$\bar{\mathbf{Q}} = \begin{bmatrix} (s_1\, m_1 + m_2\, a)\, g\, \sin(\varphi_1) + +(F_{S1}\, s_1 + F_{S2}\, a\, \cos(\varphi_1) \\ +s_2\, m_2\, g\, \sin(\varphi_2) + F_{S2}\, s_2\, \cos(\varphi_2) \end{bmatrix} \tag{3.26}$$

denotes the vector of moments due to other forces.

The demand torque $\mathbf{E}$ is calculated using

$$\mathbf{E} = \mathbf{M} \cdot [-\mathbf{K_d}\,(\dot{\boldsymbol{\varphi}} - \dot{\boldsymbol{\varphi}}_\mathbf{d}) - \mathbf{K_p}\,(\boldsymbol{\varphi} - \boldsymbol{\varphi}_\mathbf{d})] + \mathbf{b} + \bar{\mathbf{Q}} \tag{3.27}$$

with $\boldsymbol{\varphi}$ as the current generalized angle vector, $\dot{\boldsymbol{\varphi}}$ the current generalized angular velocity vector, $\boldsymbol{\varphi}_\mathbf{d}$ the demand angle vector, and $\dot{\boldsymbol{\varphi}}_\mathbf{d}$ the demand angular velocity vector. The factors $\mathbf{K_d}$ and $\mathbf{K_p}$ denote penalty factors for the difference between the internal controller model representation and the outside model (FE or MB).

Additional information on the controller used within the thesis can be found in Steidl [Ste12].

Figure 3.29 shows the main concept of the controller and the necessary user input quantities. The controller output torque vector $\mathbf{E}$ will be transformed into an actuator force vector $\mathbf{F}$ by using the geometric information of actuator and joint positions. This is done so it is possible to use the co-simulation approach, which only accepts forces as an input for the FE or MB model. In order to get a more realistic model behavior, the controller takes into account a reaction time Tr, which is a delay time from maneuver start to the actual force generation of the controller. As stated above, for the torque is calculated by determining the difference between demand angles represented by $\boldsymbol{\varphi_d}$ and the current outside model angles represented by $\boldsymbol{\varphi}$ as well as the difference between demand velocities $\dot{\boldsymbol{\varphi}}_\boldsymbol{d}$=0 (hence not included) and the current outside model angular velocities $\dot{\boldsymbol{\varphi}}$. These differences are scaled by applying $\boldsymbol{K_p}$ and $\boldsymbol{K_d}$ penalty factor vectors. Within these vectors two sets of values per joint have to be distinguished: $\boldsymbol{K_{p,High}}$ or $\boldsymbol{K_{p,Low}}$ and $\boldsymbol{K_{d,High}}$ or $\boldsymbol{K_{d,Low}}$. $\boldsymbol{K_{p,Low}}$ and $\boldsymbol{K_{d,Low}}$ are the parameters used before the maneuver is perceived and therefore responsible for the postural control of the model. $\boldsymbol{K_{p,High}}$ and $\boldsymbol{K_{d,High}}$ represent the parameters that are used to control the model after perceiving the maneuver. The controller gain parameters were determined using volunteer data as an input for an optimization. For the sled test series, as well as the emergency braking and lane change maneuvers of vehicle test series A and B, a planar controller approach was used. Model kinematics were controlled by one actuator element per revolute joint, resulting in a total of two actuators for frontal maneuvers and two for lateral maneuvers. For the combined maneuver to the left and right side, a superposition of two decoupled planar controllers was used. This approach allows for the application of

the same controller concept as for the other maneuvers but for a multi-dimensional load case. One weakness of this approach is that it does not take into account the change of inertia caused by lateral movement for the frontal load cases and the frontal movement for the lateral load cases. This results in a discrepancy between the actual needed and the calculated force. Due to large intra and inter-subject differences identified during testing, this influence was omitted.

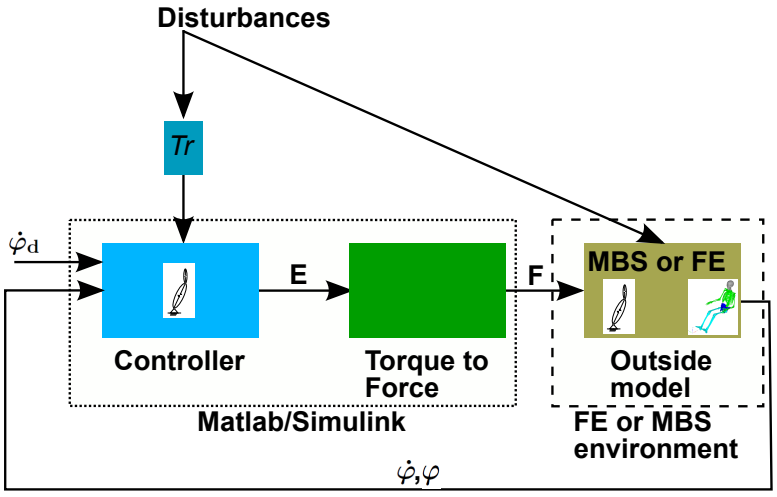

Figure 3.29.: Main controller concept. Torque vector $\boldsymbol{E}$, actuator force vector $\boldsymbol{F}$, demand angle vector $\boldsymbol{\varphi_D}$, current outside model angle vector $\boldsymbol{\varphi}$, current outside model angular velocity vector $\dot{\boldsymbol{\varphi}}$ and disturbances

Detailed information on the controller approach can be found in [Ste12].

4. Results

This chapter summarizes the main results of the movement studies and simulations conducted. The simulation results are compared to individual volunteer responses for the sled testing series and to derived volunteer relative angle corridors for testing series A and B.

4.1. Sled tests and 2D sled test model

Sled testing considered the kinematic responses and muscle activity of a total of 11 volunteers. A subset of four volunteers was investigated using the Vicon motion capture system. Since this system was also used for the subsequent vehicle tests, the discussion of the results will therefore on this subset. Maneuvers were repeated three times for each subject. As the first trial was crucial (explained in the Discussion section below), results of sled testing and simulation will concentrate on the first trial, during which the volunteers were unaware of the oncoming test (also refered to as *unaware* state). In contrast, for trials 2 and 3, a habituation effect and perception could have affected the volunteer kinematics. The coordinate system for the description of acceleration, velocities and occupant movements was in accordance with IS0 8855/70000, with the x-axis as the longitudinal vehicle axis, the z-axis representing the vertical vehicle axis and pointing to the sky, and the y-axis pointing from the passenger right side to the left with line of sight in the positive x-axis direction. Figure 4.1 shows the coordinate system.

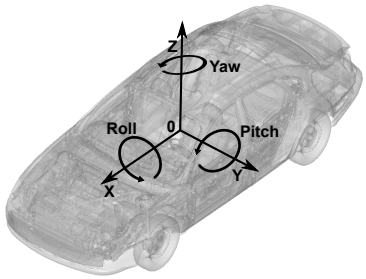

Figure 4.1.: Vehicle coordinate system based on IS0 8855/70000

4.1.1. Emergency braking maneuver 0.8g and 12 km/h

Emergency braking data was collected using an inverse volunteer position (i.e., volunteers were positioned on the sled with their direction of sight in the opposite direction of sled movement). The maneuvers were carried out on a sled test bench using a rope system that is normally used to accelerate vehicles to a defined velocity before a crash. The accelerometer was placed in the middle of the sled (near to the reference seat mounting). Figure. 4.2(a) shows an overlay of the measured longitudinal acceleration a_x for the four volunteers' first trials filtered according to ISO 6487:2000. As is evident, particularly in the phase from maneuver start to about 0.3 s, the characteristics differ by about 0.2g. This indicates that the acceleration characteristics in this phase are not highly repeatable due to the test bench controller. Furthermore, the measured acceleration signals of volunteer3 and 4 show large differences over time, indicating sensor problems. Peak values of a_x for volunteer1 and 4 are at in the same level of around 0.8g. For the emergency braking maneuver, a velocity change Δv of 12 km/h was targeted. The velocity plot in Fig. 4.2(b) shows an overlay of the velocities. As the figure shows, sled velocity after 1.4 s for volunteers 2 to 4 was 12 km/h, while for volunteer1 it was about 11 km/h.

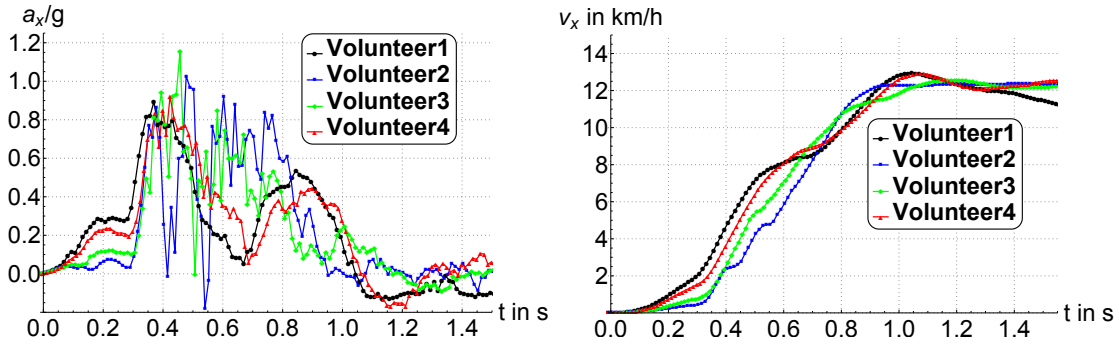

(a) Sled acceleration a_x

(b) Sled velocity v_x

Figure 4.2.: Sled test data for the frontal unaware trials of four subjects tested with the Vicon capture system

Due to the deviations of the acceleration characteristics, for simulation of frontal maneuver, occupant volunteer1 and 4 were chosen.

the simulation consisted of two phases. In order to allow for stabilization of the model, within the first phase, the model was exposed only to gravity. This phase lasted for 0.3 s. After 0.3 s, the second phase started. In this phase, the model was also exposed to the sled test pulse. Since results are presented for the second phase, the stabilization phase is not included. Simulation results for both an FE model as well as for a two-segment MB model are compared to volunteer data. Figure 4.3 shows the acceleration pulse of volunteer1 which was used for simulation.

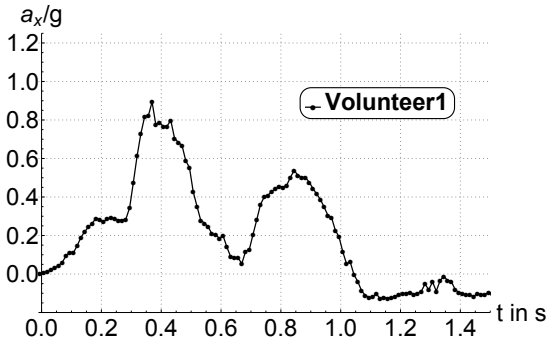

Figure 4.3.: Simulation acceleration pulse volunteer1

For the two simulation models, the controller gain parameters K_p and K_d were determined iteratively. Table 4.1 shows an overview of the controller parameters identified for volunteer1, which were used for simulating the kinematic response.

Table 4.1.: Overview of controller parameters identified for volunteer1 for torso and head/neck for frontal emergency braking maneuver at 12 km/h

Segment name	**Controller parameter name**				
	$K_{p,Low}$	$K_{d,Low}$	$K_{p,High}$	$K_{d,High}$	Tr in s
Head and neck	153.38	25.12	157.26	29.97	0.08
Torso and upper extremities	100.83	10.96	30.28	9.50	0.08

Figure 4.4(a) shows an overlay of the relative torso angles for the test data, MB model and FE model response for volunteer1. The relative angle $\varphi_{y,Torso}$ was measured with respect to the initial position. The subscript y denotes the rotation axis, and Torso denotes the considered segment. The comparison of simulation model responses and volunteer data shows that the simulation models did not reach the minimum volunteer relative torso angle of -7.3 degrees. The simulation model response shows a delay of 0.05 s for simulation peak angle compared to volunteer data. The relative torso angles of the FE and MB model differ by 0.7 degrees.

Figure 4.4(b) shows an overlay of the relative head angles of test data, MB model and FE model response for volunteer1. Visual inspection of the relative torso angles for volunteer data and simulation model response shows similar characteristics. The maximum volunteer relative head angle of 5.9 degrees was reached after 0.43 s. Simulation model peak angles were reached after 0.5 s. FE simulation model head responses show an overshoot compared to volunteer data of more than 1 degree, whereas the MB model head response differs from the volunteer maximum by less than 0.02 degrees.

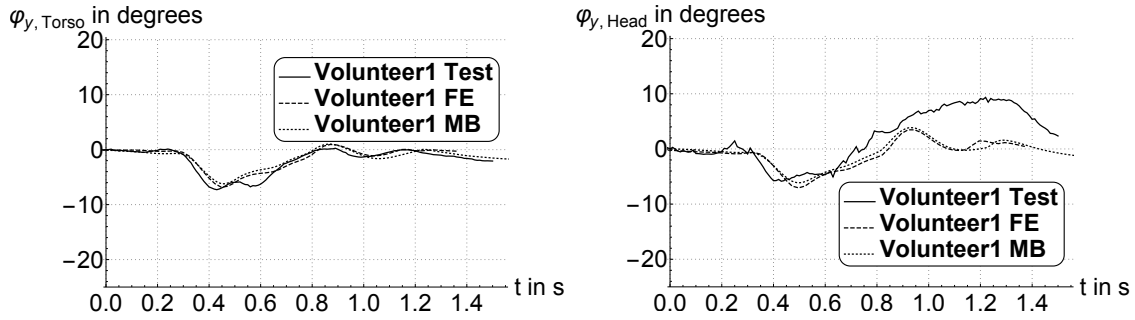

(a) Relative torso angles for volunteer1

(b) Relative head angles for volunteer1

Figure 4.4.: Overlay of relative torso and relative head angles of FE and MB model with volunteer data of emergency braking maneuver at 12 km/h

Table 4.2 shows the controller parameters used for the second investigated subject, volunteer4.

Table 4.2.: Overview of controller parameters identified for volunteer4 for torso and head/neck during frontal emergency braking maneuver at 12 km/h

Segment name	**Controller parameter name**				
	$K_{p,Low}$	$K_{d,Low}$	$K_{p,High}$	$K_{d,High}$	Tr in s
Head and neck	170.73	22.44	10.02	28.65	0.13
Torso and upper extremities	199.03	1.10	14.01	5.29	0.13

For simulation, a duration of 0.3 s for model stabilization was used once again. Figure 4.5 shows the acceleration pulse used for the simulation with volunteer4.

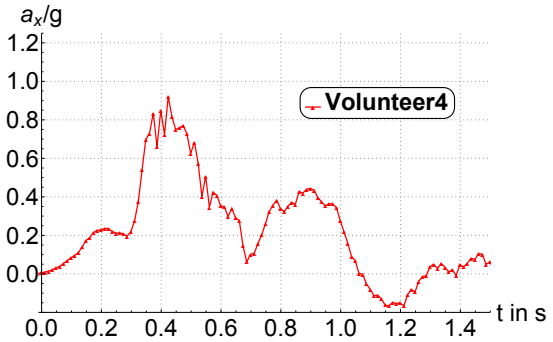

Figure 4.5.: Simulation acceleration pulse volunteer4

Figure 4.6(a) shows an overlay of the relative torso angles of test data, MB model and FE

model response for volunteer4. As the figure shows, the minimum volunteer torso angle was −20.5 degrees after 0.73 s. This shows the large differences in volunteer kinematic response, when it is compared to the maximum relative torso angle of volunteer1. The simulation results show a delay of more than 0.05 s at maneuver start. Simulation model torso response shows a steeper decrease than volunteer data. After 0.73 s, the relative torso angle of the volunteer reaches its minimum. The simulation FE model relative torso angle reaches its minimum after about 0.76 s, with a peak value of about −19 degrees . At more than −15 degrees, the MB simulation model peak relative torso angle is significantly higher than the FE model. This comparison indicates differences between the MB and FE model.

Figure. 4.6(b) shows an overlay of the relative head angles of test data, MB model and FE model response for volunteer4. As with the relative torso angles of volunteer4, the relative head angle is also more than twice as high as for volunteer1. For the relative head angles, the model response did not reproduce volunteer kinematics accurately. FE model response was about 1.6 times higher than volunteer relative head angle. Volunteer response characteristics could not be reproduced by both models. The characteristics also differ from the relative head angle characteristics of volunteer1. The increase in head angle lasts about 0.4 s for volunteer4, whereas for volunteer1, the main increase lasts about 0.1 s.

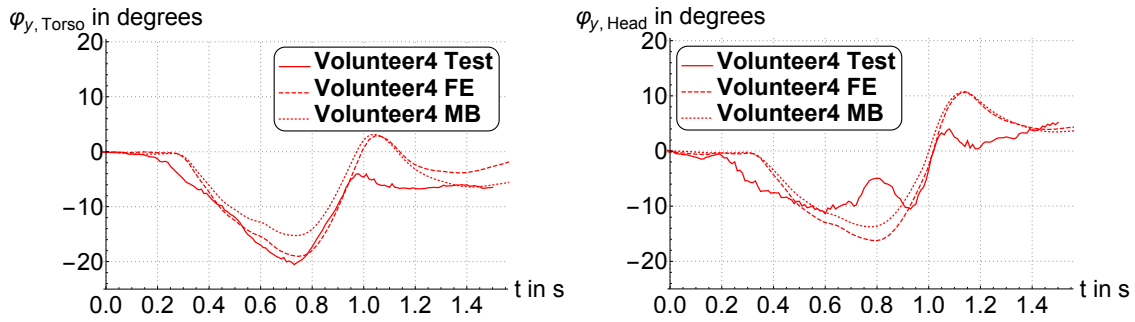

(a) Relative torso angles volunteer4

(b) Relative head angles volunteer4

Figure 4.6.: Overlay of relative torso and relative head angles of FE and MB model with volunteer data of emergency braking maneuver at 12 km/h

4.1.2. Lateral maneuver at 0.4g and 10 km/h

As described above, every volunteer first performed three longitudinal maneuvers and then three lateral ones. Here again, the accelerations and velocities of the sled test maneuver will be presented first. The lateral acceleration was also described in the sled coordinate system. Due to the rotation of the reference seat, the acceleration directions remained the same. Therefore, the lateral acceleration has therefore the same subscript

as for frontal maneuvers. In addition, for volunteer relative angles, the rotation axis remained the y-axis. Figure 4.7(a) shows the lateral accelerations for all four volunteers tested. Despite the increased maximum magnitude of about 0.4g, the acceleration characteristics differ by about 0.2g.

For lateral maneuvers, a velocity change $\Delta v = 10\,\text{km/h}$ should be reached. Figure 4.7(b) shows the velocity plot for the unaware volunteers and indicates that the sled final velocity was about 10.5 km/h for all four subjects.

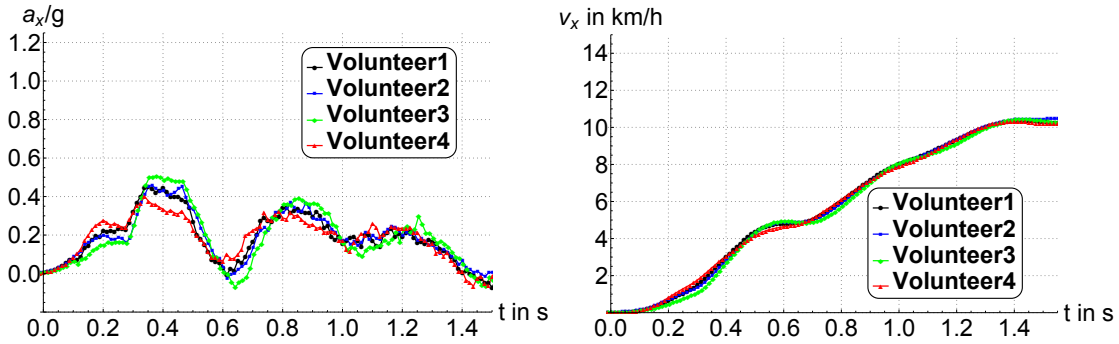

(a) Sled acceleration a_x

(b) Sled velocity v_x

Figure 4.7.: Sled test data for the lateral unaware trials of four subjects tested with Vicon capture system

The results for two volunteers for lateral simulation will be presented. In order to investigate the responses of the two remaining volunteers as well, volunteers 2 and 3 were chosen for simulation. Table 4.3 shows the controller parameters used for simulating the lateral maneuver of volunteer2.

Table 4.3.: Overview of controller parameters identified for volunteer2 for torso and head/neck for lateral maneuver at 10 km/h

Segment name	**Controller parameter name**				
	$K_{p,Low}$	$K_{d,Low}$	$K_{p,High}$	$K_{d,High}$	Tr in s
Head and neck	165.24	26.95	17.36	14.90	0.14
Torso and upper extremities	132.92	26.54	10.01	3.31	0.14

The model stabilization phase was again 0.3 s. Figure 4.8 shows the acceleration pulse of volunteer2 which was used for simulation.

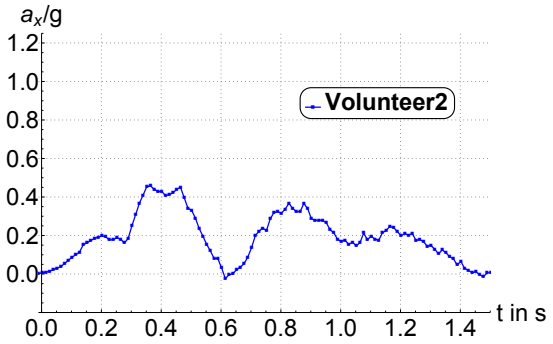

Figure 4.8.: Simulation lateral acceleration pulse volunteer2

Figure 4.9(a) shows an overlay of the relative torso angles of the test data, MB model and FE model response for volunteer2. The peak volunteer relative torso angle was close to −11.2 degrees. Volunteer characteristics showed a large plateau at about 0.8 s. The simulation results of the MB and FE models show large differences, and neither could reproduce volunteer response adequately.

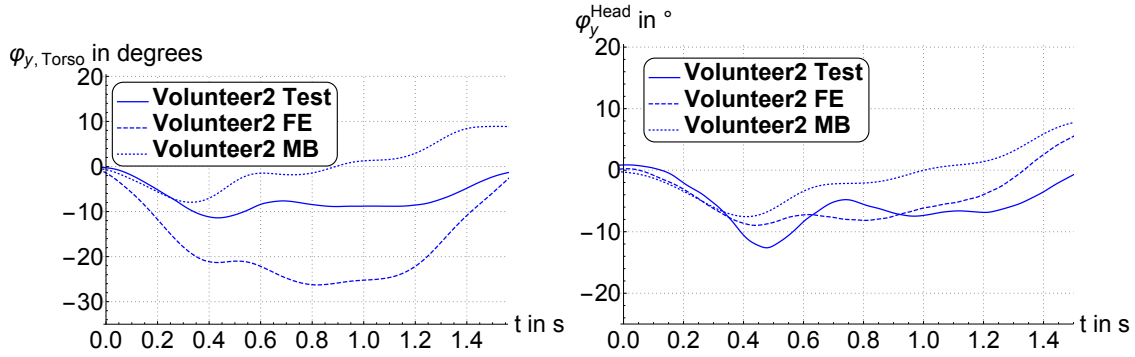

(a) Relative torso angles volunteer2

(b) Relative head angles volunteer2

Figure 4.9.: Overlay of relative torso and relative head angles of FE and MB models with volunteer data of lateral maneuver at 10 km/h

Figure 4.9 (b) shows an overlay of the relative head angles of the test data, MB model and FE model response for volunteer2. For head response, the MB and FE models reproduce volunteer response up to about 0.35 s. After this point in time the FE and MB model relative head angles separate, leading to a peak value of −9 degrees for the FE model and more than −8 degrees for the MB model. Neither model was able to reach the volunteer minimum relative head angle of about −13 degrees.

Table 4.4 shows the controller parameters used for the simulation of lateral maneuver for volunteer3.

Table 4.4.: Overview of controller parameters identified for volunteer3 for torso and head/neck for lateral maneuver at 10 km/h

Segment name	**Controller parameter name**				
	$K_{p,Low}$	$K_{d,Low}$	$K_{p,High}$	$K_{d,High}$	Tr in s
Head and neck	89.23	30	10.05	9.23	0.12
Torso and upper extremities	188.29	29.99	10	1.02	0.12

Figure 4.10 shows the acceleration pulse used for simulation.

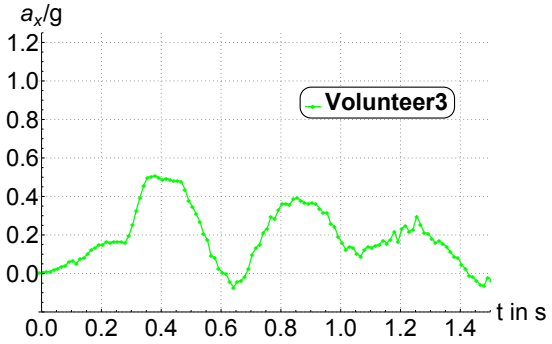

Figure 4.10.: Simulation lateral acceleration pulse volunteer3

Figure 4.11(a) shows an overlay of the relative torso angles of the test data, MB model and FE model response for volunteer3. The minimum volunteer relative torso angle was about −17 degrees. As with volunteer2, the MB and FE model responses deviated from the volunteer response and showed large differences of more than 20 degrees from minimum values.

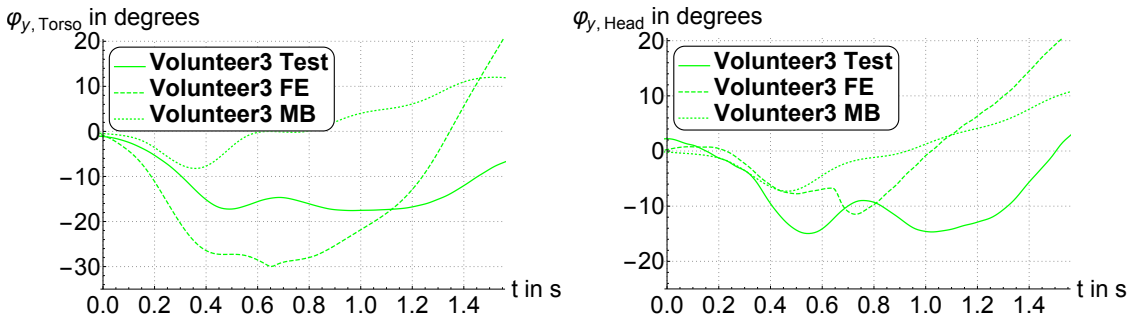

(a) Relative torso angles volunteer3

(b) Relative head angles volunteer3

Figure 4.11.: Overlay of relative torso and relative head angles of FE and MB model with volunteer data of lateral maneuver at 10 km/h

Figure 4.11(b) shows an overlay of the relative head angles of the test data, MB model and FE model response for volunteer3. For relative head angle, the model response is similar but the magnitude is about half as high as that identified for volunteer3. Neither model reached the volunteer relative head angle peak value of about 15 degrees, as the maximum reached was less than 8 degrees.

4.2. Vehicle tests and 2D vehicle model

The second test series was vehicle testing. The results from this series were intended to reveal if the large spread between volunteer responses that was identified during sled tests for a small subset of 4 volunteers could also be observed for a larger population. Model development concentrated on frontal maneuvers, in particular on an *unaware* state of volunteers, which this testing series identified as the most important with respect to the maximal torso and head excursions.

4.2.1. Emergency braking maneuver at 12 km/h

Test data analysis started with a check of the repeatability of the maneuvers. Figure 4.13(a) shows the longitudinal acceleration a_x and Fig. 4.14 the lateral acceleration a_y time histories for the emergency braking maneuver at 12 km/h. The peak longitudinal acceleration a_x was 1g, and the plateau in the measured data indicates that acceleration data was cut by the measurement system at 1g because it was beyond the acquisition range. Individual accelerations might be slightly higher than 1g. Especially from the maneuver start (t=0) to about the acceleration, the curves of individual volunteers show smaller differences than those identified during sled tests. This can also be seen in the corridor plot shown in Fig. 4.13(b). The midcurve in this plot (large dashed) represents the median, the small dashed the 16 percent quantile, and the solid line the 84 percent quantile. Quantiles where chosen to represent about $\pm\sigma$ from the median. This means that within the whole corridor about 68 percent of volunteer accelerations are included. The median acceleration was used for simulation. The lateral acceleration a_y was equal to zero, showing that the longitudinal acceleration a_x was dominant for the emergency braking maneuver.

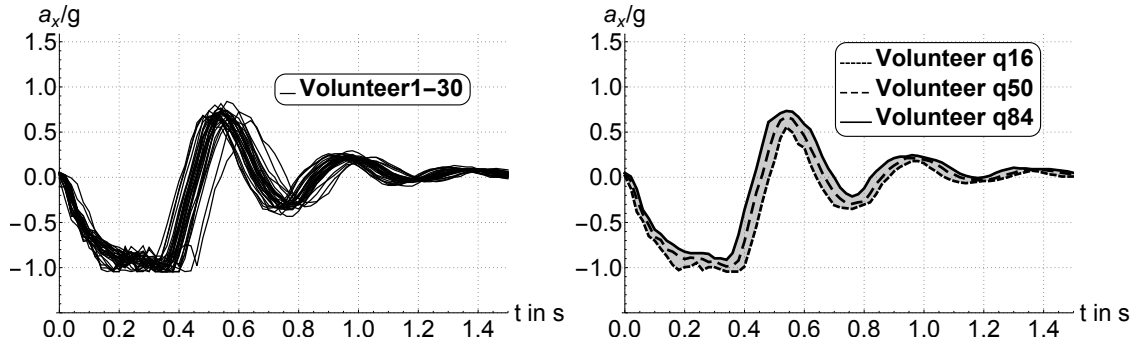

(a) Vehicle acceleration a_x (b) Vehicle acceleration a_x corridor

Figure 4.12.: Vehicle acceleration a_x for emergency braking at 12 km/h for 30 investigated volunteers

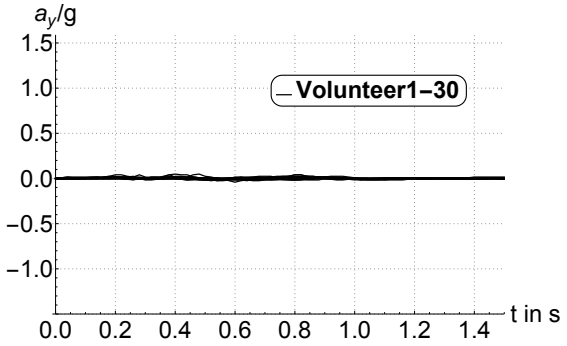

Figure 4.13.: Vehicle acceleration a_y for emergency braking at 12 km/h for 30 investigated volunteers

Due to the large number of volunteers investigated, it was decided that the simulation would concentrate on representative subjects.

The results of three simulations close to the outer bounds and the median of the relative torso angle are presented here. Depending on their peak angles, volunteers were referred to as *slack*, *average* and *tense* types (see Fig. 4.14). For the three different simulations, the following controller parameters were used:

Table 4.5.: Overview of *slack type* controller parameters for torso and head/neck for frontal emergency braking maneuver with lap belt at 12 km/h

Segment name	**Controller parameter name**				
	$K_{p,Low}$	$K_{d,Low}$	$K_{p,High}$	$K_{d,High}$	Tr in s
Head and neck	149.72	29.81	49.18	11.29	0.13
Torso and upper extremities	120.54	1.10	10.06	23.96	0.13

Table 4.6.: Overview of *average type* controller parameters for torso and head/neck for frontal emergency braking maneuver with lap belt at 12 km/h

Segment name	**Controller parameter name**				
	$K_{p,Low}$	$K_{d,Low}$	$K_{p,High}$	$K_{d,High}$	Tr in s
Head and neck	188.06	29.97	21.83	29.93	0.10
Torso and upper extremities	26.67	1	10	2.17	0.10

Table 4.7.: Overview of *tense type* controller parameters for torso and head/neck for frontal emergency braking maneuver with lap belt at 12 km/h

Segment name	**Controller parameter name**				
	$K_{p,Low}$	$K_{d,Low}$	$K_{p,High}$	$K_{d,High}$	Tr in s
Head and neck	196.16	30	39.81	29.90	0.13
Torso and upper extremities	1.49	1	10	7.37	0.13

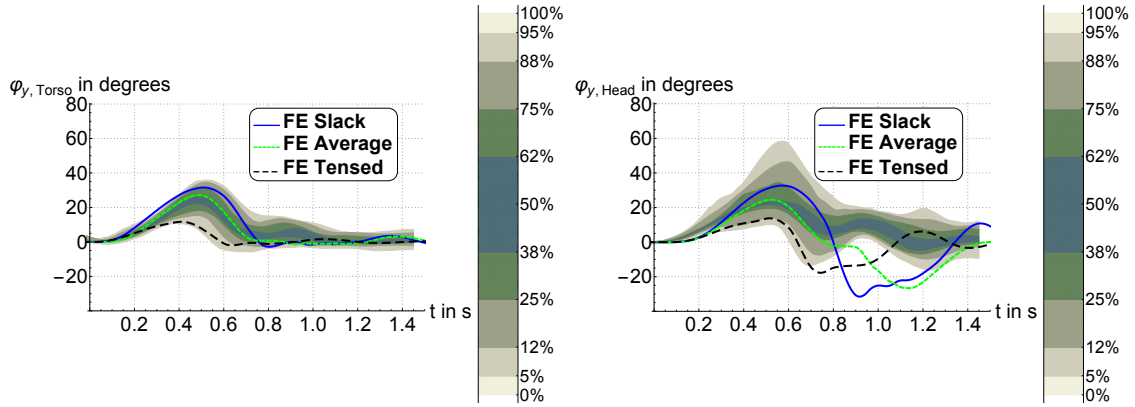

(a) Relative torso angle

(b) Relative head angle

Figure 4.14.: Overlay of relative torso and relative head angle volunteer corridor and FE model responses for *slack*, *average* and *tense* volunteer type for emergency braking maneuver at 12 km/h

Figure 4.14(a) shows the three FE simulation model angles for the torso plotted over the derived corridors. The legend on the right hand side of Fig. 4.14(a) and (b) shows the quantiles, including all investigated volunteers. The FE simulation model responses for relative torso and head angle lie within the corridors derived from the volunteer tests. The volunteer relative torso angle shows a maximum of 35.8 degrees at 0.54 s, whereas the minimum value was 0.6 degrees. As the data reveals, it was possible to achieve the main aim of simulating the outer bounds and the median value of the the volunteer responses. Simulation focussed on the phase up to about 0.6 s, which was the point in time when the vehicle stopped. After this phase, an oscillation in the acceleration signal was observed, which was also seen in the volunteer torso and head responses.

Figure4.14(b) shows the three FE simulation model relative head angles plotted over the derived corridors. The FE simulation model responses show good accordance with volunteer data for relative head angle as well. The corridor plot for the relative head angles shows the differences in the volunteer responses. Whereas about 68 percent of the volunteers remained within a range of 20 degrees , the consideration of all volunteers shows differences of more than 51.3 degrees. This indicates the differences in individual responses.

4.3. Vehicle tests and 2.5D vehicle model

As stated above, the vehicle tests in test series B were an extension of the tests of series A, but with more complex boundaries. Tests were again performed on a closed test track with a professional test driver, and six different maneuvers were investigated:

emergency braking maneuvers at 12 km/h and 50 km/h, a lane change maneuver to the left at 50 km/h, a lane change to the right at 50 km/h, and combined (braking and steering) maneuvers to the left and the right at 50 km/h. As with vehicle test series A, the first maneuver, with occupants in an *unaware* state, was investigated. The objective of the simulation for this test series was to verify the applicability of the 2.5D modeling approach. This approach superpositions two planar controllers. Due to the symmetry of the seat and the lock of the rotational degree of freedom around the vertical model axis, results are presented for the braking maneuver, the lane change maneuver to the left and a combined maneuver to the right.

4.3.1. Emergency braking maneuver at 12 km/h

As with testing series A, the maneuvers were investigated in terms of their repeatability. Figure 4.15(a) shows the longitudinal acceleration a_x and Fig. 4.16 the lateral acceleration a_y time histories for the emergency braking maneuver at 12 km/h. The peak longitudinal acceleration a_x was -1.04g, whereby two volunteers showed smaller acceleration levels with maximums of 0.8g and 0.9g. Once again, the lateral acceleration a_y was zero. Figure 4.15(b) shows the derived acceleration corridors for the frontal braking maneuver in testing series B. The difference between the minimum and maximum value at 0.2 s is 0.26g.

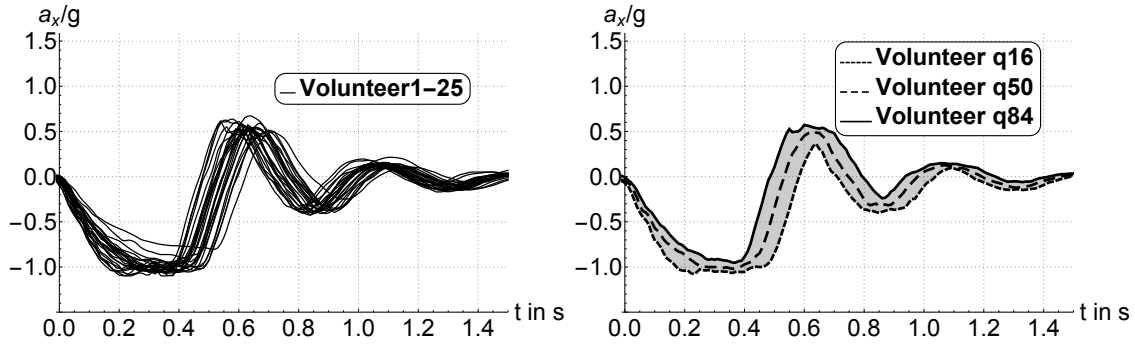

(a) Vehicle acceleration a_x

(b) Vehicle acceleration a_x corridor

Figure 4.15.: Vehicle acceleration a_x for emergency braking at 12 km/h for 25 investigated volunteers

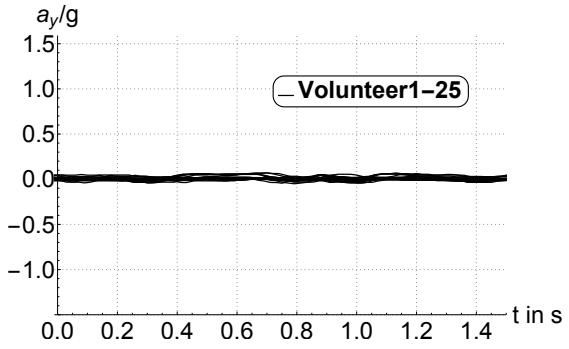

Figure 4.16.: Vehicle acceleration a_y for emergency braking at 12 km/h for 30 investigated volunteers

Figure 4.17 shows the longitudinal velocity v_x for 25 volunteers. The initial vehicle velocity was between 11 and 15 km/h.

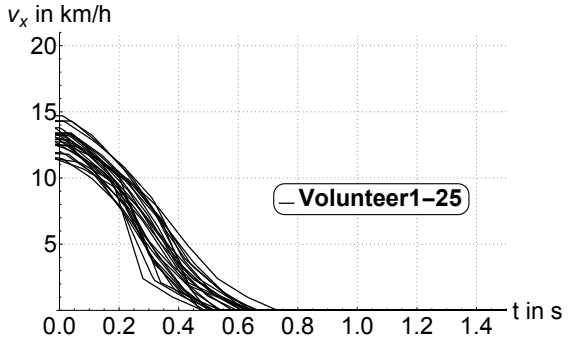

Figure 4.17.: Vehicle longitudinal velocity v_x for 25 investigated volunteers

For the simulation, the aim was to determine if the 2.5D approach can simulate the identified volunteer kinematics of torso and head. Table 4.8 shows the set of controller parameters used. Because it was possible to use a planar modeling approach, controller values are only shown for controlling the model in the dominant acceleration direction.

Table 4.8.: Overview of frontal controller parameters for torso and head/neck for frontal emergency braking maneuver with three-point belt at 12 km/h

Segment name	**Controller parameter name**				
	$K_{p,Low}$	$K_{d,Low}$	$K_{p,High}$	$K_{d,High}$	Tr in s
Head and neck	66.89	29.86	159.78	29.99	0.10
Torso and upper extremities	2.48	10.09	10.30	1.85	0.10

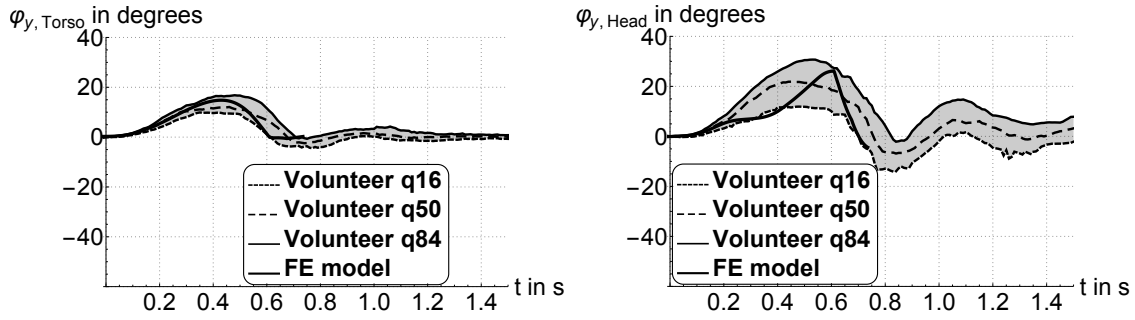

(a) Relative torso angle

(b) Relative head angle

Figure 4.18.: Overlay of relative torso and relative head angle volunteer corridor and FE model for emergency braking maneuver at 12 km/h

Figure 4.18(a) shows an overlay of the relative torso angle corridor based on 25 subjects and the FE model response. As the figure shows, the FE model response remains within the volunteer corridor and shows a maximum of 14.8 degrees after 0.42 s. Furthermore, the simulation ended after about 0.9 s. Therefore, the vehicle rebound phase was not simulated, because the vehicle already had a velocity of zero km/h, and the subsequent acceleration characteristic is vehicle dependent.

Figure4.18(b) shows an overlay of the relative head angle corridor based on 21 subjects and the FE model response. As with the relative torso angle, the relative head angles also lie within the corridor, except for a short phase after 0.3 s.

4.3.2. Lane change maneuvers to the left and right at 50 km/h

The second load case investigated was the lateral maneuver. Lateral maneuver was a lane change maneuver to the left and the right sides at 50 km/h. Figure 4.19(a) shows the longitudinal acceleration a_x for a lane change maneuver to the left. The figure shows that a_x was close to zero for this maneuver. The same holds true for the longitudinal acceleration a_x for a lane change maneuver to the right, which is shown in 4.19(b).

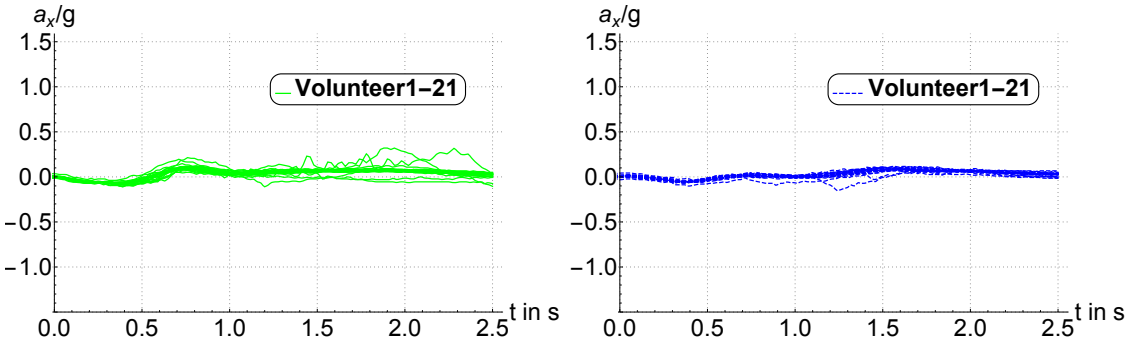

(a) Vehicle acceleration a_x

(b) Vehicle acceleration a_x

Figure 4.19.: Vehicle acceleration a_x for lane change maneuvers to the left (a) and to the right(b) at 50 km/h for 21 investigated volunteers

Figure 4.20 shows an overlay of the lateral acceleration a_y for the lance change to the left (solid green) and to the right (blue dashed). This figure shows that lateral acceleration was the dominant one within this maneuver, and the peak accelerations for both sides were about 1g.

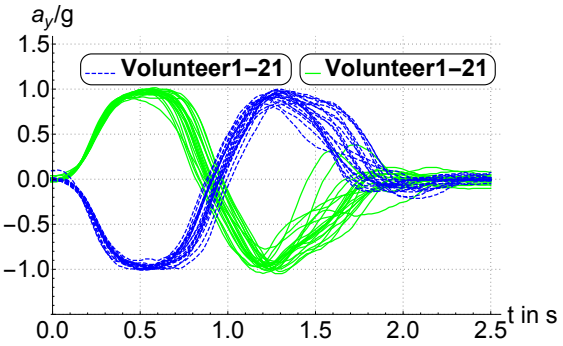

Figure 4.20.: Overlay of vehicle acceleration a_y lane change to the left (solid green) and to the right (blue dashed) for 21 investigated volunteers

Maneuver longitudinal velocities for both maneuvers can be seen in Fig. 4.21. The initial velocities for the lane change maneuver to the left and to the right for 21 volunteers were between 48 km/h and 50 km/h, and there was no braking for this maneuver. The decrease in speed is a result of the steering and the lane change of the vehicle.

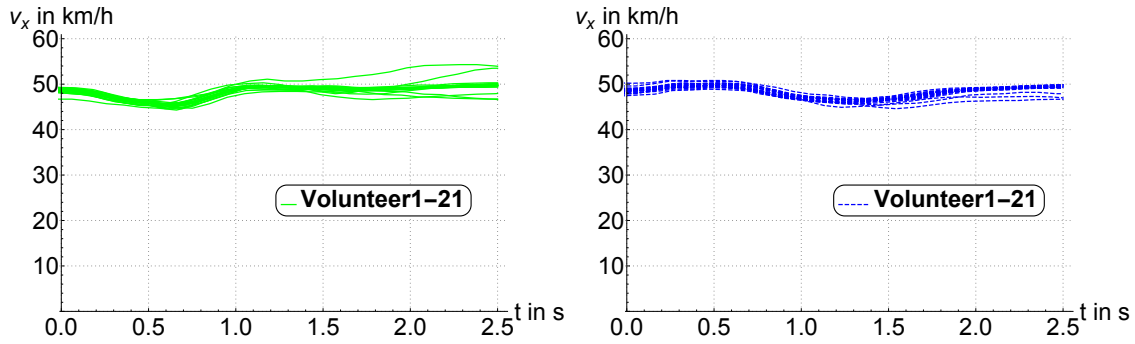

(a) Vehicle velocity v_x (b) Vehicle velocity v_x

Figure 4.21.: Vehicle velocity v_x for lane change maneuvers to the left (a) and to the right(b) at 50 km/h for 21 investigated volunteers

Due to the symmetry of the maneuvers, Fig. 4.22(a) only shows the acceleration corridor for the lane change to the left. The corridor shows a difference of less than 0.05g between 16 percent and 84 percent quantile. Figure 4.22(b) shows the corridor for the steering wheel angle. The maneuver was initiated by a steering of about 200 degrees to the left. After 0.4 s, the counter-steering to stabilize the vehicle begins. This phase lasts for about 0.7 s. The last part of the maneuver was returning the steering to the neutral position, which is reached after 1.8 s.

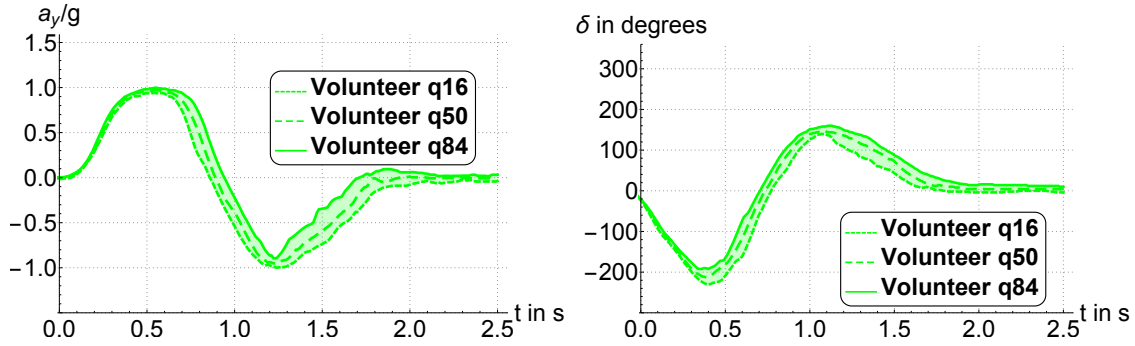

(a) Vehicle acceleration a_y corridor (b) Steering wheel angle δ corridor

Figure 4.22.: Vehicle acceleration a_y and steering wheel angle δ for lane change maneuvers to the left at 50 km/h

Due to the symmetry of the acceleration characteristics to the left and to the right, and the fact that the symmetry of the modeling approach omitted the belt influence and therefore the rotation around the vertical axis, the simulation concentrated on one load case. Simulation results are shown for the lane change to the left. Table 4.9 shows the parameters that were used for simulation.

Table 4.9.: Overview of lateral controller parameters for torso and head/neck for lane change maneuver to the left with three point belt at 50 km/h

Segment name	**Controller parameter name**				
	$K_{p,Low}$	$K_{d,Low}$	$K_{p,High}$	$K_{d,High}$	Tr in s
Head and neck	126.10	28.00	78.92	24.26	0.11
Torso and upper extremities	55.72	18.92	10.01	21.31	0.11

Figure 4.23(a) shows an overlay of the volunteer relative torso angle corridor and the FE model response. The simulation model and volunteer relative angle characteristics are completely different. Whereas the median of the volunteer data shows a magnitude of 13.4 degrees within the first phase, simulation model response shows only 1 degree of this magnitude.

Figure 4.23(b) presents an overlay of the volunteer relative head angle corridor and the FE model response.The simulation model shows different characteristics for relative head angle as well. The volunteer head remains in the upright position. The simulation model shows a maximum of 15.65 degrees .

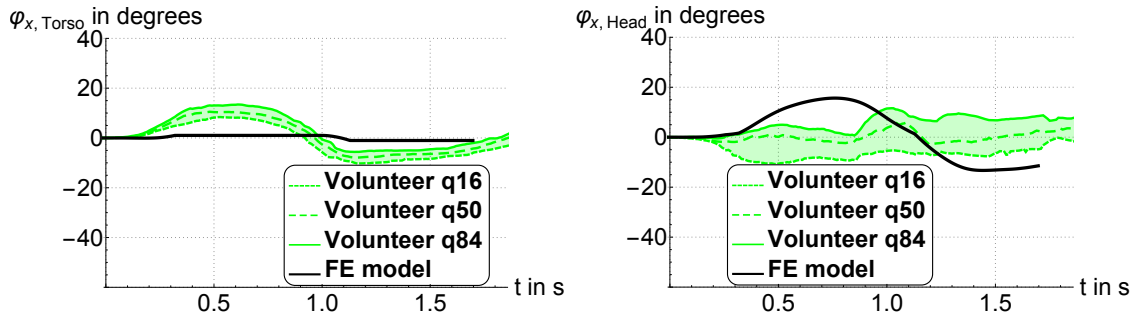

(a) Relative torso angle

(b) Relative head angle

Figure 4.23.: Overlay of volunteer relative torso and relative head angle corridor and FE model for lane change maneuver to the left at 50 km/h

4.3.3. Combined maneuver to the left and right at 50 km/h

The combined maneuvers were the new maneuvers compared to vehicle test series A and also compared to the current state of the art. Hence, these maneuvers extended the range of total investigated maneuvers and showed the necessity of having a model which can imitate the volunteer 3D movement. Figure 4.24(a) shows the longitudinal acceleration a_x for the combined maneuver to the left and Fig. 4.24(b) for the combined maneuver to the right. Compared to the lane change maneuver, a_x was not zero. This was due to the

combination of braking and steering resulting in a longitudinal and lateral acceleration. Due to the initial velocity of 50 km/h, this maneuver lasted for approximately 1.5 s. Once again, the same holds true for longitudinal acceleration of the combined maneuver to the right, as shown in Fig. 4.24 (b).

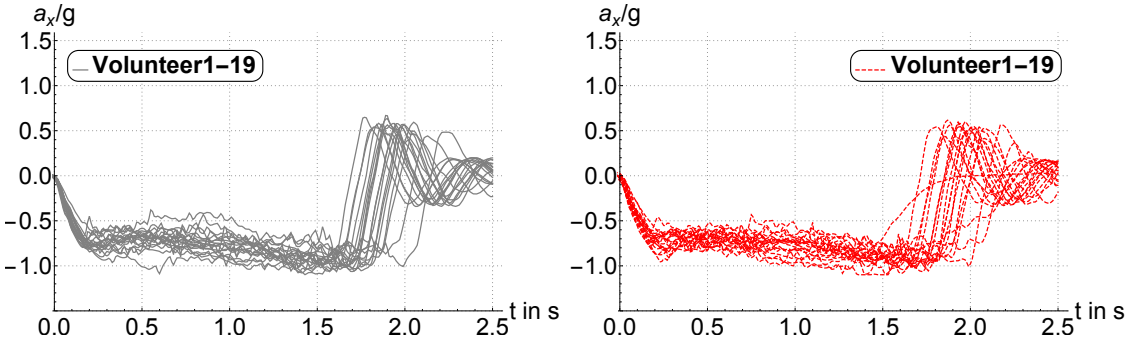

(a) Vehicle acceleration a_x (b) Vehicle acceleration a_x

Figure 4.24.: Vehicle acceleration a_x for combined maneuvers to the left (a) and to the right(b) at 50 km/h for 19 investigated volunteers

Figure4.25 shows an overlay of the lateral acceleration a_y for the combined maneuver to the left and to the right. Compared to the lane change maneuver, the lateral acceleration component a_y did not reach the maximum of 1g. The peak acceleration for maneuvers to the left and right was about 0.85g. The long duration of the maneuver can be observed for this acceleration component.

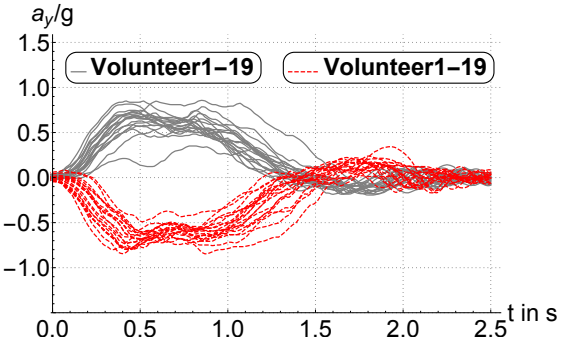

Figure 4.25.: Overlay of vehicle acceleration a_y combined to the left in gray solid and to the right in red dashed line for 19 investigated volunteers

Figure 4.26(a) and (b) show te velocity time histories. The initial vehicle velocity average was 49 km/h. After about 2.0 s, the vehicle had stopped. Few volunteers reached the point with a vehicle velocity of 0 km/h after 2.2 s.

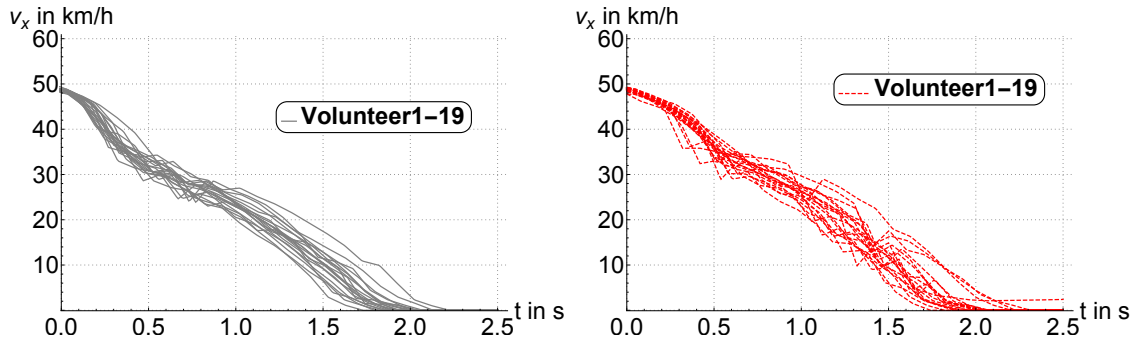

(a) Vehicle velocity v_x

(b) Vehicle velocity v_x

Figure 4.26.: Vehicle velocity v_x for combined maneuvers to the left (a) and to the right(b) at 50 km/h for 19 investigated volunteers

Here again, due to the symmetry of the maneuvers, corridors are only presented for the maneuver to one side. Figure 4.27(a) shows the derived acceleration corridor for a_x and 4.27(b) the derived acceleration corridor for ay for the combined maneuver to the right side. As the chart shows, 68 percent of the volunteers longitudinal and lateral accelerations up to 1.7 s lie within 0.2g, which demonstrates the high repeatability of the maneuver.

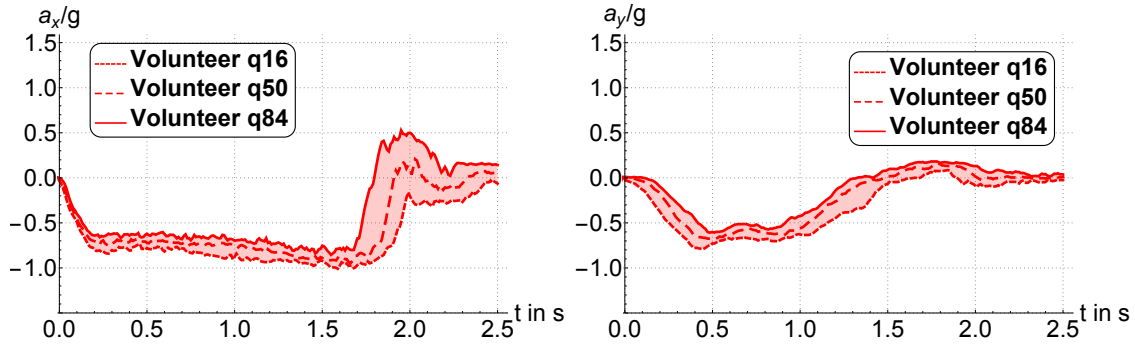

(a) Vehicle acceleration a_x corridor

(b) Vehicle acceleration a_y corridor

Figure 4.27.: Vehicle velocity v_x for combined maneuvers to the left (a) and to the right(b) at 50 km/h for 19 investigated volunteers

Due to the maneuver symmetry and the simplification of locking the degree of freedom around the vertical axis, the simulation results are once again presented for one maneuver side. Due to the belt influence, which restricts volunteer movement to the right side, the maneuver to the right was chosen which causes a volunteer movement to the left. Table 4.10 shows the controller parameters used for simulation. In contrast to the other load cases presented, the simulation of this load case required the use of a controller

superposition. The name of the segment indicates whether controller parameters were used for frontal or lateral controller.

Table 4.10.: Overview of frontal controller parameters for torso and head/neck for combined maneuver to the right with three-point belt at 50 km/h

Segment name	**Controller parameter name**				
	$K_{p,Low,f}$	$K_{d,Low}$	$K_{p,High}$	$K_{d,High}$	Tr in s
Head and neck front	177.26	29.34	24.69	28.96	0.10
Torso and upper extremities front	40.86	24.73	10.03	11.40	0.10
Head and neck lateral	17.02	2.46	83.86	14.67	0.10
Torso and upper extremities lateral	48.15	20.81	107.11	25.10	0.08

Figures 4.28(a) and 4.28(b) show an overlay of the relative torso and head angle around the global y-axis volunteer corridor and the FE model response. Figures 4.29(a) and 4.29(b) show an overlay of the relative torso and head angle around the global x-axis volunteer corridor and the FE model response. Due to the combined maneuver, two angles must be considered for torso and head. The first one is around the y-axis representing the volunteer and model forward movement, the second one is the rotation around the x-axis representing volunteers' and models' lateral rotational movement. For the relative torso angle around the y-axis, the FE simulation characteristic and volunteer response show good accordance up to after about 0.4 s. The volunteer response shows a local maximum of 6 degrees after 0.3 s, whereas the simulation model reaches a global maximum of about 8.6 degrees after 0.49 s. After this point in time, the simulation model show a decrease in relative torso angle up and reaches its initial position after 1.8 s. The volunteer characteristics show a global maximum after 1.84 s with a value of 8.3 degrees. Volunteers reach their initial position after 2.02 s.

For relative head angle around the y-axis, the simulation model response cannot reproduce the long-lasting plateau of volunteer response with a duration of 1.5 s. The relative torso angle around the x-axis remains within the volunteer corridors and shows a minimum of -10.4 degrees. For relative head angle around the x-axis, the simulation model response is within the corridors identified during volunteer tests. The comparison of the relative torso and head angles shows the larger variations in the volunteer responses.

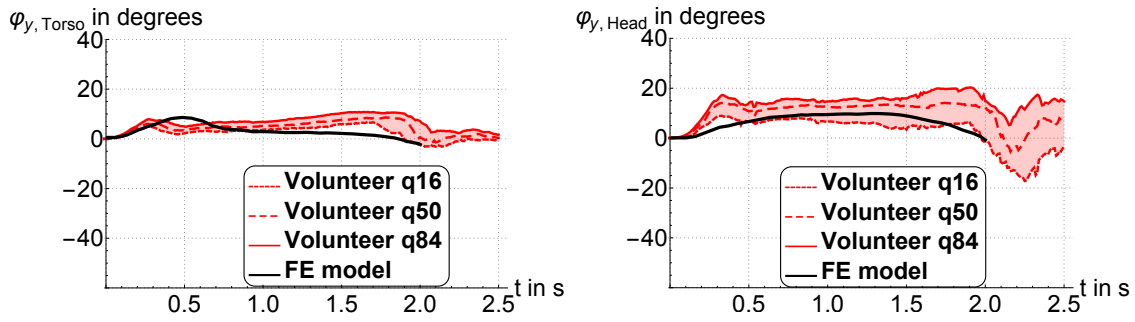

(a) Relative torso angle (b) Relative head angle

Figure 4.28.: Overlay of volunteer relative torso and relative head angle corridor around global y-axis and FE model for combined maneuver to the left at 50 km/h

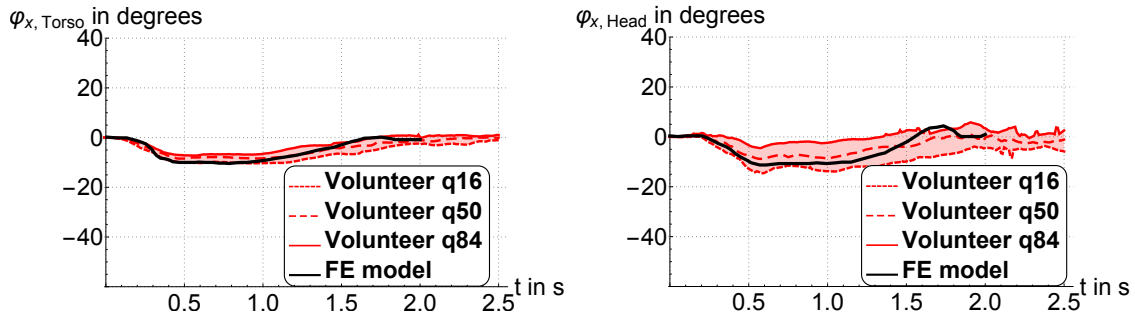

(a) Relative torso angle (b) Relative head angle

Figure 4.29.: Overlay of volunteer relative torso and relative head angle corridor around global x-axis and FE model for combined maneuver to the left at 50 km/h

5. Discussion

5.1. Discussion of movement studies

The movement studies performed within this thesis were designed to determine the occupant kinematics during several maneuvers. The aim of the movement studies was to collect data for the development of the methodology for incorporating reactive occupant kinematics. As explained above, the volunteer anthropometry, relevant load cases and boundary conditions were chosen based on the simulation. The volunteer experiments conducted were divided into three test series. The maneuvers will be discussed in chronological order.

5.1.1. Choice of relevant load cases

As stated in section 3.2, relevant load cases were determined based on traffic safety data from 2008, published by NHTSA [Adm08]. Specifically, the accident statistics were prioritized by the initial point of impact in the total number of crashes, including single-vehicle and multiple-vehicle crashes, and three different crash severities: fatal, injured and property damage only. Based on this information, the load cases for the movement studies were derived. The data published by NHTSA does not contain detailed information on the driving state, the primary safety features of the vehicle or the awareness states of the drivers. Therefore, this data also includes accidents where the driver may have been distracted and no actions prior to the collision took place, or one or several primary safety measures may have intervened, thereby changing the accident outcome. Hence, a wide range of possible set-ups of the collision opponents and driving states could lead to such initial points of impact. To derive the load cases presented in this thesis, it was assumed that the driver was fully aware of the upcoming accident before the collision. Furthermore, it was assumed that the drivers attempted to avoid the accidents with or without the aid of primary safety features by actively steering, braking or performing combined maneuvers. This assumption is also supported by the data presented by [EZO$^+$09], which was obtained from the Institute for Traffic Research and Data Analysis (ITARDA) in Japan from 1993-2004. For 52% of a total of 860 frontal impacts, the driver performed an evasive braking or steering action. The emergency braking and the single lane change maneuver were chosen due to volunteer safety and the repeatability of the tests.

5.1.2. Sled tests

Sled tests were carried out on a crash test bench. The occupant kinematics under laboratory conditions were investigated for velocities of about 12 km/h for frontal emergency braking and about 10 km/h for the lateral maneuver. This was due to the combination of the reference seat with the "lap-belt-only" configuration, which made it necessary to decrease the test velocity in order to avoid possible injuries. The investigated frontal velocity difference of Δv= 12 km/h is slightly higher than those reported by Beeman et al. [BKMD11] and Kemper et al. [KBMD14], who used a velocity difference of Δv= 10 km/h for their medium severity load cases at 5g. In contrast to these studies, occupants were tested in an inverse test set-up. Furthermore volunteers were instructed to keep their arms resting on their thighs, similar to the study presented by [ABS$^+$09]. Acceleration level of 0.8g for frontal studies is significantly lower than the acceleration levels investigated in the studies above and equal to the study presented by [EZO$^+$09].

The lateral sled maneuver presented within this thesis is comparable to a study published by Ejima et al. in 2012 [EIS$^+$12]. Based on three male volunteers, they also investigated the effects of pre-impact swerving/steering on the physical motion of the volunteer in the low-speed side impact tests. Tests also used a rigid seat without lateral support, and volunteers were secured to the seat using a lap belt. In addition to the load case investigated within this thesis, which focused on an acceleration of 0.4g and a relaxed muscle state, Ejima et al. investigated two acceleration levels of 0.4g and 0.6g, as well as a relaxed and a tensed muscle state. In general, the investigated accelerations of about 0.8g for the emergency braking maneuver and 0.4g for the lateral maneuver are smaller than those identified during vehicle test series A and B, and the subset of investigated volunteers was significantly smaller. Nevertheless, the test data can be used, especially for the first modeling steps (i.e., evaluating the co-simulation approach and the joint modeling, as well as the muscle/actuator implementation).

The results presented for the four volunteers whose kinematics were determined using a Vicon motion capture system showed large variations in the acceleration characteristics of the sled, especially from the beginning of the maneuver up to about 0.3 s for emergency braking and lateral maneuver. Although the difference between the acceleration characteristics up to 0.3 s is smaller for the lateral maneuvers due to the lower peak acceleration levels which should be reached for such cases, there is still a maximum difference of 0.1g for lateral maneuver after 0.2 s. The test bench controller did not allow for changing the characteristics of the accelerations. Hence, the original goal of using a ramp acceleration characteristic could not be achieved. The results of volunteer kinematics for emergency braking for two volunteers showed differences for duration, as well as for the peak angles for torso and head. Due to the differences in acceleration characteristics, it was not possible to determine whether the source of these differences was the acceleration or the individual contributions of the subjects. Furthermore, the volunteer preparation process and the laboratory set-up may also have affected volunteer kinematics. These influences could not be quantified. However, the measured EMG signals did not show bracing effects before testing.

The relative torso angles of the lateral sled maneuvers were compared to the angle values reported for T1 by Ejima et al. The two investigated volunteers showed a relative torso angle of 11 and 17 degrees, which was less than the average value of 22 degrees reported by Ejima et al. For the head center of gravity, Ejima et al. reported an average value of 15 degrees, which is in good accordance with the relative head angles identified within this thesis: 13 and 15 degrees.

5.1.3. Vehicle tests

Vehicle testing was a major step for generating high quality data for a bigger subset of the 50^{th}-percentile male population. In contrast to the sled test series, this testing part was performed on a closed test track. A reference seat was mounted in a production car, a Mercedes-Benz S-500 with a modified passenger door, a removed windshield and Vicon cameras mounted on a frame on both the vehicle roof and the hood of the car.

The vehicle tests were performed with a professional driver. Using a driver instead of a robot or an automated system may cause problems regarding the repeatability of the maneuvers. However, the results demonstrated the high repeatability and therefore the quality of the collected data within the movement studies of this thesis. Acceleration levels were close to 1g (10.0 ± 0.3 m/s^2). This is about the maximum value which can be reached with a production car with conventional tires on a dry track with standard asphalt.

The acceleration characteristics for emergency braking at 12 km/h show a change in sign after about 0.6 s. At this point in time, the plot of the vehicle velocity already indicates the stand-still of the car. Acceleration after this point in time is the result of vehicle kinematics due to inertia, elasticities and chassis suspension.

For the lane change maneuver, a median peak acceleration close to 1g was also reached. The whole lane change maneuver was divided into two phases: an initial maneuver phase and a counter-steering phase. In the first phase, the maneuver was initiated by a steering wheel rotation of about 200 degrees. After this phase, the steering wheel was rotated by about 360 degrees in order to stabilize the vehicle and return the steering wheel to the initial position. Each of these two phases lasted for about 0.9 s, leading to a total maneuver duration of 1.8 s. In particular, in the first phase of the first part of the maneuver up to 0.55 s, the fact that $2\,\sigma < 0.1$g for lateral peak acceleration shows the high repeatability. Within the second phase, the spread is larger, resulting in a standard deviation of $2\,\sigma = 0.18$g for lateral peak acceleration. This difference is mainly explained by differences in the timings of the counter-steering.

For the combined maneuver, which was a combination of steering and braking, a decrease of the maximum acceleration in the longitudinal direction and an increase in the lateral acceleration can be observed. These can be explained by the limitation of the combined tire forces (see [HW13]). Due to the higher velocity of 50 km/h , the whole maneuver lasts for about 2 s.

As is evident, the total number of volunteers investigated per maneuver changes, due to the fact, that occupant kinematics data was not available for all volunteers. Acceleration and velocity data was presented for the *unaware* volunteer state. The choice to focus on the unaware condition was based on the findings from this test series. In 2011, Kirschbichler et al. [KSP+11] stated that with repeated maneuvers, the forward excursions decreased. Although this effect was not observed for all sled test volunteers, it was hypothesized that the cause of the decrease might be some habituation or training effect due to the knowledge of the maneuvers. The small number of 11 volunteers did not allow to prove this on a valid data basis. The movement studies of test series A were used to determine if the variation in duration and peak values for relative torso and head angles could also be observed for a larger subset of the 50^{th}-percentile male population. Whereas the increased number of volunteers addressed the inter-subject differences, the intra-subject differences were investigated using the three different awareness states. These awareness states were *unaware*, *anticipated* and *informed*. Kirschbichler et al. [KHP+14] presented a comparison of the maximum relative excursion of the torso and head in the frontal direction for vehicle test series A and series B, as well as the maximum relative excursion in the lateral direction for the lane change maneuver. The white line in the middle of the colored box represents the median. Furthermore, the 25 percent and 75 percent quantiles (lower and upper limits of the box), the extreme values indicated by error bars and the number of subjects are shown. Figure 5.1 shows the results of the analysis performed by Kirschbichler et al. [KHP+14] for the frontal emergency braking maneuver, and Fig. 5.2 for the lateral maneuver. The legend shows the investigated awareness states *unaware, anticipated and informed* for the emergency braking maneuver in vehicle test series A at 12 km/h, as well as the *unaware* condition of series B at 50 km/h. The abbreviation *rep*, which stands for repeated test of the emergency braking maneuver of series B at 12 km/h, is comparable to the *anticipated* condition of series A. For the emergency braking maneuver at 50 km/h, only the first trial, which was an *unaware* condition, is shown. The data for the frontal maneuvers shows that the median for maximum relative frontal torso excursion and head decreased from the *unaware* to the *informed* awareness state. Thus, with increasing knowledge of the maneuver, there was a tendency that the median head and torso excursion decreased, but the spread between volunteer kinematic response also increased. The lower forward torso excursions for the emergency braking maneuvers in series A and B at 12 km/h show the influence of the belt system on torso kinematics. As stated above, different boundary conditions were used for these two load cases: a lap belt and seat without lateral support for vehicle test series A, and a three-point belt and seat with lateral support for vehicle test series B. Based on these results for the emergency braking maneuvers, the simulation model development and validation focussed on the *unaware* state due the larger volunteer torso and head excursions that are particularly relevant for secondary safety measure development. However, the presented simulation methodology is not limited to the *unaware* state. For the single lane change maneuvers, no clear trend with respect to awareness state could be identified.

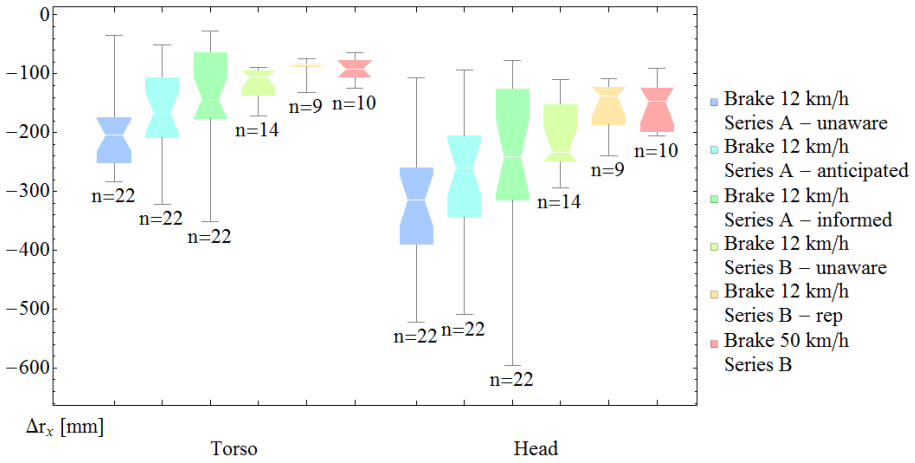

Figure 5.1.: Comparison of relative torso and head center point forward excursion Δr_x for frontal maneuver for different awareness states and for the two vehicle test series A and B [KHP+14]

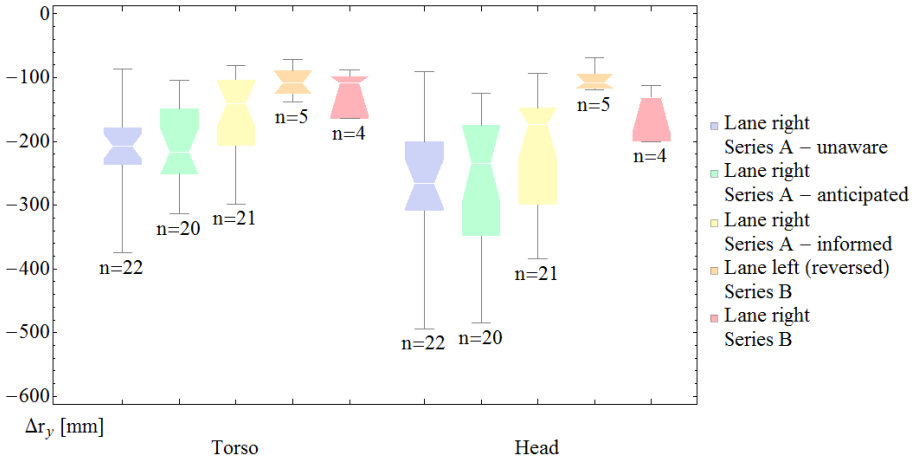

Figure 5.2.: Comparison of relative torso and head center point forward excursion Δr_y for lateral maneuver for different awareness states and for the two vehicle test series A and B [KHP+14]

In addition to human volunteer testing, another goal was to test the hypothesis that the dummy is too stiff to be used within the pre-collision phase. Therefore, a HybridIII dummy was also put into the same suit as the volunteers, equipped with reflective markers, and placed in the vehicle according to the 50$^{\text{th}}$-percentile positioning procedure for crash test application. In order to reduce possible errors caused by movement of the dummy, maneuvers were performed three times with a re-positioning between the tests. Figure 5.3(a) shows an overlay of the relative torso angles of three dummy emergency

braking trials at 12 km/h and the volunteer corridors, and Fig. 5.3(b) shows the relative head angles of three dummy trials overlayed with volunteer corridors. As the figures show, the dummy response up to 0.5 s shows slight differences. The volunteer corridor with a relative torso angle average maximum of 12 degrees and a relative head angle average maximum of 17 degrees, represents a stiff behavior. Dummy response was also investigated for the lane change maneuver at 50 km/h. Figures 5.5(a) and 5.5(b) show the overlays of HybridIII dummy relative torso angles and relative head angles with volunteer corridors for the lane change maneuver. Especially for the lane change maneuver the main weakness of the dummy is evident. For the lane change maneuver at 50 km/h, the dummy moves to the side and remains in this position after about 1.2 s. Safety measures developed based on this position would not adequately protect a human being. The dummy tests, show the importance of volunteer data and a simulation model capable of reproducing volunteer data for a lap belt only configuration.

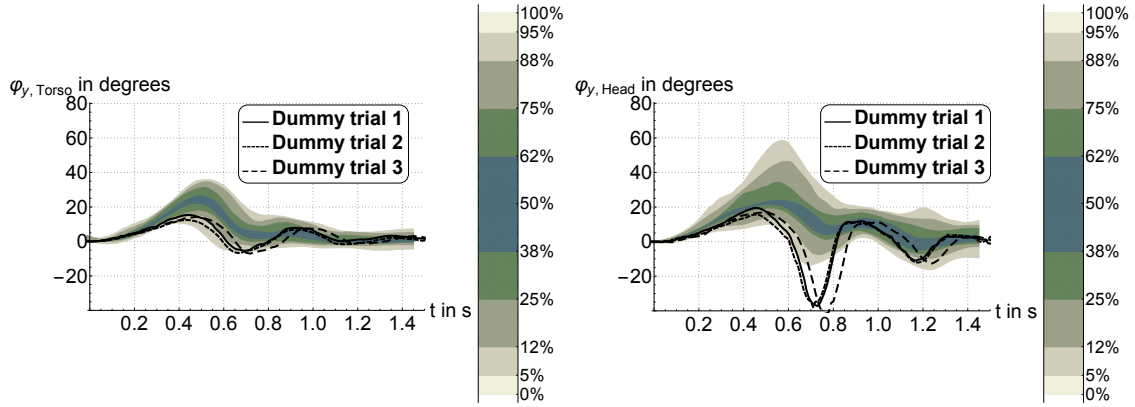

(a) Relative torso angle

(b) Relative head angle

Figure 5.3.: Overlay of relative HybridIII dummy torso angles and volunteer corridor for three emergency braking trials at 12 km/h

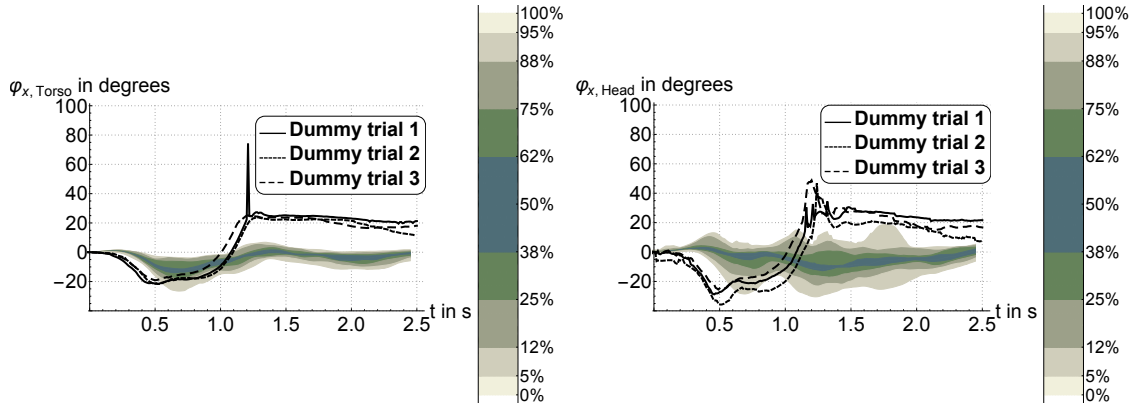

(a) Relative torso angle

(b) Relative head angle

Figure 5.4.: Overlay of relative HybridIII dummy torso angles and volunteer corridor for three lane change trials at 50 km/h

For vehicle test series A, no comparable study with similar boundary conditions and a similar focus on occupant kinematics, has been published to date. The occupant kinematics data of vehicle test series B is similar to the study performed by Òlafsdòttir et al. [OsDB13], who have published the results of their investigation into passenger kinematics and muscle responses in autonomous braking events. In this study, kinematics and EMG data for a total of 20 volunteers (11 male and 9 female) was collected. Vehicle frontal accelerations were comparable to the vehicle test series B presented within this thesis. Volunteers were also subjected to acceleration pulses of about 1.1g, and the initial vehicle velocity was 70 km/h, with the objective to achieve a Δv of 50 km/h. In contrast to vehicle test series B, where braking was initiated by an experienced driver, the maneuvers presented in this study were initiated autonomously. Furthermore, the maneuvers were performed on light-traffic public roads. As with the current study (Mercedes S500), a production car (Volvo V60 T4) was used. They replaced the standard seat belt with an Active Seatbelt retractor, which allowed for reversible pre-tension but could also be used in passive mode without tension. The upholstered leather seat was not altered.

Table 5.1 shows a comparison of the the volunteer subject information presented within this thesis for vehicle test series B and data presented by Òlafsdòttir et al. As the table shows, the data on autonomous braking without pre-tension was also collected for female and male volunteers with comparable mass and height. Hence, the kinematics results could be compared.

The torso and head excursions for vehicle test series B were presented by Kirschbichler et al. in 2014 [KHP+14]. The subjects' torso forward excursion for frontal braking maneuver at 50 km/h of -93±20 mm are smaller than the values presented by Òlafsdòttir et al., which found average values of about 140 mm for male and female subjects. In addition, the average forward head excursion of -151±43 mm was smaller than the values

Table 5.1.: Comparison of average and standard deviation values for volunteer number, gender, mass, height and age, of test series B and data presented by Òlafsdòttir et al. [OsDB13]

Test series B				
Number of volunteers	**Gender**	**Mass in kg**	**Height in cm**	**Age in years**
27	Male	77.8 ± 8.4	179.1 ± 4.7	25.4 ± 9.6
6	Female	63.0 ± 10.4	169.0 ± 4.1	31.5 ± 9.3
Autonomous braking [OsDB13]				
Number of volunteers	**Gender**	**Mass in kg**	**Height in cm**	**Age in years**
11	Male	77.5 ± 5.6	178.2 ± 5.2	32.7 ± 12.5
9	Female	59.4 ± 5.2	166.6 ± 5.0	28.8 ± 5.9

reported by Òlafsdòttir et al., which had an average value of about 200 mm for males and females.[1] In addition to differences in the volunteer responses, deviations in the location of the points used for comparison could also be an explanation.

5.2. Simulation

Chapter 3 explained that a total of three different models were created within this thesis: a 2D sled test model, a 2D vehicle test model and a 2.5D vehicle test model. For the creation of all three models, a THUMS®-D version was used to derive the masses and inertia properties of the surrogate model. As stated above, the main motivations for using surrogate models were the reduction of computational effort and the stiffness of the THUMS®. The stiffness requires modifications of material assignments in order to use it for pre-collision investigations [YWK+14]. This is also in accordance with results presented by Muggenthaler 2006 [Mug06], who concluded that the HUMOS was also too stiff to reproduce low-impact volunteer tests. Changing the material stiffness of the model might lead to a different model response for simulations of the collision phase, and the computational effort is still too high to allow for a controller development. By using the surrogate model, the simulation run was decreased to 1/10 of the original duration using the standard model.

5.2.1. Sled test model

Model development started with sled tests. As described in chapter 3, the presented sled test model used a simplified modeling approach, where the COG of the model was not coincident with the original THUMS®, and the mass moment of inertia values were

[1] Negative value is due to the different coordinate system used

not adjusted to the values identified for THUMS®. Furthermore, the human vertebral column was approximated using a two-segment rigid body model, representing the torso and head/neck segments of the human body. The anatomical details of muscles were not taken into account, and the muscle lines of action were not anatomically correct. Muscle attachment points were fixed to virtual points in space connected to rigid bodies. The results were presented for two unaware volunteers for frontal and for lateral maneuver.

Despite these limitations, the MB and FE model relative angle responses for torso and head for the frontal maneuver presented for the two volunteers can qualitatively reproduce the volunteer characteristics. A quantitative comparison of the FE and MB model responses to volunteer data for the first investigated volunteer showed a delay of 0.05 s for relative torso angle maximum of the simulation model responses. The FE and MB model responses show differences of 0.7 degrees for relative torso angle. For the relative head angle, this difference is in approximately the same range.

The second volunteer response that was simulated showed about twice the relative torso and head angles as the first volunteer. For relative torso angle, the volunteer characteristic was reproduced qualitatively. Once again, the FE and MB model showed differences that might be caused by model differences with respect to the location of the center of gravity. For relative head angle response, FE and MB models did not reproduce the volunteers' kinematics, which showed a backward and forward movement between 0.7 s and 0.8 s that was observed for volunteer1.

For the simulation of the lateral maneuver, the volunteer kinematics could not be reproduced. The FE and MB model responses showed differences of more than 100 percent compared to volunteer data. This shows the inadequacy of modeling the human using only added masses.

5.2.2. Vehicle models

To simulate vehicle test series A and B, two different models were developed. For the model of test series A, the basic concept of the sled test model with respect to joint location, joint modeling and muscle implementation was maintained. Hence, a planar modeling was used again, but with adjusted COG and mass moment of inertia values according to THUMS®-D version with rotated arms and hip. The simulation boundary conditions remained the same, with a lap-belt configuration and a reference seat with no lateral support.

The simulation results were presented for the frontal braking maneuver at 12 km/h, which was prioritized in this model development stage. The simulation of the lateral maneuver was considered to be of lower priority due to the lap-belt and reference seat combination. Due to the small distance between the volunteer and the B-pillar, as well as the missing lateral support, psychological factors may have also influenced volunteer kinematics.

The main objective of the simulation was to determine if the chosen modeling approach was able to reproduce occupant kinematics, especially in the phase from the start of

the maneuver to the relative angle peak values and, partially, the backward movement. Three volunteers representing the whole data set were chosen. Volunteers were chosen based on their relative torso angle peak values. The three volunteers, referred to as *slack*, *average* and *tense* type were close to the outer bounds and median of the data set. Simulation results were presented for the FE simulation model only. The simulation results indicate that the chosen modeling approach in combination with the controller concept can cover the large inter-subject differences observed during vehicle test series A. Volunteer angles show large variations of more than 20 degrees for relative torso angle and about 50 degrees for relative head angle. It is important to mention is that the types identified for relative torso angles do not necessarily have to be the same for relative head angle. Investigation of individual subjects showed variety in torso and head angles. Hence, no trend for the combination of relative torso and head angle could be found.

Vehicle test series B extended the maneuvers of test series A. The configuration change of using a three-point belt and the reference seat with lateral support elements, as well as the consideration of combined load cases, required the development of a new modeling approach because volunteer movement cannot longer be assumed to be planar. To be able to simulate volunteer behavior, the reference seat had to be equipped with lateral support elements, and a three-point belt was integrated. Once again, the seat was modeled as a rigid body omitting the deformation of the reference seat used within the tests. The simulation results for the frontal emergency braking maneuver showed that the relative torso angle response of the 2.5D model is within the volunteer corridor. For the emergency braking maneuver at 12 km/h a time interval of 0.7 s was again investigated because the emergency braking maneuver had already ended after this duration. The relative head angle response was within the corridor, omitting the time interval between 0.3 s and 0.4 s. Although the simulation lies within the corridor, the characteristics are not similar. The volunteers showed a smoother forward and backward movement. This is attributable to the combination of the reaction time and a large actuator force output within the controller, in combination with a decreasing acceleration.

For the lane change maneuvers, the relative torso peak angle is significantly smaller than the identified volunteer corridors. This can be explained by the fact that the THUMS® simulation model makes contact with the lateral support of the seat after 2 degrees of lateral movement. Due to the rigid surface of the seat and the rigid surface of the THUMS® outer surface, there is no deformation of these components. This can also be observed in the characteristics of the head resulting in a larger relative head angle than those of the volunteers. Considering this relative angle plot, one can see that the median volunteer angle is close to zero.

Thus, this thesis shows that the co-simulation in combination with a simplified THUMS® model can be used for pre-collision simulations. Further work must concentrate on the validation of the approach for different HBMs as well as for different codes.

This indicates that the human tries to hold the head in an upright position, despite the fact that the torso shows a change in relative angle. This is in agreement with the results

of the qualitative study by Morris and Cross [MC05]. The results chapter showed the vehicle longitudinal and lateral accelerations, for both the emergency braking maneuvers and the lane change maneuvers. It was demonstrated that the longitudinal accleration was dominant the emergency braking maneuver, while the lateral accelerations were dominant for the lane change maneuver, with the other component being close to zero. For the emergency braking maneuver, this justifies the use of a planar model and controller approach. For the lane change maneuver, a single consideration of the longitudinal and lateral acceleration does not allow for this because the vehicle yaws due to the steering input. Depending on the occupant location with respect to the vehicle center of gravity, this can introduce longitudinal movement components. Hence, the occupant movement components were investigated in order to support the decision to use a planar approach. Figure 5.5 shows the vehicle yaw rate ω corridor for the lane change maneuver to the left.

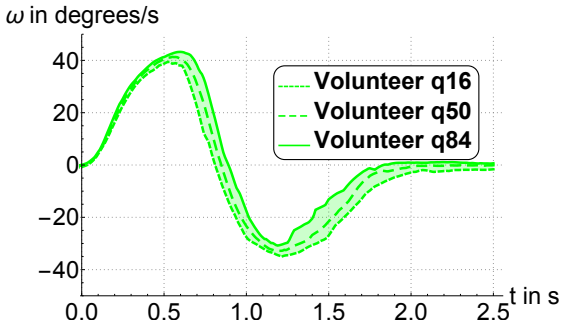

Figure 5.5.: Vehicle yaw rate ω corridor for lane change maneuver to the left at 50 km/h

Figures 5.6(a) and (b) show the displacement components of the torso centroid in the x- and y-directions for the lane change maneuver to the left. Figures 5.7(a) and (b) show the displacement components of the head centroid in the x- and y-direction for the lane change maneuver to the left as well. As with the accelerations, for the displacements, the dominant occupant movement direction for the lane change maneuver is also the y-direction, which justifies the planar modeling and controller approach for lane change maneuver as well.

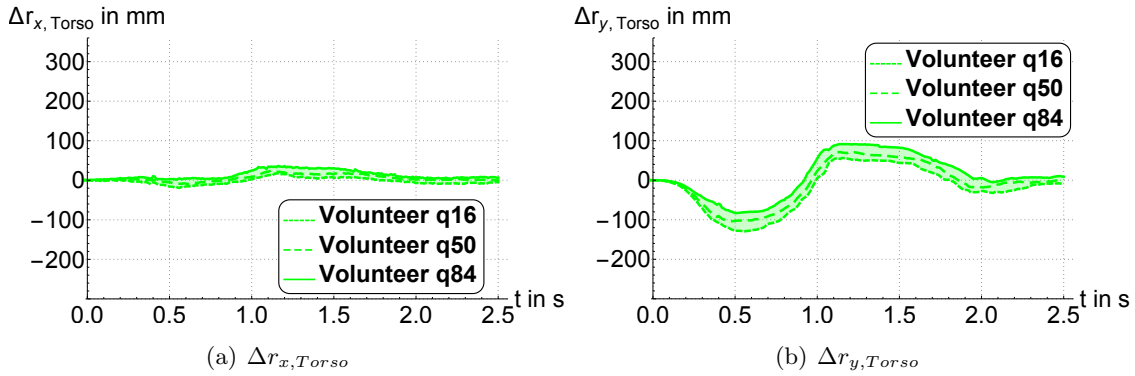

(a) $\Delta r_{x,Torso}$ (b) $\Delta r_{y,Torso}$

Figure 5.6.: Torso segment centroid displacement components $\Delta r_{x,Head}$ and $\Delta r_{x,Head}$ for lane change maneuver to the left at 50 km/h

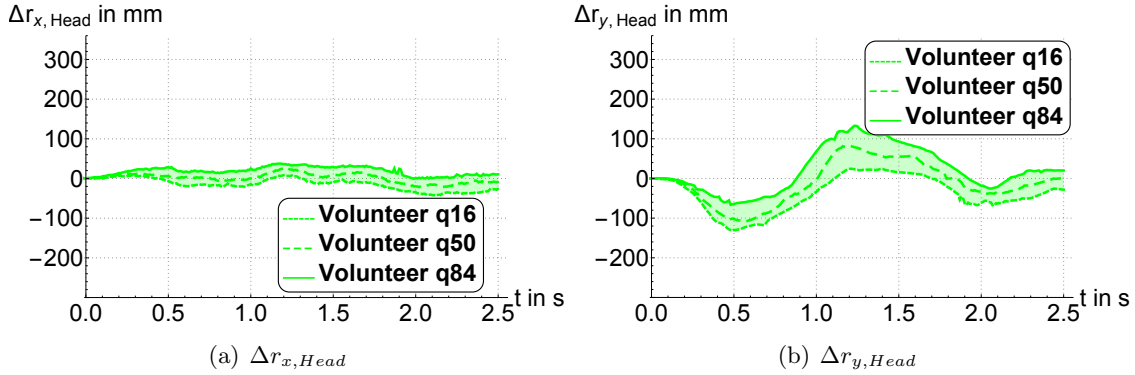

(a) $\Delta r_{x,Head}$ (b) $\Delta r_{y,Head}$

Figure 5.7.: Head segment centroid displacement components $\Delta r_{x,Head}$ and $\Delta r_{x,Head}$ for lane change maneuver to the left at 50 km/h

The last maneuver that was investigated was the combined maneuver to the right side. Due to the fact that research on this load case is still ongoing, the results should viewed qualitatively. This load case was the main reason for the development of the 2.5D model. The relative torso angle $\varphi_{y,Torso}$ of the simulation model remains within volunteer corridors up to 0.4 s. After 0.4 s, the model response shows a further increase in relative torso angle, whereas the volunteer median showed a decrease. This leads to an overestimation of approximately 100 percent. After 0.5 s, the model moves backwards and reaches its initial position after about 1.8 s. The volunteer responses show a different behavior by reaching their initial position at 2 s. The volunteer backward movement starts after 1.8 s. For $\varphi_{x,Torso}$, the simulation model response lies within the volunteer corridor up to 1.8 s. Hence, the model is able to reproduce the lateral torso rotation. The $\varphi_{x,Head}$ simulation model response also lies within the volunteer corridor. For the head rotation around the y-axis, the simulation model leaves the volunteer corridor in the first phase

of the maneuver after 0.1 s. From 0.4 s to 1.75 s, the simulation model response is within the volunteer corridors. In general, the simulation model response shows a smaller slope than the volunteer characteristics up to 0.3 s which might be a result of inertia differences between the model and the volunteers.

5.3. Limitations and recommendations

The results section of this thesis showed that the developed methodology is capable of reproducing the volunteer-determined kinematics for frontal and lateral maneuvers. A more generalized reconsideration of the work with respect to the testing and simulation portion will provide a better understanding of the limitations and help to suggest potential future research topics.

The aim of OEMs with respect to vehicle safety systems is to improve them in order to save lives and to gain a reputation for building safe cars, which has become an important factor in worldwide competition over the years. Cars should be sold to a wide range of people, no matter what anthropometry, sex, age or ethnic background they have.

Obviously, it is not possible to include all of these aspects for the testing and simulation of occupant kinematics. As stated previously, the testing phase was divided into three different parts. In all of the movement studies, an anthropometry close to the 50^{th}-percentile male was chosen. This decision was made with respect to simulation, in particular based on the models available. Human body models were developed for the simulation of the collision phase to augment conventional dummy models. As with the dummy models, the development of HBMs prioritized a 50^{th}-percentile male adult with about 175 cm and a mass of about 77 kg ([SRPS83]). To date, the THUMS® occupant model is only available for this population [Dyn14].

In addition to the anthropometry restriction, this work also focussed mainly on the young male population. The small amount 6 female volunteers investigated within this study and 9 females within the studies published by Òlafsdòttir et al. [OsDB13] for front passenger and Oesth et al. [OsDB13] for driver do not allow for solid statistical analysis of gender-related differences in the kinematic responses. There might also be a difference between volunteer groups of other ages, which needs to be quantified. Another factor for the selection of volunteers is the physical condition. The volunteers who participated in these movement studies where mainly athletic people. People who are not physically fit could show different pre-collision kinematics.

In addition racial differences were not considered. The psychological state of the vehicle occupants is another relevant factor for testing which was not omitted from this thesis. The question of, how and to what extent psychological factors (e.g., stress, happiness) combine physiological parameters (e.g.,fatigue, physical fitness) to influence vehicle occupant kinematics remains open.

The boundary conditions that were used for the testing also have to be considered. Ve-

hicle tests were performed with one certain vehicle type with altered seat and restraint systems. Changing the vehicle type might affect the occupant kinematics due to psychological factors (e.g., feeling unsafe) and also due to the change in the vehicle dynamics. The vehicle occupants were also assumed to be sitting in a standard position prior to the start of the maneuver, which is often not the case in reality. The velocities and accelerations were chosen based on volunteer safety and also maximum values that could be achieved with a production car. The large range of velocities of 38 km/h between the different frontal emergency braking maneuvers invites a question about whether or not the occupant responses for velocities between 12 km/h and 50 km/h, as well as for acceleration levels between 0.5g and 1g, remain the same, or if there are different strategies and patterns that could be identified.

Clearly, there is a wide range of aspects that can be considered within testing. From the author's point of view, the most important aspects that should be addressed by subsequent research are gender and anthropometry, followed by a variation of the load cases (different acceleration levels and velocities).

On the simulation side, there are also limitations of which the reader should be aware. The development of the implementation method was based on the THUMS® occupant model. To check the universality of the controller concept in combination with the HBM, it is necessary to cross-check THUMS® with other models, such as the Global Human Body Models Consortium's (GHBMC) human body model [PKC+13]. The cross-check would make it possible to determine the differences in mass distributions and model configuration and therefore indicate whether or not the controller concept has to be adjusted.

The simulation results showed that the surrogate models can reproduce the occupant kinematics for both the frontal maneuvers and the combined maneuvers. However, for the pure lateral maneuver, the simulation could not reproduce the occupant kinematics. As stated above, both the seat and the outer surface of the model were modeled as rigid bodies. Using the reference seat with wooden plates covered with leather increased the stiffness compared to the original production seat, but due to the use of the standard mounting, this seat still has elasticities which were neglected for the simulation boundaries. Furthermore the movement of the seat due to rolling and pitching of the sled and the vehicle were also not modeled. For the sled test with the rigid sled the rolling and pitching of the sled is less than one degree. The analysis of the pitch angles demonstrated that the maximum pitch of the test vehicle during full braking is 1.85 degrees. The pitching effect was therefore negligible. Modeling the outer model surface as a rigid body also does not represent reality and leads to the effect that the simulation results are more sensitive to the initial position of the model in the seat than they might be in reality.

The presented implementation approach splits the human spine into two segments. Considering the complexity of the human spine, this is a rough approach. The question that has to be answered is where are the limits of this approach and how can the current results be viewed in the context of cybernetic approaches? The approach presented

here is a technical top-down approach with the main aim of reproducing the occupant kinematics without a detailed modeling of the underlying biological system. Cybernetic approaches (e.g., [REK+15]) consider both the internal and the external dynamics of a biological system. Due to the high number of volunteers required, the main aim of having a reasonable kinematics model with low computational effort, and the novelty of the approach, the cybernetic approach was rejected. Although the computational efforts can be reduced to 1/10 of the original run time when changing the complex FE model to a simple surrogate model, there is also one major drawback: As mentioned above, HBMs were developed for simulations of the collision phase and are used to determine injuries and injury mechanisms during this phase. Even though no injuries might occur within the pre-collision phase, both the change in position and the activity of the muscles influence the internal load distributions of the occupant. By rejecting the cybernetic approach and using a surrogate model as presented within this thesis, information on the internal stresses is lost. In order to increase the model complexity further and achieve the goal of having one specific model to simulate the pre-collision and the collision phases, this issue needs to be addressed. Purely technical approaches require the expertise of cybernetics in order to manage the transition from pre-collision to the collision phase. Hence, from the author's point of view, the goal of having one model can only be achieved if the knowledge and strengths from these different research disciplines can be combined.

The consideration of the data from test series B indicates that the current two-segment approach needs to be extended for the lane change maneuver, in order to enable the reproduction of a shearing movement (translational spine movement without segment angle change). The co-simulation approach basically allows for the arbitrary increase of the number of segments, but the analytical solution of the model equations is limited to four segments. As stated previously, the rotation of the torso and head/neck segments around the vertical axis was not considered within the presented modeling approach. Due to the maneuver set up of the sled test and vehicle test series A, where the volunteer movement could be modeled as planar movement, head rotation could be omitted. For vehicle test series B, since the three-point belt influences the degree of freedom around the vertical model axis, it may also be necessary to control that degree of freedom as well. Further work must therefore concentrate on a reconsideration of the collected test data in order to quantify and evaluate these influences on occupant kinematics.

The controller within this thesis uses relative demand and actual segment values for bothe the head/neck segment and the torso segment. The main concept was described in the methodology chapter of this thesis. To determine the joint torques and via the muscle/actuator force for the beam elements via geometry information, the controller uses an internal representation of the outside model, which could be either an MB or FE model. In the modeling approach presented, this internal model was a two-segment model with masses and mass moment of inertia derived from THUMS®. The DoF and COG positions of individual parts of the internal model were adjusted to the outside model as accurately as possible. The simulation results are strongly dependent on the

modeling differences within the internal and the outside model. Therefore, increasing the number of segments used to represent the head/neck and the torso regions would also require an adjustment of the controller concept and an exact determination of the mass and inertia properties.

As stated in previous chapters, a lap-belt configuration was used for both the sled and vehicle test series A. This lap belt was manually tightened, and it was assumed that the pelvis movement was therefore constrained. Based on this assumption, the torso joint was also assumed to be restrained. A qualitative estimation of the relative movement between the subject and the reference seat showed that this assumption holds true for the sled testing and vehicle test series A. For vehicle test series B, a three-point belt was used, and the lower part of the belt was not fixed. During maneuvering, webbing could be paid out until the seat belt retractor locked. The pelvis was therefore no longer locked, and a relative movement between volunteer and reference seat could occur. The relative movement was estimated based on the marker trajectory of a seatbelt marker attached to the lap belt part of the three-point belt. Due to occlusions of this marker point, data was not available for all subjects. However, data of individual subjects showed excursions of the seatbelt marker of more than 100 mm.

Three different volunteer types (*slack*, *average* and *tensed*) were identified, and controller gains were derived by using an optimization algorithm. Although the onset latencies are close to biologically reasonable ranges (e.g., [EOH$^+$07], [HCD$^+$13]), the current technical implementation of the controller in combination with the optimization does not allow for the identification of clear patterns of the controller gain parameters $K_{p,High}$, $K_{p,Low}$, $K_{d,High}$ and $K_{d,Low}$. If the model is to be used by a broader community, sets of default values must be given, and once again, a connection between the technical and the cybernetic approach must be found.

The simulations of vehicle test series B used a simplified belt model with characteristics related to the stiffness of a beam element within the model. As mentioned above, for test series B, the belt force was measured. Analysis of the belt force showed large variations of belt force. Figure 5.8 shows the measured belt force for emergency braking maneuver at 12 km/h for 25 volunteers. The results showed that the measured minimum shoulder belt force is close to about 0.12 kN, while the maximum shoulder belt force is close to 0.35 kN. These measured belt forces are in accordance with the belt forces measured by Òlafsdòttir et al. [OsDB13]. Comparing the results of vehicle test series A and B, it is evident that the three-point belt significantly influences volunteers' forward excursion. In addition, for simulation a difference in model response using different belt setups was found. These results are in accordance with the study of Morris and Cross [MC05], who identified seatbelt use as one pre-event factors for occupant kinematics, as well as Carlsson and Davidsson [CD11], who also hypothesized that seat belt properties influence volunteer forward movement. In order to further validate the simulation model responses, further testing must provide additional information on the belt forces to verify the data collected during vehicle test series B.

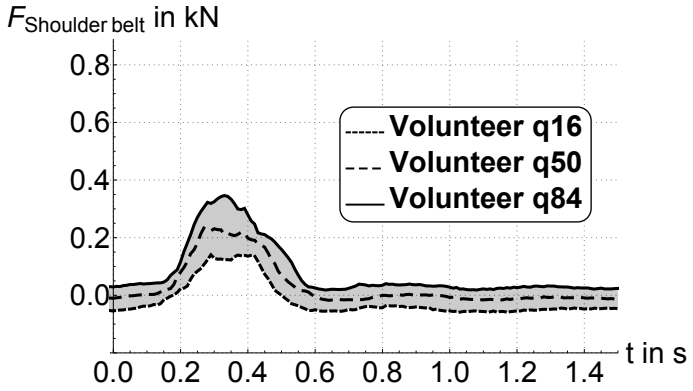

Figure 5.8.: Shoulder Belt force $F_{Belt}^{Shoulder}$

Due to the importance of active and reactive HBMs for the future development of advanced safety systems, the author anticipates an increase in the number of research initiatives dealing with active and reactive human body modeling. The large number of parameters that might influence the occupant kinematics makes it nearly impossible for all of the testing to be done within the scope of a single initiative. To facilitate the sharing of a data and its inclusion in subsequent simulation models, standard points have to be defined. Within the literature, single marker trajectories are often presented. This leads to problems if the size of the subjects varies and is not presented within the publications, or if marker points are occluded due to the setup. One suggestion might be to also agree on a set of calculated points based on the trajectories of several markers, which would increase the stability. For this task in particular, the author sees the strong benefit of corporation between experts in the field of vehicle safety and biomechanics, in order to define a reasonable and stable solution.

6. Summary

This thesis developed a methodology for incorporating reactive occupant kinematics in a human body model (HBM). Reactive human kinematics within this thesis is the kinematics of human occupants caused by muscle contributions that counteract external low-acceleration disturbances (up to several g). HBMs are developed as an additional tool for the assessment of secondary safety measures. Simulations using both numerical dummy models and HBMs allow for the reproducible, effective and efficient development of secondary safety features, as the model kinematics show good accordance with testing data. Beyond kinematics investigations, the use of HBMs can provide a direct insight into injuries and injury mechanisms, which is an additional advantage over conventional numerical dummy models. The major drawbacks of using mechanical and numerical dummy models, as well as passive HBMs for the development of primary safety features are their high stiffness and their lack of active muscle components. For pre-collision scenarios with low acceleration levels, muscle contribution has been identified as a major component that influences human kinematics.

This thesis addresses this lack of passive HBMs by presenting an approach that makes it possible to take into account such contributions for the simulation of human pre-collision kinematics. The presented approach is based on co-simulation, which is the main difference compared to common approaches. The controller that influences the model kinematics and the model itself are split. This approach makes it possible to use the same controller for different underlying FE, as well as for multi-body models. The development of the implementation methodology was divided into several steps. The first step was an analysis of the state of the art with respect to testing. The results showed that mainly two types of testing could be distinguished: sled testing and vehicle testing. Studies within the literature were performed with acceleration levels up to 5g.

To ensure a solid development of the implementation methodology, tests were performed. This should allow for an exact definition of boundaries and extend the data pool of available literature on occupant pre-collision kinematics. The test series within this thesis were divided into two categories: sled and vehicle testing. Specifically, three different series were performed. One sled test series and two vehicle test series referred to as vehicle test series A and test series B. The maneuvers investigated within these test series were chosen based on accident statistics, which identified frontal, lateral and rear initial points of impact as the most relevant. Using this information, two different maneuvers, were primarily chosen for occupant kinematics investigations: an emergency braking maneuver and a single lane change maneuver. Prior to the sled testing series, the co-simulation approach was tested on simple surrogate models of the lower extremities

using shell element as parts of the BIORIDII/HybridIII 50^{th}-percentile dummy models. After demonstrating the functionality on the simple surrogate models, work continued on HBMs. For the development of the methodology, a THUMS® model with refined mesh was used. The high stiffness and large computational effort of this HBM would not enable a proper methodology development. Hence, it was decided to create surrogate models. The surrogate models were created by removing the flesh and inner organs and introducing two kinematic joints in the lumbar and cervical area of the THUMS® version. The remaining skeletal parts were assigned the mass and mass moment of inertia properties of the original THUMS® model.

Specifically, three different surrogate models corresponding to the three different testing series were created. These three different models were necessary to be able to increase model and controller complexity step-by-step and address the different boundary conditions of the testing series. The different surrogate models created were a 2D sled test model, a 2D vehicle model and a 2.5D vehicle model. The designation 2.5D refers to an approach where two 2D controllers were superpositioned in order to simulate volunteer 3D responses. The sled test model was built using sled test series data. For the creation of this model, the human vertebral column was divided into two parts, which represented the torsos and the heads of the human volunteers. Due to the set-up of sled testing maneuvers, the introduced kinematic joints were modeled as revolute joints, with one frontal rotational degree of freedom for frontal maneuvers and one rotational lateral degree of freedom for lateral maneuvers, which resulted in one planar model per investigated maneuver. For this first model creation step, the mass moment of inertia properties of the original model were not taken into account. Model kinematics were controlled with a planar movement controller. The presented 2D inertia model was the next major step in methodology development. It is a more realistic model based on vehicle test series A, using a reference seat and lap-belt configuration. This model takes into account the mass moment of inertia properties of the THUMS®-D model. Here again, this model is planar. In combination with a planar controller, this model makes it possible to imitate the complete range of volunteer responses identified during frontal testing. This was demonstrated by taking three representative volunteer responses, which were close to the outer bounds and the median of volunteer responses.

The last model shown in this thesis is a 2.5D model. This model is based on vehicle testing series B, which used a seat with lateral support and a three-point belt. This model uses a modeling approach that enables the representation of a 3D volunteer movement. The rotational DoF are separated, and a superposition of two 2D controllers to a simulated 3D volunteer response is used. The simulation results show that the co-simulation approach makes it possible to simulate the whole range of volunteer responses for frontal maneuvers that was identified within the tests. For pure lateral and combined maneuvers, the method is also applicable.

To sum up the main findings, the presented approach is a further step towards the goal of using HBMs to assess of primary safety measures. The data collected to determine occupant pre-collision kinematics extends the current state of the art. The strong con-

nection of testing and simulation allowed for an exact definition of boundary conditions. Due to the bottom-up approach using surrogate models, the current problem of an excessively stiff HBM was eliminated. Furthermore, this approach permits an flexible increase of both model and controller complexity, which makes it possible to incorporate more realistic models of muscles with respect to insertion and origin, as well as with respect to the force creation. If a deformable model is to be used in the FE environment instead of the rigid body formulation, one must incorporate further joints and muscle/actuator elements.

The presented approach provides the basis for further work towards the goal of having a fast and reliable development process for the improving integrated safety systems.

List of Figures

List of Tables

Bibliography

[ABS+09] K. B. Arbogast, S. Balasubramanian, T. Seacrist, M. R. Maltese, J. F.F. García-España, T. Hopely, E. Constans, F. J. Lopez-Valdes, R. W. Kent, H. Tanji, and K. Higuchi. Comparison of kinematic responses of the head and spine for children and adults in low-speed frontal sled tests. *Stapp Car Crash J*, 53:329–372, Nov 2009.

[Adm08] National Highway Traffic Safety Administration. Traffic safety facts 2008 - a compilation of motor vehicle crash data from the fatality analysis reporting system and the general estimates system. Technical report, National Center for Statistics and Analysis U.S. Department of Transportation Washington, DC 20590, 2008.

[Age10] European Environment Agency. Occupancy rates of passenger vehicles (term 029). Available at http://www.eea.europa.eu/data-and-maps/indicators/occupancy-rates-of-passenger-vehicles/occupancy-rates-of-passenger-vehicles-1#data_specifications, July 2010. Accessed on 01 October 2014.

[Age11] European Environment Agency. Size of the vehicle fleet (term 032). Available at http://www.eea.europa.eu/data-and-maps/indicators/size-of-the-vehicle-fleet/size-of-the-vehicle-fleet-2, January 2011. Accessed on 01 October 2014.

[BB02] M. Bárány and K. Bárány. Biochemistry of muscle contraction. Available at http://www.uic.edu/classes/phyb/phyb516/index.htm, 2002. Accessed on 01 October 2014.

[BBY+12] J. Broughton, C. Brandstatt, G. Yannis, P. Evgenikos, P. Papantoniou, M. Candappa, M. Cristoph, K. Van Duijvenvoorde, and M. Vis. Basic fact sheet "main figures", 2012. Deliverable D3.9 of the EC FP7 project DaCoTa.

[BCUM10] D. Bose, J.R. Crandall, C.D. Untaroiu, and E.H. Maslen. Influence of pre-collision occupant parameters on injury outcome in a frontal collision. *Accident Analysis & Prevention*, 42(4):1398 – 1407, 2010.

[Ben14] M. Benedikt. Regelungstechnische aspekte bei der nicht-iterativen co-simulation. *Automatisierungstechnik*, 62(8):p. 598 – 606, 2014.

[BKM+12] S. M. Beeman, A. R. Kemper, M. L. Madigan, C. T. Franck, and S. C. Loftus. Occupant kinematics in low-speed frontal sled tests: Human vol-

unteers, hybrid III ATD, and PMHS. *Accident Analysis & Prevention*, 47:128–139, Jul 2012.

[BKMD11] S. M. Beeman, A. R. Kemper, M. L. Madigan, and S. M. Duma. Effects of bracing on human kinematics in low-speed frontal sled tests. *Ann Biomed Eng*, 39(12):2998–3010, Dec 2011.

[BM07] H. Burg and A. Moser. *Handbuch Verkehrsunfallrekonstruktion*. ATZ/MTZ-Fachbuch. Vieweg & Teubner Verlag, 2007.

[BS13] H.H. Braess and U. Seiffert. *Vieweg Handbuch Kraftfahrzeugtechnik*. ATZ/MTZ-Fachbuch. Springer Fachmedien Wiesbaden, 2013.

[BW76] K.-J. Bathe and E. L. Wilson. Numerical methods in finite element analysis. 1976.

[BW13] M. Benedikt and A. Watzenig, D.and Hofer. Modelling and analysis of the non-iterative coupling process for co-simulation. *Mathematical and Computer Modelling of Dynamical Systems*, 19(5):451–470, 2013.

[CD11] S. Carlsson and J. Davidsson. Volunteer occupant kinematics during driver initiated and autonomous braking when driving in real traffic environments. In *International IRCOBI Conference on the Biomechanics of Impact*, pages 125–136, 2011.

[CDCD+05] L. Chiari, U. Della Croce, D., A. Leardini, and A. Cappozzo. Human movement analysis using stereophotogrammetry: Part 2: Instrumental errors. *Gait & Posture*, 21(2):197 – 211, 2005.

[CDCLC05] A. Cappozzo, U. Della Croce, A. Leardini, and L. Chiari. Human movement analysis using stereophotogrammetry: Part 1: theoretical background. *Gait & Posture*, 21(2):186 – 196, 2005.

[CEKL99] H.-Y. Choi, H.-W. Eom, S.-T. Kho, and I.-H. Lee. Finite element human model for crashworthiness simulation. *SAE Technical Paper 1999-01-1906*, 1999.

[CLCC05] U. D. Croce, A. Leardini, L. Chiari, and A. Cappozzo. Human movement analysis using stereophotogrammetry: Part 4: assessment of anatomical landmark misplacement and its effects on joint kinematics. *Gait & Posture*, 21(2):226 – 237, 2005.

[Com11] European Commission. White paper on transport. Available at http://ec.europa.eu/transport/themes/strategies/doc/2011_white_paper/white-paper-illustrated-brochure_en.pdf, March 2011. Accessed on 11 September 2014.

[Com14a] Euopean Commission. Vehicle safety. Available at http://ec.europa.eu/transport/road_safety/specialist/knowledge/vehicle/index_en.htm, June 2014. Accessed on 11 September 2014.

[Com14b] European Commission. EU road fatalities. Available at http://ec.europa.eu/transport/road_safety/pdf/observatory/trends_figures.pdf, March 2014. Accessed on 05 December 2014.

[CRS09] R. Cresnik, A. Rieser, and H. Schluder. Dynamic simulation of mechatronic systems. In *7th European LS-Dyna Conference, Graz, Austria*, 2009.

[Dea79] P.M. Deane. *The First Industrial Revolution*. Cambridge University Press, 1979.

[dJB94] J. G. de Jalón and E. Bayo. *Kinematic and dynamic simulation of multibody systems*. 1994.

[DL93] C. J. De Luca. The use of surface electromyography in biomechanics. *Journal of Applied Biomechanics*, 13 (2):135–163, 1993.

[DL03] G. De Luca. Fundamental concepts in emg signal acquisition. *Copyright Delsys Inc*, 2003.

[Dyn11] Dynamore. Thums-training within om4is project. February 2011.

[Dyn14] Dynamore. Human model. Available at http://www.dynamore.de/en/products/models/human, 2014. Accessed on 06 December 2014.

[EBB05] J. D. Enderle, S. M. Blanchard, and J. D. Bronzino. *Introduction to biomedical engineering*. Academic Press, 2005.

[Eck01] E. Eckermann. *World History of the Automobile*. Society of Automotive Engineers (SAE), 2001. Warrendale, USA, 2001.

[Eic10] A. Eichberger. Contributions to primary, secondary and integrated traffic safety, May 2010. Habilitation Thesis.

[EIS+12] S. Ejima, D. Ito, F. Satou, K. Mikami, K. Ono, K. Kaneoka, and I. Shiina. Effects of pre-impact swerving/steering on physical motion of the volunteer in the low-speed side-impact sled test. In *International IRCOBI Conference on the Biomechanics of Impact*, pages 352–366, 2012.

[EOH+07] S. Ejima, K. Ono, S. Holcombe, K. Kaneoka, and M. Fukushima. A study on occupant kinematics behaviour and muscle activities during preimpact braking based on volunteer tests. In *International IRCOBI Conference on the Biomechanics of Impact*, pages 31–45, 2007.

[Eur13] Eurostat. Energy, transport and environment indicators, 2013. Pocketbook 2013 edition.

[EZO+09] S. Ejima, Y. Zama, K. Ono, K. Kaneoka, I. Shiina, and H. Asada. Prediction of pre-impact occupant kinematic behavior based on the muscle activity during frontal collision. In *21st ESV Conference*, number 09-0913, 2009.

[EZS+08] S. Ejima, Y. Zama, F. Satou, S. Holcombe, K. Ono, K. Kaneoka, and I. Shiina. Prediction of the physical motion of the human body based on muscle activity during pre-impact braking. In *International IRCOBI Conference on the Biomechanics of Impact*, pages 36: 163–176, 2008.

[Fre12] D. Fressmann. Vehicle safety using the thums human model,. In *11th German LS-Dyna Forum, Ulm*, 2012.

[GHJ66] A. M. Gordon, A. F. Huxley, and F. J. Julian. The variation in isometric tension with sarcomere length in vertebrate muscle fibers. *Journal of Physiology*, 184:170–192, 1966.

[GHS08] D. Gross, W. Hauger, and J. Schröder. *Technische Mechanik 1: Statik*. Springer Verlag, 10. Auflage edition, 2008.

[GHSW06] D. Gross, W. Hauger, J. Schröder, and W. A. Wall. *Technische Mechanik 3: Kinetik*. Springer Verlag, 10. auflage edition, 2006.

[GL18] H. Gray and W. H. Lewis. *Anatomy of the human body*. Philadelphia, Lea & Febiger, 1918. Published May 2000 by Bartleby.com.

[Hat74] H. Hatze. The meaning of the term 'biomechanics'. *Journal of Biomechanics*, 7(2):189–190, 1974.

[HCD+13] P. Huber, M. Christova, G. A. D'Addetta, E. Gallasch, S. Kirschbichler, C. Mayer, A. Prüggler, A. Rieser, W. Sinz, and D. Wallner. Muscle activation onset latencies and amplitudes during lane change in a full vehicle test. In *Proceedings of the IRCOBI Conference*, pages pp: 628–640, 2013.

[HCM11] P. Huber, C. Cagran, and W Müller. An algorithm to correct for camera vibrations in optical motion tracking systems. *Journal of Biomechanics*, 44(11):2172–2176, July 2011.

[HFP+01] L. Herda, P. Fua, R. Plänkers, R. Boulic, and D. Thalmann. Using skeleton-based tracking to increase the reliability of optical motion capture. *Human Movement Science*, 20(3):313 – 341, 2001.

[HHK+98] R. Happee, M. Hoofman, A.J. van den Kroonenberg, P. Morsink, and Wismans J. A mathematical human body model for frontal and rearward seated automotive impact loading. In *42nd Stapp Car Crash Conference*, number 983150. SAE, 1998.

[Hil38] A. V. Hill. The heat of shortening and the dynamic constants of muscle. *Proceedings of the Royal Society of London B*, 126:136–195, 1938.

[HKAS14] P. Huber, S. Kirschbichler, Prüggler A., and T. Steidl. Three-dimensional occupant kinematics during frontal, lateral and combined emergency maneuvers. In *International IRCOBI Conference on the Biomechanics of Impact, Berlin, Germany*, 2014.

[HKC94a] Y. Huang, A. I. King, and J. M. Cavanaugh. Finite element modelling of gross motion of human cadavers in side impact. In *38th Stapp Car Crash Conference*, number 942207, pages 35–53. SAE, 1994.

[HKC94b] Y. Huang, A.I. King, and J. M Cavanaugh. A madymo model if near side-human occupants impact. *Journal of Biomedical Engineering*, Vol. 111:116(2):228–35, May 1994.

[Hub13] P. Huber. Reactive human body models. In *Grazer Safety Update 2013*. Carhs, September 2013.

[Hum14a] Humanetics. Biorid-ii. Available at http://www.humaneticsatd.com/crash-test-dummies/rear-impact/biorid-ii, 2014. Accessed on 01 October 2014.

[Hum14b] Humanetics. Hybrid III 50th male dummy. Available at http://www.humaneticsatd.com/crash-test-dummies/frontal-impact/hybrid-iii-50th, 2014. Accessed on 01 October 2014.

[Hux57] A. F. Huxley. Muscle structure and theories of contraction. *Progress in Biophysics and Biophysical Chemistry*, page 7:255–318, 1957.

[HW13] W. Hirschberg and H. Waser. Fahrzeugdynamik. Vorlesungskript, May 2013.

[IKW+02] M. Iwamoto, Y. Kisanuki, K. Watanabe, I. Furusu, K. Miki, and J. Hasegawa. Development of a finite element model of the total human model for safety (thums) and application to injury reconstruction. In *International IRCOBI Conference on the Biomechanics of Impact*, pages 31–42, 2002.

[KBD11] A. R. Kemper, S. M. Beeman, and S. M. Duma. Effects of pre-impact bracing on chest compression of human occupants in low-speed frontal sled tests. In *22th International Technical Conference on the Enhanced Safety of Vehicles (ESV)*, number 11-0193, 2011.

[KBMD14] A. R. Kemper, S.M. Beeman, M. L. Madigan, and S. M. Duma. Human occupants in low-speed frontal sled tests: Effects of pre-impact bracing on chest compression, reaction forces, and subject acceleration. *Traffic Injury Prevention*, 15:sup1,:S141–S150, 2014.

[KHP+14] S. Kirschbichler, P. Huber, A. Prüggler, T. Steidl, W. Sinz, C. Mayer, and G. A. D'Addetta. Factors influencing occupant kinematics during braking and lane change maneuvers in a passenger vehicle. In *International IRCOBI Conference on the Biomechanics of Impact, Berlin, Germany*, 2014.

[Knu07] D. Knudson. *Fundamentals of biomechanics*. Springer, 2007.

[Kra08] F. Kramer. *Passive Sicherheit von Kraftfahrzeugen: Biomechanik-Simulation-Sicherheit im Entwicklungsprozess*. Springer, 2008.

[KSP+11] S. Kirschbichler, W. Sinz, A. Prüggler, P. Huber, and K. Steiner. Detailed analysis of 3d occupant kinematics and muscle activity during the pre-crash phase as basis for human modeling based on sled tests. In *22th International Technical Conference on the Enhanced Safety of Vehicles (ESV)*, 2011.

[LCDCC05] A. Leardini, L. Chiari, U. Della Croce, and A Cappozzo. Human movement analysis using stereophotogrammetry: Part 3. soft tissue artifact assessment and compensation. *Gait & Posture*, 21(2):212 – 225, 2005.

[LH02] G. Leen and D. Heffernan. Expanding automotive electronic systems. *Computer*, 35(1):88–93, 2002.

[LRS+98] E. Lizee, S. Robin, E. Song, N. Bertholon, and J. Y. Le Coz. Development of a 3d finite element model of the human body. In *42nd Stapp Car Crash Conference*, number 983152. SAE, 1998.

[LST10] LSTC. *LS-DYNA, Keyword user's manual - volume 1.* Livermore Software Technology Corporation (LSTC), Livermore Software Technology Corparation, P. O. Box 712, Livermore, California, May 2010.

[Mas92] Jean Massion. Movement, posture and equilibrium: interaction and coordination. *Progress in neurobiology*, 38(1):35–56, 1992.

[MAS05] H. Muggenthaler, N. Adamec, J.and Praxl, and M. Schönpflug. The influence of muscle activity on occupant kinematics. In *International IRCOBI Conference on the Biomechanics of Impact*, page 313–323, 2005.

[MBE+13] R. Meijer, J. Broos, H. Elrofai, E. de Bruijn, P. Forbes, and R. Happee. Modelling of bracing in a multi-body active human model. In *Proceedings of the IRCOBI Conference*, 2013.

[MC05] R. Morris and G. Cross. Improved understanding of passenger behaviour during pre impact events to aid smart restraint development. In *19th International Technical Conference on the Enhanced Safety of Vehicles (ESV)*, number 05-0320, 2005.

[MEBvH13] R. Meijer, H. Elrofai, J. Broos, and E. van Hassel. Evaluation of an active multi-body human model for braking and frontal crash events. In *Proceedings of the 23rd International Technical Conference on the Enhanced Safety of Vehicles (ESV)*, 2013.

[Men00] A. Menache. *Understanding Motion Capture for Computer Animation and Video Games*. Morgan Kaufmann, 2000.

[Mon14] J. A. Montagna. The industrial revolution. Available at http://www.yale.edu/ynhti/curriculum/units/1981/2/81.02.06.x.html, 2014. Accessed on 8 September 2014.

[Mug06] H. Muggenthaler. *Einfluss der Muskelaktivität auf die Kinematik auf*

die Kinematik des menschlichen Körpers und die Deformationseigenschaften des Muskels: Versuch und Simulation. PhD thesis, Institut für Rechtsmedizin der Ludwig-Maximilians-Universität München, 2006.

[Mus14] Deutsches Museum. Der motorwagen von karl benz. Available at http://www.deutsches-museum.de/sammlungen/meisterwerke/meisterwerke-i/motorwagen/motorwagen-grossansicht/, 2014. Accessed on 8 September 2014.

[MVHB+12] R. Meijer, E. Van Hassel, J. Broos, H. Elrofai, L. Van Rooij, and P. Van Hooijdonk. Development of a multi-body human model that predicts active and passive human behaviour. In *Proceedings of the International Conference on Biomechanics of Impact IRCOBI, Dublin-Ireland*, 2012.

[Nig91] B. M.: Nigg. *Biomechanics of the Musculo-skeletal System. 2.* JOHN WILEY and SONS, 1991.

[OODB13] Jonas Östh, Jóna Marín Olafsdóttir, Johan Davidsson, and Karin Brolin. Driver kinematic and muscle responses in braking events with standard and reversible pre-tensioned restraints: validation data for human models. *Stapp Car Crash J*, 57:1–41, Nov 2013.

[OsDB13] J.M. Ólafsdóttir, J. Östh, J. Davidsson, and K Brolin. Passenger kinematics and muscle responses in autonomous braking events with standard and reversible pre-tensioned restraints. In *International IRCOBI Conference on the Biomechanics of Impact*, pages 602–617, 2013.

[Pan01] M. G. Pandy. Computer modeling and simulation of human movement. *Ann. Rev. Biomed. Eng.*, Vol 3, 2001.

[PHR+11] A. Prüggler, P. Huber, A. Rieser, K. Steiner, S. Kirschbichler, and A. Eichberger. Implementation of reactive human behavior in a numerical human body model using controlled beam elements as muscle element substitutes. In *22th International Technical Conference on the Enhanced Safety of Vehicles (ESV)*, 2011.

[PKC+13] G. Park, T. Kim, JR Crandall, C. Kim T, Arregui-Dalmas, and J. Luzon-Narro. Comparison of kinematics of ghbmc to pmhs on the side impact condition. In *Proceedings of the Ircobi Conference*, pages 368–379, 2013.

[Pla09] W. Platzer. *Taschenatlas Anatomie, Band 1: Bewegungsapparat.* Thieme, 2009.

[REK+15] TK Rupp, W Ehlers, N Karajan, M Günther, and S Schmitt. A forward dynamics simulation of human lumbar spine flexion predicting the load sharing of intervertebral discs, ligaments, and muscles. *Biomechanics and modeling in mechanobiology*, pages 1–25, 2015.

[RHMY06] M. B. I. Reaz, M. S. Hussain, and F. Mohd-Yasin. Techniques of emg signal analysis: detection, processing, classification and applications. *Biol Proced Online*, 8:11–35, 2006.

[Rob01] S. Robin. Humos: Human model for safety - a joint effort towards the development of refined human-like car occupant models. In *17th International Technical Conference on the Enhanced Safety of Vehicles (ESV)*, number 297, 2001.

[Roo11] L. van Rooij. Effect of various pre-crash braking strategies on simulated human kinematic response with vary ing levels of driver attention. In *Proceedings of the 22nd ESV Conference*, 2011.

[RPdCJ13] L. van Rooij, J. Pauwelussen, O. O. den Camp, and R. Janssen. Driver head displacement during (automatic) vehicle braking tests with varying levels of distraction. In *Proceedings of the 23rd ESV-Conference*, number 13-0403, 2013.

[SBB+06] T. Serre, C. Brunet, K. Bruyere, J. P. Verriest, D. Mitton, S. Bertrand, and W. Skalli. Humos (human model for safety) geometry: From one specimen to the 5th and 95th percentile. In *Digital Human Modeling for Design and Engineering Conference*, number 2006-01-2324. SAE, 2006.

[SEB+11] G. Sammer, K. Eder, W. Berger, E. Strieder, M. Meschik, F. Vohryzka, U. Raich, J. Grafenauer, J. Stark, and E. Stierschneider. C- verkehrsnachfrage und mobilität, October 2011.

[SG14] U. Seiffert and M. Gonter. *Integrated Automotive Safety Handbook*. SAE International, Warrendale, Pennsylvania, USA, February 2014.

[SNW04] K.-U. Schmitt, P. Niederer, and F. Walz. *Trauma biomechanics*. Springer, 2004.

[SRPS83] L. Schneider, D. H. Robbins, M. A. Pflüg, and R. G. Snyder. Development of anthropometrically based design specifications for an advanced adult anthropomorphic dummy family. Final Report UMTRI-83-53-1, University of Michigan, Transportation Research Institute, 2901 Baxter Road. Ann Arbor, Michigan 48109, December 1983.

[SS08] V. Schindler and I. Sievers. *Forschung für das Auto von Morgen: Aus Tradition entsteht Zukunft*. Springer-Verlag, Berlin and Heidelberg, 2008.

[Öst14] J. Östh. *Muscle responses of car occupants- Numerical modelin and volunteer experiments under pre-crash braking conditions*. Thesis for the degree of doctor of philosophy in maschine and vehicle systems, Chalmers University of Technology, Division of Vehicle Safety, Department of Applied Mechanics, Chalmers University of Technology, SE-41296 Gothenburg Sweden, April 2014.

[Ste12] Thomas Steidl. Regelungstechnische Nachbildung der Kinematik des men-

schlichen Oberkörpers für ausgewählte Fahrmanöver. Master's thesis, Graz University of Technology, 2012.

[Tas10] Tass. *Madymo Theory Manual Release 7.2*. Tass, Schoemakerstraat 97 2628 VK Delft, The Netherlands, January 2010.

[TLPM13] T. Toroyan, K. Laych, M. Peden, and Martial Missimikim. Global status report on road safety 2013. Technical report, World Health Organisation, 2013.

[Wes10] T. Westermann. *Modellbildung und Simulation: Mit einer Einführung in ANSYS*. Springer Berlin Heidelberg, 2010.

[WS87] J. M. Winters and L. Stark. What is gained and what is lost by varying model complexity. *Biological Cybernetics*, 55:403–420, 1987.

[WSA+02] G. Wu, S. Siegler, P. Allard, C. Kirtley, A. Leardini, D. Rosenbaum, M. Whittle, D. D. D'Lima, L Cristofolini, H. Witte, O. Schmid, I. Stokes, Standardization, and Terminology Committee of the International Society of Biomechanics. ISB recommendation on definitions of joint coordinate system of various joints for the reporting of human joint motion–part i: ankle, hip, and spine. international society of biomechanics. *J Biomech*, 35(4):543–548, April 2002.

[WvdHV+05] G. Wu, F. C. T. van der Helm, H. E. J. Veeger, M. Makhsous, P. Van Roy, C. Anglin, J. Nagels, A. R. Karduna, K. McQuade, X. Wang, F. W. Werner, and B. Buchholz. Isb recommendation on definitions of joint coordinate systems of various joints for the reporting of human joint motion–part ii: shoulder, elbow, wrist and hand. *Journal of Biomechanics*, 38(5):981–992, May 2005.

[YHWK06] K. H. Yang, J. Hu, N. A. White, and A. I. King. Development of numerical models for injury biomechanics research: A review of 50 years of publications in the stapp car crash conference. *Stapp Car Crash Journal, pp. 429-490*, Vol. 50, November 2006.

[YWK+14] E. Yigit, J. Weber, M. Kröger, P. Huber, A. Prueggler, and S. Kirschbichler. Influence of soft tissue material model on occupant kinematics in low g scenarios using fe human body models. In *5th International Symposium Human Modeling and Simulation in Automotive Engineering*. Carhs, October 2014.

[Zie71] O.C. Zienkiewicz. *The finite element method in engineering science*. McGraw-Hill, 1971.

[ZN05] J. Zhao and G. Narwani. Development of a human body finite element model for restraint system r&d applications. In *19th International Technical Conference on the Enhanced Safety of Vehicles (ESV)*, number 05-0399, 2005.

A. Appendix

In addition to the controller model files and the standard simulation model files, an user-mat, a coupling block (s-function) in Matlab/Simulink® and two text files (referred to as "kopplungsvorgabe.dyn" and "Steuerbeams.dyn") were required as additional files for the FE simulation. The coupling of a controller developed in Matlab/Simulink® to the LS-Dyna® FE model required the setting of several inputs. Figure A.1 shows the s-function block and the input parameters, which are the IP address, the port number, the number of computer cores used for the simulation, the number of actuators which should be used, the number of outputs. These represent the quantities that the controller requires. The last two parameters are a time scaling factor, which enables the use of this coupling for FE models with different unit systems, and a time receive factor in ms, which is used to determine the end of the simulation based on communication issues.

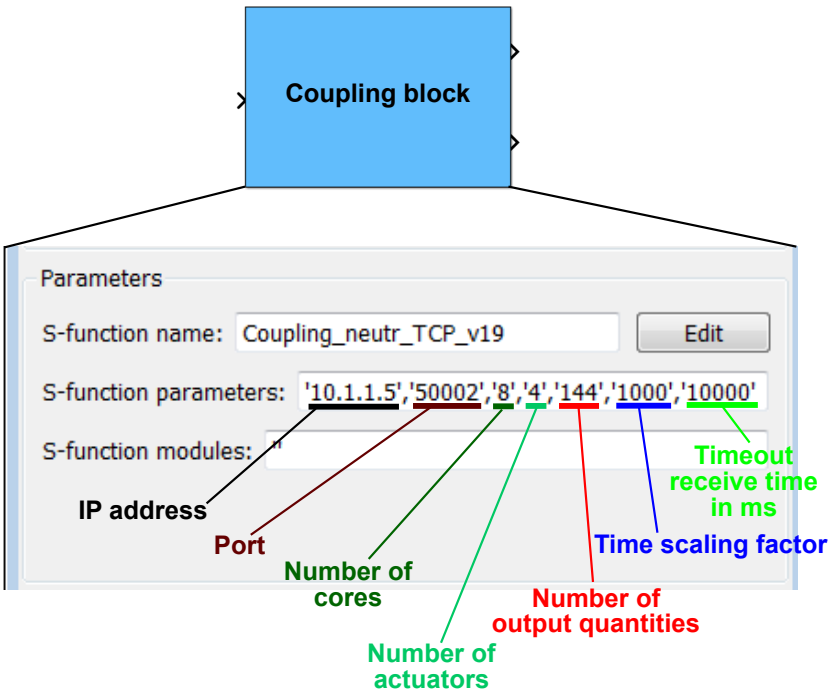

Figure A.1.: Input parameters of coupling block

The required additional input file "kopplungsvorgabe.dyn" is needed to define which

quantities should be passed from the FE environment to the controller. Figure A.2 shows an example of a kopplungsvorgabe.dyn file and outlines the main input parameters. The first line of this file describes the time interval for the exchange of data between Matlab/Simulink® and LS-Dyna® as a multiple of simulation time steps. Starting with the second row the LS-Dyna® output quantities are set. The first column entry in the second and following rows represents the node number. The second column entry represents the type of the exchanged quantity, which could be node displacements (indicated by the number 3), node velocities (indicated by the number 2) or node accelerations (indicated by the number 1). The third and final column in this file defines the direction of the quantity in the global coordinate system. Number 1 indicates the global x- axis, number 2 the global y-axis and number 3 the global z-axis direction. The total number of exchanged quantities is the number of outputs set in the coupling block.

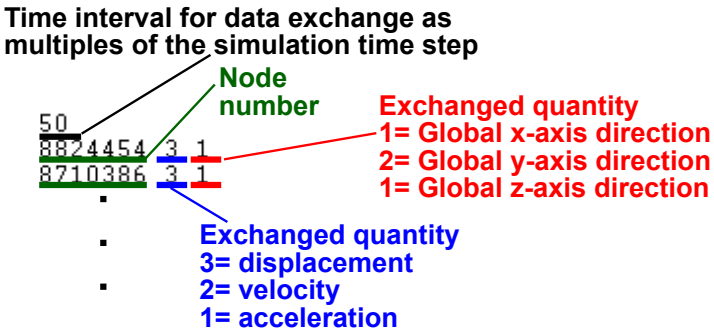

Figure A.2.: Example and description of the entries in kopplungsvorgabe.dyn file

The second additional file was "Steuerbeams.dyn". This file provides the actual definition of the actuator elements represented by the beam elements. The basic structure of the file is similar to a conventional beam definition in LS-Dyna®. A beam is specified by assigning a part, a section and an underlying material model. Information on the individual entries is available in the manual [LST10]. The main difference is the material model. The actuator elements use a userdefined material. The user has to define the beam element as an actuator by using the number 41, and an actuator identifier must be set as well. This ensures that the generated force will be applied to the specific beam element. The total number of defined actuators is the number set in the coupling block. Figure A.3 shows an example of Steuerbeams.dyn file.

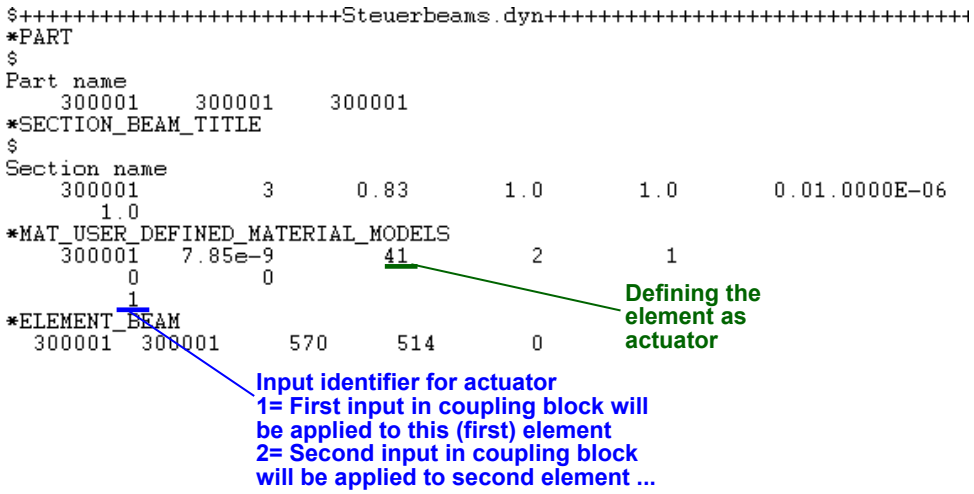

Figure A.3.: Example and description of the entries in Steuerbeams.dyn file